学位論文

Outflows in Distant Star Forming Galaxies Probed by Lyman Alpha Spectra

(Lyα スペクトルで探る遠方星形成銀河のアウトフロー)

Takuya Hashimoto

橋本 拓也

東京大学大学院理学系研究科天文学専攻

平成26年12月　博士(理学)申請

Doctoral Dissertation

Outflows in Distant Star Forming Galaxies

Probed by Lyman Alpha Spectra

(Ly αスペクトルで探る遠方星形成銀河のアウトフロー)

35-127074
Takuya Hashimoto

橋本 拓也

Department of Astronomy, Graduate School of Science

The University of Tokyo

December, 2014

Abstract

In galaxy formation and evolution, gas exchanges between galaxies and the ambient intergalactic medium (IGM), i.e., outflows and inflows, are thought to play important roles. Outflows have been ubiquitously found in nearby and high redshift (high-z) galaxies. However, at high-z, outflow studies are limited in luminous massive galaxies such as Lyman Break Galaxies (LBGs). While some authors have argued the importance of outflows from low mass galaxies in chemical enrichment (e.g., Larson, 1974), the presence and properties of outflows in them are not well examined due to their faintness.

Recently, Nakajima *et al.* (2012) have constructed the largest Lyman Alpha Emitter (LAE) photometry sample at $z \sim 2.2$ containing as many as ~ 4000 LAEs. LAEs are selected by virtue of their strong Lyα emission. Previous studies have shown that LAEs are less massive than other galaxy populations at the same redshift. Several spectroscopic follow-up observations have been performed to detect rest-frame UV and optical lines which are essential for understanding outflows. Thanks to these observations, now it is practical to inspect the presence of outflows in LAEs. In this thesis, we first examine the presence of outflows in 12 LAEs at $z \sim 2.2$ based on high spectral resolution Lyα data taken by Magellan/MagE ($R \sim 4000$) and Keck/LRIS ($R \sim 1100$), and nebular emission lines by Magellan/MMIRS, Keck/NIRSPEC, and Subaru/FMOS. Specifically, a Lyα line of four objects have been obtained by MagE, that of six objects by LRIS, and that of two objects by the both spectrographs. We have detected both Lyα and nebular emission lines in all the 12 objects. In a stacked spectrum of the four MagE spectra, we have also detected several low ionization state (LIS) metal absorption lines in LAEs for the first time (Hashimoto *et al.* 2013). LIS absorption lines are additionally detected in three individual spectra of LRIS object (Shibuya *et al.* 2014a). In order to probe outflows in LAEs, after determining the systemic velocity from nebular emission lines, we examine the velocity properties of Lyα and LIS absorption lines. We have confirmed that all the 12 objects have a main Lyα peak redward of the systemic, and 5 out of the 12objects additionally

have a weak Lyα emission blueward of the systemic, so called "blue bump". We find that most of the Lyα profiles are asymmetry with a red tail and a blue sharp cut off, and the main red peak is redshifted with respect to the systemic velocity by $\Delta v_{\mathrm{Ly}\alpha,\mathrm{r}} \simeq 200$ km s^{-1}. Finally, we have measured the blueshift of LIS absorption lines with respect to the systemic redshift, to find that they are blue shifted by $|\Delta v_{\mathrm{abs}}| \simeq 100 - 200$ km s^{-1}. These three results are all consistent with a scenario that LAEs have outflows. Thus, we have confirmed the presence of outflows in LAEs with a large sample and several techniques.

The finding that LAEs have outflows is also important to understand Lyα escape mechanisms in LAEs. Many theoretical works have investigated how galaxy properties affect the Lyα escape and emergent Lyα profile. Using a Monte Carlo technique, the Lyα radiation transfer has been in general computed through idealized spherically symmetric shells of homogeneous and isothermal neutral hydrogen gas. The ultimate goal of these studies is to understand the physical nature of galaxies using the Lyα line. Several works have compared observed Lyα lines with those predicted by models both in LBGs (e.g., Verhamme *et al.* 2008; Kulas *et al.* 2012) and LAEs (Chonis *et al.* 2013). Verhamme *et al.* (2008) have shown that their expanding shell model can well reproduce observed Lyα profiles. On the other hand, Kulas *et al.* (2012) and Chonis *et al.* (2013) have argued that such models can not reproduce observed Lyα lines well, especially the position and flux of a blue bump. There are some problems to be solved in these studies. First, Verhamme *et al.* (2008) have determined the best fit model parameters by eye, not by the statistics. This prevents one from estimating errors of the best-fit parameters, as well as examining degeneracies among the parameters. Second, Kulas *et al.* (2012) have fitted a stacked spectrum of 12 LBGs. As recently pointed out by several authors, stacking analysis generates an imaginary spectrum rather than a typical spectrum of the 12 LBGs. It is possible that the discrepancies are caused by the stacking analysis. Finally, while Chonis *et al.* (2013) have fitted three individual Lyα spectra, those spectra have similar Lyα profiles and Lyα luminosities. This also prevents them from a definitive conclusion of the origin of the discrepancies. In addition to these problems, Kulas *et al.* (2012) and Chonis *et al.* (2013) have not compared the best fit parameters with observables.

In this thesis, we have applied the Lyα radiative transfer code constructed by Verhamme *et al.* (2006) and Schaerer *et al.* (2011) to our data on the individual basis. Unlike the sample in Chonis *et al.* (2013), our 12 objects have a wide variety of Lyα profiles and Lyα luminosities. We also determine the best-fit parameters and their associated errors from the χ^2 statistics. In addition, since various observables of our objects have been

examined, we can statistically compare best fit parameters with them. Thus, we can solve the problems in previous studies. We also try to understand our finding in Hashimoto *et al.* (2013) that LAEs have smaller $\Delta v_{\mathrm{Ly}\alpha,\mathrm{r}}$ than those in LBGs. From this, we infer the key properties on Lyα escape mechanisms. We have found that all the Lyα profiles in our objects are well reproduced. For the objects without blue bump, model parameters are broadly consistent with the observables. However, for objects with the blue bump, we find that an intrinsic FWHM of Lyα, $\mathrm{FWHM_{int}}$(Lyα), is significantly larger than that of nebular lines. We infer that the parameter $\mathrm{FWHM_{int}}$(Lyα) is the key to well reproduce observed profiles. We propose that if we introduce an additional source of Lyα emission such as gravitational cooling, the large $\mathrm{FWHM_{int}}$(Lyα) and the existence of the blue bump can be simultaneously explained. We have then examined four possibilities of the origin of small $\Delta v_{\mathrm{Ly}\alpha,\mathrm{r}}$ in LAEs: a large galactic outflow velocity, the presence of a peculiar ISM with a unity covering fraction, $CF = 1$, a patchy ISM with a neutral gas covering fraction below unity, $CF < 1$, and the low neutral hydrogen column density (N_{Hi})of the gas. We find that the small $\Delta v_{\mathrm{Ly}\alpha,\mathrm{r}}$ can be quantitatively well explained by the low N_{Hi} scenario. Their typical N_{Hi} is as low as $\log(N_{\mathrm{Hi}}) \sim 10^{19}$ cm^{-2}, which is more than one order of magnitude lower than that in LBGs. Such a low column density could be consistent with the recent findings of LAEs having high ionization parameter (Nakajima & Ouchi 2014) or low HI gas mass (Pardy *et al.* 2014). Thus, we show quantitatively that N_{Hi} is the key for the Lyα escape in LAEs for the first time.

We finally discuss two implications for reionization studies. First, in estimating the neutral fraction of the IGM from Lyα emissivity, $\Delta v_{\mathrm{Ly}\alpha}$ is assumed to be 400 km s^{-1}. If LAEs at $z > 6$ have similarly small $\Delta v_{\mathrm{Ly}\alpha,\mathrm{r}}$ values as derived in this study, the amount of Lyα photons scattered by the IGM, as used to constrain the epoch of reionization, may be in need of revision. Second, from our finding that high EW(Lyα) objects tend to have small $\Delta v_{\mathrm{Ly}\alpha,\mathrm{r}}$ and the finding in Verhamme *et al.* (2014) that objects with ionizing photon leaking should have small $\Delta v_{\mathrm{Ly}\alpha,\mathrm{r}}$, we propose that targeting high EW(Lyα) objects would be an efficient way to search for LyC leaking galaxy candidates from photometry alone.

Contents

List of Figures

List of Tables

Chapter 1

Introduction

1.1 Galaxies

Galaxies are self-gravitating systems consisting of stars, interstellar medium (ISM), dust, and dark matter. Galaxies show variety of appearance from ordered disk-like elliptical shapes to irregular shapes. Since they are a basic component of the Universe, it is important to understand how they evolved with time. How can we study past galaxies ? Because the speed of light is limited, one can study them by observing distant galaxies. Selecting distant galaxies from a literally "astronomical" number of objects in the sky is the first step to study them. The most direct and secure way to determine the distance to objects is spectroscopy. One can determine it by measuring how much spectral lines are shifted into longer wavelengths with respect to their rest-frame wavelengths (redshift; z). However, the number of objects which can be simultaneously observed by spectroscopy is limited. In addition, due to the sensitivity limit, it is quite difficult to perform spectroscopy for faint objects. Instead, using the characteristic galaxy Spectral Energy Distributions (SEDs), two photometric techniques are commonly used to search for high redshift (high-z) galaxies as described below.

1.2 High-Redshift Galaxies

1.2.1 Lyman Break Galaxies

Young massive O- and B-type stars in star forming galaxies efficiently emit ionizing photons ($\lambda \leq 912$ Å). Those photons are absorbed by neutral hydrogen atoms in the inter stellar medium (ISM) and used for their ionization. In addition to that, photons with

$\lambda \leq 1215.67$ Å are resonantly scattered by neutral hydrogen in the inter galactic medium (IGM) along the line of sight. The break in SEDs at $\lambda \leq 1215.67$ Å made by these two effects is called Lyman Break. Thus, using the color excess between two broad-bands, one at the wavelength $\lambda \gtrsim 1215.67$ Å and the other at $\lambda \lesssim 1215.67$ Å, one can efficiently select star forming galaxies. Star forming galaxies selected in this technique are called Lyman Break Galaxies (LBGs). Large surveys have found thousands of LBGs from $z \sim 2$ up to $z \gtrsim 10$ (e.g., Ellis *et al.* 2013) and have revealed that they are moderately massive galaxies (10^{10} - 10^{11} $M_{\odot}$ Shapley *et al.* 2004; Erb *et al.* 2006b). A weak point of this method is that FUV continuum has to be detected, which introduce a selection bias toward UV bright objects.

1.2.2 Lyman Alpha Emitters

Another technique to search for high-z galaxies uses the HI Lyα line ($\lambda_{\rm rest} = 1215.67$Å). Ly$\alpha$ is the most prominent UV emission line, and is emitted when an electron falls from quantum level $n = 2$ to $n = 1$. It is produced by several astronomical phenomena; recombination radiation following photoionization by young massive O- and B type stars in HII regions (e.g., Partridge & Peebles 1967) and by fluorescence in intergalactic medium (IGM) (e.g., Cantalupo *et al.* 2005; Kollmeier *et al.* 2010), collisional excitation radiation following gravitational cooling (e.g., Faucher-Giguère *et al.* 2010; Rosdahl & Blaizot 2012). The Lyα technique uses the color excess of Lyα against FUV continuum, where Lyα emission is observed by a narrow band filter and FUV continuum by a broadband filter. Objects selected by this method, with large Lyα equivalent width of EW(Lyα)$\gtrsim 20 - 30$ Å, are called Lyα Emitters (LAEs). The merit of this technique is that one can efficiently search for galaxies very faint in continuum emission (i.e., low mass objects). LAEs are now commonly seen in both the local and high-z universes (local: Deharveng *et al.* 2008; Cowie *et al.* 2011, high-z: Hu & McMahon 1996; Rhoads & Malhotra 2001; Ouchi *et al.* 2008, 2010). Previous studies based on SED have revealed that typical LAEs are low-mass galaxies with a small dust content ($\lesssim 10^9 M_{\odot}$ e.g., Nilsson *et al.* 2007; Gawiser *et al.* 2007; Guaita *et al.* 2011; Nakajima *et al.* 2012), although there are some evolved LAEs with moderate mass and dust (Ono *et al.* 2010a; Hagen *et al.* 2014). Morphological studies have shown that LAEs are typically compact (e.g., Bond *et al.* 2009, 2010) and their typical size does not evolve with redshift (Malhotra *et al.* 2012). Thus, LAEs are among the building block candidates in the Λ Cold Dark Matter (CDM) model, where smaller

and less massive galaxies merge to be larger and massive ones (Rauch *et al.*, 2008). In contrast to their importance in galaxy evolution and formation, their properties are not fully understood due to their faintness.

1.3 Previous Studies Related to LAEs

In §1.2.2, we have summarized what are LAEs and their basic properties revealed by their SEDs and morphologies. In this section, first, we briefly summarize the previous studies utilizing LAEs which examine the high-z large scale structure (§1.3.1) and the epoch of cosmic reionization (§1.3.2). Then, we summarize recent studies which examine properties of LAEs (§1.3.3).

1.3.1 Clustering Analysis of LAEs

Each galaxy is enveloped by a dark matter halo, a self-gravitating system composed of dark matter. Therefore, studying dark matter halo masses and their redshift evolution leads to understanding the history of stellar mass assembly. While it is difficult to directly investigate them, theoretical studies have shown that a massive dark matter halo has stronger clustering strength (e.g., Sheth & Tormen 1999, Mo&White 02). The clustering strength of dark matter halos can be probed by those of galaxies. In fact, utilizing the extremely large field view of e.g., Subaru/Suprime-Cam, previous studies have discovered numerous LAEs and analyzed their clustering strength (e.g., Ouchi *et al.* 2008; Guaita *et al.* 2010). These studies have revealed that LAEs reside in dark matter halos which are among the lowest mass halos at a given redshift.

1.3.2 LAEs as a Probe of Cosmic Reionization

380,000 years after the Big Bang ($z \sim 1100$), ionized hydrogen experienced recombination due to the expansion and cooling of the Universe. Since there are no stars nor galaxies, this is called the "dark age" of the Universe. On the other hand, it is known that the Universe is fully ionized, indicating that the Universe is re-ionized by UV ionizing photons emitted by stars and galaxies at some epoch. This is called "cosmic reionization". However, how and when reionization has happened are not fully understood. The nature of ionizing sources is also an open question.

Fan *et al.* (2006) have examined absorption in high-z QSOs continua at wavelengths shorter than 1215.67 Å. This technique utilizes the resonant nature of Lyα: QSO continuum emission is seen redshifted as 1215.67Å and is absorbed by the neutral hydrogen in the foreground IGM. Thus, this probes the neutral fraction of the IGM, $x_{\rm HI}$, between the QSOs and us. They have shown that reionization has completed as late as $z \sim 6$.

LAEs are also used as a probe of reionization because the Lyα line is sensitive to $x_{\rm HI}$. We introduce two methods related to LAEs commonly used in reionization studies. First one is to examine the evolution of the Lyα luminosity function. At the epoch of reionization (EoR), the observed number density of LAEs should be decreased because Lyα photons are scattered by neutral hydrogen atoms in the IGM. Indeed, Kashikawa *et al.* (2006); Ouchi *et al.* (2010); Kashikawa *et al.* (2011) have demonstrated that the Lyα luminosity function rapidly decreases from $z = 5.7$ to $z = 6.6$. Taking into account the fact that UV luminosity function remains unchanged during this period (e.g., Kashikawa *et al.* 2011), these results indicate that reionization has been completed at $z \gtrsim 6$. Second one is to investigate the evolution of the fraction of galaxies with Lyα emission among LBGs, Lyα fraction. Stark *et al.* (2010, 2011) have shown that lower UV luminosity LBGs have larger Lyα fractions, and that the fraction increases from $z \sim 4$ to $z \sim 6$. However, later studies (e.g., Ono *et al.* 2012; Schenker *et al.* 2012, 2014) have demonstrated that the fraction decrease from $z \sim 6$ to $z \sim 8$. This is also interpreted as a result of a rapid increase in $x_{\rm HI}$, from being fully ionized at $z \sim 6$ to a volume-averaged neutral fraction as high as $\sim 60\%$ at $z \sim 8$ (Jensen *et al.* 2013; Stark *et al.* 2014).

1.3.3 Recent Findings of LAEs

Until recently, near-infrared spectroscopy for LAEs is quite difficult due to their faintness. It is not until 2011 that nebular emission lines have been successfully detected in LAEs (McLinden *et al.* 2011; Finkelstein *et al.* 2011). Since then, thanks to the recent advent of high sensitivity near-infrared spectroscopy instruments, and to the establishment of LAE catalogues for the nebular emission line spectroscopy, the number of LAEs whose nebular emission lines have been detected is rapidly increasing. Finkelstein *et al.* (2011) have successfully derived the gas phase metallicity in two $z \sim 2$ LAEs for the first time using the 1σ upper limit on the [NII] flux with the $N2$ index (e.g., Pettini & Pagel 2004). They have claimed that at least one LAE does not obey to the well-established mass-metalliciy relation (e.g., Tremonti *et al.* 2004; Erb *et al.* 2006a) in the sense that it has much lower

gas phase metallicity than those of LBGs at a given stellar mass (see also Song *et al.* 2014). Nakajima *et al.* (2013) have remarkably succeeded in deriving both gas phase metallicity and gas ionization parameter using the diagram of the $R23$ index versus the [OIII]/[{sc Oii] flux ratio (Pagel *et al.* 1979; Kewley & Dopita 2002). They have shown that LAEs have lower gas phase metallicity and higher gas ionization parameter than those of LBGs. These findings are further confirmed by Nakajima & Ouchi (2014) with a large sample containing both local and high-z galaxies.

Several studies have investigated the position of LAEs in the diagram of star formation rate against stellar mass. It is known that normal star-forming galaxies make a main sequence whereas starburst galaxies such as ULIRGS and/or submm galaxies lie above the main sequence (e.g., Daddi *et al.* 2007). Therefore, the diagram is useful to understand the mode of star formation. Hagen *et al.* (2014) have examined stellar populations of bright LAEs discovered by HETDEX pilot survey. Interestingly, they have found that those LAEs are burst-like galaxies (see also Chonis *et al.* 2013; Rhoads *et al.* 2014; Vargas *et al.* 2014). Recently, Kusakabe *et al.* (2014) have investigated rest-frame IR luminosity to examine dust properties of LAEs utilizing Spitzer/MIPS 24 μm and Herschel/PACS data. They have found that rather than Calzetti dust extinction law (Calzetti *et al.* 2000) which is commonly adopted, the Small Magellanic Cloud attenuation curve (Pettini *et al.* 1998) is more appropriate for the averaged LAEs. After carefully correcting SFR for dust extinction, they have claimed that at least the averaged LAEs are consistent with the main sequence.

1.4 Open Questions concerning LAEs

We describe two open questions concerning LAEs: the presence of outflows and the Lyα photon escape mechanism.

1.4.1 The Presence of Outflows

Gas exchanges between galaxies and the ambient intergalactic medium (IGM), i.e., outflows and inflows, are thought to play important roles in galaxy evolution. Outflows are driven by supernovae (SNe), stellar winds from massive stars, and AGN activity (Heckman *et al.*, 1990; Murray *et al.*, 2005; Choi & Nagamine, 2011). Galaxies which lost cold gas via outflows may experience a reduction or even termination of subsequent star formation. In contrast, cold gas supplied by inflows may increase the star formation, especially when

they come in the form of dense, filamentary gas streams ('cold accretion'; e.g. Dekel *et al.* 2009). Gas exchanges will also affect the chemical evolution of galaxies and the IGM, and thus have played important roles in establishing the mass-metalliciy relation across cosmic time (e.g., Larson 1974; Tremonti *et al.* 2004; Erb *et al.* 2006a; Yabe *et al.* 2015).

Outflows have been found in nearby starburst galaxies (Heckman *et al.*, 1990), nearby ULIRGs (Martin, 2005), LBGs at $z \sim 2-3$ (Pettini *et al.*, 2002; Shapley *et al.*, 2003), and BX/BM galaxies at $z \sim 2$ (Steidel *et al.*, 2010). These studies have made use of the fact that FUV low-ionization interstellar (LIS) absorption lines, which are generated when continuum photons encounter the outflowing gas, are blue-shifted with respect to the systemic redshift measured by nebular emission lines such as Hα originated from HII regions in the galaxy.

Examining the incidence of outflows in LAEs is of interest, because LAEs are generally low mass galaxies and thus have shallow gravitational potentials. Some authors have argued the importance of outflows from less massive galaxies in chemical enrichment (e.g., Larson, 1974). However, FUV continua of LAEs are too faint for LIS absorption lines to be reliably measured with current facilities.

Lyα is also used to probe the gas kinematics. The Lyα line is known to have complex profiles caused by its resonant nature. Many theoretical and observational studies have shown that outflowing gas leads to a redshifted Lyα line with respect to the systemic redshift (e.g., Verhamme *et al.*, 2006; Steidel *et al.*, 2010), giving a positive Lyα offset velocity, $\Delta v_{\mathrm{Ly}\alpha,\mathrm{r}}$. This also leads to an asymmetric Lyα profile with a red tail and a blue sharp cut off. In the case of an outflow, back-scattered (i.e., redshifted) Lyα photons have more chance of escape because they drop out of resonance with the foreground gas. However, it is very difficult to obtain high-resolution nebular emission spectra for LAEs because they are faint compared to strong sky emission.

Prior to Hashimoto *et al.* (2013), only four LAEs have both high-resolution Lyα and nebular line spectra: two from McLinden *et al.* (2011) and two from Finkelstein *et al.* (2011). Objects in McLinden *et al.* (2011) have $\Delta v_{\mathrm{Ly}\alpha,\mathrm{r}} = 125 \pm 17.3$ and 342 ± 18.3 km s^{-1}, respectively, and objects in Finkelstein *et al.* (2011) have $\Delta v_{\mathrm{Ly}\alpha,\mathrm{r}} = 288 \pm 37$ (photometric) $\pm$ 42 (systematic) and $189 \pm 35 \pm 18$ km s^{-1}, respectively. The fact that all four have $\Delta v_{\mathrm{Ly}\alpha,\mathrm{r}} > 0$ suggests that outflows are common in LAEs. However, due to the small sample sizes obtained so far, there has not been a statistical discussion of the gas motions of LAEs. The presence of outflows in LAEs should be examined with a larger sample.

1.4.2 The Lyα Escape Mechanism

Another important question in LAEs is their Lyα escape mechanism. Due to the resonant nature of Lyα photons, Lyα photons would be easily absorbed by dust grains after their long light paths. However, LAEs have strong Lyα emission, suggesting that they have low dust extinction and/or some mechanisms that make light paths of Lyα photons short. Taking into account the fact that a large fraction (75%) of young galaxies have strong Lyα emission (Cowie *et al.* 2011), studying the Lyα escape mechanism is important for understanding the physical nature of galaxies at the early stage of galaxy evolution.

Some observational studies at the local universe have proposed that outflows facilitate the escape of Lyα photons from galaxies (e.g., Kunth *et al.*, 1998) as they reduce the number of resonant scattering. Likewise, others (e.g., Kornei *et al.* 2010; Atek *et al.* 2014) have shown that dust content correlates with Ly escape fraction. While these effect would certainly at work, there has been no decisive conclusion.

On the other hand, using a Monte Carlo technique, the Lyα radiation transfer (RT) has been in general computed through idealized spherically symmetric shells of homogeneous and isothermal neutral hydrogen gas. These theoretical studies have investigated how galaxy properties affect the Lyα escape and emergent Lyα profiles. These studies have shown that Lyα RT is a complicated process altered by galactic outflows/inflows (e.g., Verhamme *et al.* 2006; Dijkstra & Loeb 2009), the neutral hydrogen column density and dust content of the ISM (e.g.,Zheng & Miralda-Escudé 2002; Verhamme *et al.* 2006), and the inclination of the galaxy disk (e.g., Verhamme *et al.* 2012; Zheng & Wallace 2014), as well as by the properties of the IGM surrounding the galaxy (e.g., Kollmeier *et al.* 2010; Laursen *et al.* 2013). One of the goals in these theoretical studies is to aid understanding the galaxy properties from the observed Lyα line, and to identify the key factors for the Lyα escape.

To understand Lyα RT and escape by a close comparison of observed and modeled Lyα lines, it is important to obtain spectral lines other than the Lyα line. The line centroid and the velocity dispersion of nebular emission lines (e.g., Hα and [OIII]) offer information on the galaxy's systemic redshift and an internal motion of HII regions, respectively. On the other hand, as described above, a blue-shift of LIS metal absorption lines with respect to the systemic redshift reveals the galactic outflow velocity, and the width of the LIS lines can be interpreted as the thermal velocity of the outflowing gas. These lines would

disentangle the complicated Lyα RT and help to understand the Lyα escape. However, as described in §1.4.1, it has been difficult to obtain LIS metal absorption lines nor nebular emission lines in LAEs.

Recent successful detections of both Lyα and nebular emission lines have opened up studies which compare observed and modeled Lyα lines in the context of a spherical outflowing gas shell not only in LBGs (e.g., Verhamme *et al.* 2008; Kulas *et al.* 2012) but also in LAEs (Chonis *et al.* 2013). On one hand, utilizing the shell model constructed by Zheng & Miralda-Escudé (2002) and Kollmeier *et al.* (2010), Kulas *et al.* (2012) and Chonis *et al.* (2013) have shown that the expanding shell model can not well reproduce observed Lyα profiles, especially a secondary emission blue-ward of the systemic velocity. On the other hand, based on the expanding shell model constructed in Verhamme *et al.* (2006), Verhamme *et al.* (2008) have shown that the expanding shell model can well reproduce observed profiles as well as other observed properties such as the dust content. There are, however, some problems to be solved in these studies. First, the best fit parameters in Verhamme *et al.* (2008) have been determined by eye, not by the statistics. This prevent us from determining the best fit parameters and its associated errors, as well as the degeneracy among the parameters. Second, Kulas *et al.* (2012) have compared a stacked spectrum of 12 LBGs with modeled Lyα lines. As recently pointed out by several authors (e.g., Vargas *et al.* 2014), stacking analysis provides a poor representation of individual objects. This would cause a discrepancy between observed and modeled Lyα lines. On the other hand, Chonis *et al.* (2013) have compared observed and modeled Lyα lines on the individual basis for three objects. As described in Chonis *et al.* (2013), these three objects have very similar Lyα profiles and Lyα luminosities. Thus, a larger sample with various Lyα profiles and physical properties (e.g., stellar mass, Lyα luminosity) is needed, in order to understand how well the expanding shell model can reproduce observed Lyα profiles and observables. This question is quite important because many observational studies make use of the expanding shell model to interpret observed Lyα profiles. Since Kulas *et al.* 2012; Chonis *et al.* 2013 could not fitted their Lyα profiles, there has been no discussion related to Lyα escape mechanism in these studies. Thus, first we need to quantitatively examine the validity of the expanding shell, then investigate the Lyα escape mechanisms.

As we show in §3, we examine the Lyα and absorption velocity properties and compare them with those of LBGs. Interestingly, LAEs and LBGs have similar velocity properties except for $\Delta v_{\mathrm{Ly}\alpha,\mathrm{r}}$. LAEs have $\simeq 200$ km s^{-1} which is significantly smaller than those in

LBGs, $\simeq 400$ km s^{-1} (Steidel *et al.* 2010; Rakic *et al.* 2011; Kulas *et al.* 2012). In addition, Hashimoto *et al.* (2013) have shown that $\Delta v_{\mathrm{Ly}\alpha,\mathrm{r}}$ anti-correlates with EW(Lyα), which is confirmed with larger samples in Shibuya *et al.* (2014a) and Erb *et al.* (2014). Thus, understanding the origin of the small $\Delta v_{\mathrm{Ly}\alpha,\mathrm{r}}$ through the detailed Lyα modeling should shed light on the Lyα RT and escape in LAEs.

1.5 Open Questions Concerning Cosmic Reionization

Understanding high-z LAEs properties such as the Lyα escape mechanism is also important for reionization studies.

As described in §1.3.2, some studies utilizing LAEs have suggested that the neutral fraction of IGM, x_{HI}, has rapidly increased from being fully ionized at $z \sim 6$ to a volume-averaged neutral fraction as high as $\sim 60\%$ at $z \sim 8$ (Jensen *et al.* 2013; Stark *et al.* 2014). However, some theoretical studies point out that it is unphysical that the neutral fraction of the IGM has changed in such a short period. Indeed, aforementioned studies have put some assumptions when deriving x_{HI}. In particular, related to this thesis, these studies have assumed that Lyα lines are redshifted with respect to the systemic by $\Delta v_{\mathrm{Ly}\alpha,\mathrm{r}} \sim 400$ km s^{-1} when they enter the IGM out of the galaxy (see also Santos 2004). If Lyα photons with a large $\Delta v_{\mathrm{Ly}\alpha,\mathrm{r}}$ enter the IGM, they would suffer less scattering since they are out of resonance from the neutral hydrogen in the IGM. Thus, without the exact value of $\Delta v_{\mathrm{Ly}\alpha,\mathrm{r}}$, one cannot precisely derive the neutral fraction of the IGM. However, it is quite difficult to obtain $\Delta v_{\mathrm{Ly}\alpha,\mathrm{r}}$ at such a high-z before the advent of *James Webb Space Telescope* (but see Stark *et al.* 2014). Therefore, it is quite important to systematically study $\Delta v_{\mathrm{Ly}\alpha,\mathrm{r}}$ at lower redshift such as $z \sim 2$.

Recently, several studies have investigated potential ionizing sources of reionization by searching for galaxies with ionizing photon leaking (Lyman Continuum; LyC). LyC emission is detected in LAEs and LBGs both spectroscopically (Shapley *et al.* 2006) and photometrically (e.g., Iwata *et al.* 2009; Nestor *et al.* 2013). In particular, Iwata *et al.* (2009) have demonstrated that the ionizing photon escape fraction is higher in LAEs than that in LBGs. Taking into account the fact that LAEs are the dominant population at high-z, they would have significantly contributed to reionization. This picture is further supported by the finding of Nakajima *et al.* (2013) and Nakajima & Ouchi (2014). They have shown that LAEs have the highest ionization parameter (i.e., the number of ionizing photons per a neutral atom) in a large sample of local and $z \sim 2-3$

galaxies. Verhamme *et al.* (2014) and Behrens *et al.* (2014) have examined Lyα profiles for two possible LyC leaking scenarios: (1) galaxies with density bounded HII regions where ionizing photons completely ionize the ISM, (2) galaxies with a neutral ISM with holes. They have demonstrated that the Lyα offset with respect to the systemic redshift, $\Delta v_{\mathrm{Ly}\alpha,\mathrm{r}}$, should be quite small in these cases. Since LAEs have small $\Delta v_{\mathrm{Ly}\alpha,\mathrm{r}}$, it is interesting to understand their Lyα profiles closely to examine a possible connection between LAEs and galaxies with high LyC escape fractions.

1.6 Goals of This Thesis

As described, LAEs are low mass galaxies and are important not only in understanding galaxy evolution and formation, but also in cosmic reionization studies. However, due to their faintness, properties such as the presence of outflows and the Lyα escape mechanism have not been fully understood. This also prevents us from putting a strong constraint on EoR.

In order to address these questions, in this thesis, we use the largest ($N \simeq 4000$ objects) $z \sim 2.2$ LAE samples in the COSMOS, the Chandra Deep Field South (CDFS), and the Subaru/*XMM-Newton* Deep Survey (SXDS) (Nakajima *et al.* 2012, 2013, and Nakajima et al. in prep.). These LAE samples are all based on Subaru/Suprime-Cam imaging observations with our custom made narrow band filter, NB387 ($\lambda_{\mathrm{c}} = 3870$Å and FWHM $= 94$Å). The redshift of $z \simeq 2.2$ is favored since we can simultaneously observe Lyα, LIS absorption lines (e.g., [SiII]), [OI], and [CII]), and optical nebular lines (e.g., [OII], Hβ, [OIII], and Hα) from the ground. Furthermore, we can compare the kinematics and Lyα radiative transfer of LAEs with those of brighter and more massive galaxies at similar redshifts, e.g., LBGs, obtained by previous studies.

We performed several follow-up spectroscopy observations for the samples. High spectral resolution Lyα lines are obtained by Magellan/MagE ($R \sim 4000$) and Keck/LRIS ($R \sim 1100$), and nebular emission lines by Magellan/MMIRS, Keck/NIRSPEC, and Subaru/FMOS. Specifically, Lyα spectra of four objects have been obtained by MagE, that of six objects by LRIS, and two objects by both spectrographs. As a result, we have successfully detected both Lyα and nebular emission lines for the 12 objects. LIS metal absorption lines are additionally detected in a stacked spectrum of the four MagE spectra and three LRIS individual spectra.

Utilizing these Lyα and nebular emission lines, we examine if they have outflows by

measuring the degree of the asymmetry of the Lyα profile and the velocity offset of the Lyα main peak with respect to the systemic redshift for the 12 objects. As described above, in the case of an outflow, the Lyα profile should be asymmetric with a positive $\Delta v_{\mathrm{Ly}\alpha,\mathrm{r}}$. In addition, for the objects with LIS absorption lines, we also measure their blueshift with respect to the systemic redshift, Δv_{abs}. Since there are only four (no) objects with measured $\Delta v_{\mathrm{Ly}\alpha,\mathrm{r}}$ (Δv_{abs}) (McLinden *et al.* 2011; Finkelstein *et al.* 2011) prior to Hashimoto *et al.* (2013), the spectra of the 12 objects enable us to discuss the presence of outflows with the highest confidence.

After confirming the presence of outflows in LAEs, we apply the Monte Carlo based Lyα radiative transfer code constructed by Verhamme *et al.* (2006) and Schaerer *et al.* (2011) to our data. This enables us (1) to examine how well the shell model can reproduce observed Lyα profiles, and (2) to understand the Lyα RT and escape mechanism in LAEs.

Concerning the first point, we compare observed and modeled Lyα profiles on an individual basis. Unlike the sample in Chonis *et al.* (2013), our 12 objects have a wide variety of Lyα profiles and physical quantities such as stellar masses derived from SED fitting. In addition, we determine the best-fit parameter and its associated error from the χ^2 statistics unlike Verhamme *et al.* (2008) who have determined the best-fit parameter by eye.

Concerning the second point, Hashimoto *et al.* (2013) have remarkably shown that the mean value of $\Delta v_{\mathrm{Ly}\alpha,\mathrm{r}}$ is significantly smaller than those of LBGs (e.g., Steidel *et al.* 2010; Kulas *et al.* 2012) even at the same stellar mass, star formation rate, and velocity dispersion of nebular lines. In addition, as we show in §3, velocity properties of Lyα and absorption lines reveal that the only significant difference in the velocity properties between LAEs and LBGs is $\Delta v_{\mathrm{Ly}\alpha,\mathrm{r}}$. Understanding it would shed light on the Lyα escape mechanism in LAEs. Theoretical studies propose four possibilities of the origin of small $\Delta v_{\mathrm{Ly}\alpha,\mathrm{r}}$ in LAEs: a large galactic outflow velocity, the presence of a peculiar ISM with a unity covering fraction, $CF = 1$, a patchy ISM with a neutral gas covering fraction below unity, $CF < 1$, and the low neutral hydrogen column density (N_{HI}) of the gas. By comparing with results of theoretical studies, we examine the origin of the small $\Delta v_{\mathrm{Ly}\alpha,\mathrm{r}}$ in LAEs. Erb *et al.* (2014) have recently successfully detected both Lyα and nebular emission lines for as many as 26 LAEs. They have also found that LAEs have small $\Delta v_{\mathrm{Ly}\alpha,\mathrm{r}}$ and tried to interpret it. However, their Lyα profiles have much lower spectral resolution compared with ours, which prevents them from a close comparison with RT models. Our high resolution Lyα spectra enable us to discuss the origin of it much more

quantitatively than Erb *et al.* (2014).

Finally, we discuss implications for reionization studies. Using measured $\Delta v_{\mathrm{Ly}\alpha,\mathrm{r}}$ values, we try to remove an important uncertainty in reionization studies. Behrens *et al.* (2014) and Verhamme *et al.* (2014) have proposed that Lyα profiles can be used as a probe of LyC leaking galaxies. They have argued that spectroscopy for objects with small $\Delta v_{\mathrm{Ly}\alpha,\mathrm{r}}$ would be an efficient way to find them. However, performing spectroscopy for many objects is unrealistic. Based on our results and those of Verhamme *et al.* (2014), we propose an efficient way to search for LyC leaking galaxy candidates from photometry alone.

The outline of the thesis is as follows. In §2, we briefly describe parent photometry LAE samples, and then spectroscopy for the 12 objects in detail. We show our observational results in §3. In particular, spectroscopic properties such as the asymmetry and the profile of the Lyα line are evaluated in §3.1. In conjunction with the blue shift of the LIS absorption lines with respect to the systemic redshift, we discuss the presence of outflows in LAEs. We also show the results of stellar population and morphology in §3.2 and §3.3, respectively. These results are used in §4 for a detailed comparison between observed and modeled Lyα profiles. In §4, we apply the expanding shell model constructed by Verhamme *et al.* (2006) Schaerer *et al.* (2011) to our data. We introduce a technique for determining the best-fit parameters and their associated errors, as well as the degeneracy among the parameters using χ^2 statistics. A detailed comparison of not only Lyα profiles but also model parameters and observables are shown. A discussion on the origin of the small $\Delta v_{\mathrm{Ly}\alpha,\mathrm{r}}$, as well as its implication is given in §5. We also discuss implications of our study for reionization studies. Finally, a summary and conclusions are described in §6.

Throughout this paper, magnitudes are given in the AB system (Oke & Gunn, 1983), and we assume a ΛCDM cosmology with $\Omega_m = 0.3$, $\Omega_\Lambda = 0.7$, and $H_0 = 70$ km s^{-1} Mpc^{-1}.

Chapter 2

Observations & Data

Our initial sample of objects are taken from large $z \sim 2.2$ LAE samples in the COSMOS, the Chandra Deep Field South (CDFS), and the Subaru/*XMM-Newton* Deep Survey (SXDS) (Nakajima *et al.* 2012, 2013, and Nakajima et al. in prep.). These LAE samples are all based on Subaru/Suprime-Cam imaging observations with our custom made narrow band filter, NB387 ($\lambda_c = 3870$Å and FWHM = 94Å). The LAEs have been selected by imposing the following color criteria:

$$u^* - NB387 > 0.5 \ \& \ B - NB387 > 0.2 (\text{COSMOS and SXDS}), \tag{2.1}$$

$$U - NB387 > 0.8 \ \& \ B - NB387 > 0.2 (\text{CDFS}). \tag{2.2}$$

The COSMOS, CDFS, and SXDS sample contains 619, 747, and 919 LAEs with EW$\gtrsim$30Å

From these, we only use 12 LAEs whose Lyα and nebular emission lines (e.g., Hα and [OIII]) are both spectroscopically confirmed. Among the 12 objects, 11 LAEs have been presented in Hashimoto *et al.* (2013) and Shibuya *et al.* (2014a). We add one new LAE with EW(Lyα)$_{\rm photo} \sim 280$Å whose detail properties will be discussed in Hashimoto et al. in prep.

In this section, we summarize our near-infrared spectroscopy (§2.1), optical spectroscopy (§2.2), and the presence of AGNs in the sample (§2.3).

2.1 Near-Infrared Spectroscopy

In order to detect nebular emission lines, we performed three near-infrared observations with Magellan/MMIRS (PI: M. Ouchi), Keck/NIRSPEC (PI: K. Nakajima), and Subaru/FMOS (PI: K. Nakajima). Canonical spectral resolutions for our observation settings are $R \sim 1120$, 1500, and 2200 for MMIRS, NIRSPEC, and FMOS, respectively.

2.1.1 MMIRS Spectroscopy and Reduction

We observed the two CDFS objects on 2010 October 21 with Magellan/MMIRS using the HK grism covering 1.254 – 2.45μm. The total exposure time was 10800s for each object. The slit width was 0.″5 resulting in $R \equiv \lambda/\Delta\lambda \sim 1120$. A two-point dither pattern (A1,B1,A2,B2,A3,B3,...) was adopted. The A0V standard star HIP-16904 was also observed. The sky was clear through our observation run, with seeing sizes of 0.″5 – 0.″9.

We reduced the MMIRS data using IRAF tasks and the COSMOS package which is the standard reduction pipeline for Magellan/IMACS. The MMIRS detector is read out non-destructively during a single exposure, and individual read-outs are stored as separate extensions in a FITS file through which we know whether and when a particular pixel is saturated. Bias subtraction and flat fielding were processed for each read-out using IRAF `mscred` package to treat data of this format. Then we ran `mmfixen` package which takes advantage of its sampling. This essentially fits a line to different values for a given pixel in each readout, and outputs the slope of this linear fit to the final collapsed image. Wavelength calibration and distortion correction were processed for each frame using the COSMOS package. Although we obtained arc lamp calibration images, we used OH lines for wavelength calibration. We then performed the following operation to remove sky background: C1 = B1 - (A1 + A2)/2, C2 = B2 - (A2 + A3)/2. After this operation, we ran `subsky` in the COSMOS package [*1] on each frame to remove residual sky lines. Resultant frames ($C1, C2$,...) are then stacked to have a final 2D frame using `sumspec-2d` and `extract-2dspec` in the COSMOS package. 1D spectrum extraction was carried out using `apall` in IRAF. The telluric absorption correction and flux calibration were conducted using the standard star frames.

Throughout the paper, we determine a line to be detected, if there exists an emission line above the 3σ sky noise around the wavelength expected from the Lyα redshift, where sky noise is calculated from the spectrum within 100 Å from the line wavelength.

We successfully detected Hα and [OIII]$\lambda\lambda$ 4959 5007 lines from the two CDFS objects.

[*1] This uses the Kelson procedure (cf, Kelson, 2003).

2.1.2 NIRSPEC Spectroscopy and Reduction

The four COSMOS objects, COSMOS-08501, COSMOS-13636, COSMOS-30679, and COSMOS-43982, were observed on 2011 February 10 and 11 with Keck-II/NIRSPEC. COSMOS-30679 was observed with NIRSPEC-3 (J band; 1.15 – 1.36μm), NIRSPEC-5 (H band; 1.48 – 1.76μm), and NIRSPEC-6 (K band; 2.2 – 2.43μm) filters in the low-resolution mode, while the rest of the four were observed with the K band alone. Furthermore, we observed CDFS-3865 with the J band targeting [OII] $\lambda\lambda 3726, 3729$. The slit width was 0.″76 for all three objects, corresponding to $R \sim 1500$ for all grisms. A two-point dither pattern was adopted. We simultaneously observed reference stars, which we used for blind offsets (see Finkelstein *et al.* 2011; Yang *et al.* 2011) because of the faintness of our targets. The A0V standard star HIP-13917 was also observed. The sky was clear in our observing nights, with seeing sizes of 0.″6 – 0.″9.

We reduced the NIRSPEC data using mainly IRAF tasks. Details of the reduction procedure is described in Nakajima *et al.* (2013).

An Hα line was detected from all of the COSMOS objects. In addition to that, an [OIII] λ5007 line was detected from COSMOS-30679. An [OII] λ3727 line was additionally detected with the J band ($1.15 - 1.36$ μm).

The flux-calibrated 1D spectra of the objects are shown in Figure 2.1.

2.1.3 FMOS Spectroscopy and Reduction

The six COSMOS and two SXDS objects, COSMOS-08357, COSMOS-12805, COSMOS-13138, COSMOS-13636, COSMOS-38380, COSMOS-43982, SXDS-10600, and SXDS-10942, were observed on 2012 December 22, 23, and 24 with Subaru/FMOS. We used $J-$ and $H-$band filters, whose spectral coverage is $0.9 - 1.8$ μm. Details of the observation and data reduction procedures are presented in Nakajima et al., in prep. We successfully detected [OIII] line(s) in all of the objects.

The flux-calibrated 1D spectra of the objects are shown in Figure 2.2.

2.2 Optical Spectroscopy

In order to detect Lyα and metal absorption lines, we carried out several observations with Magellan/MagE (PI: M. Rauch) and Keck/LRIS (PI: M. Ouchi). The spectral reso-

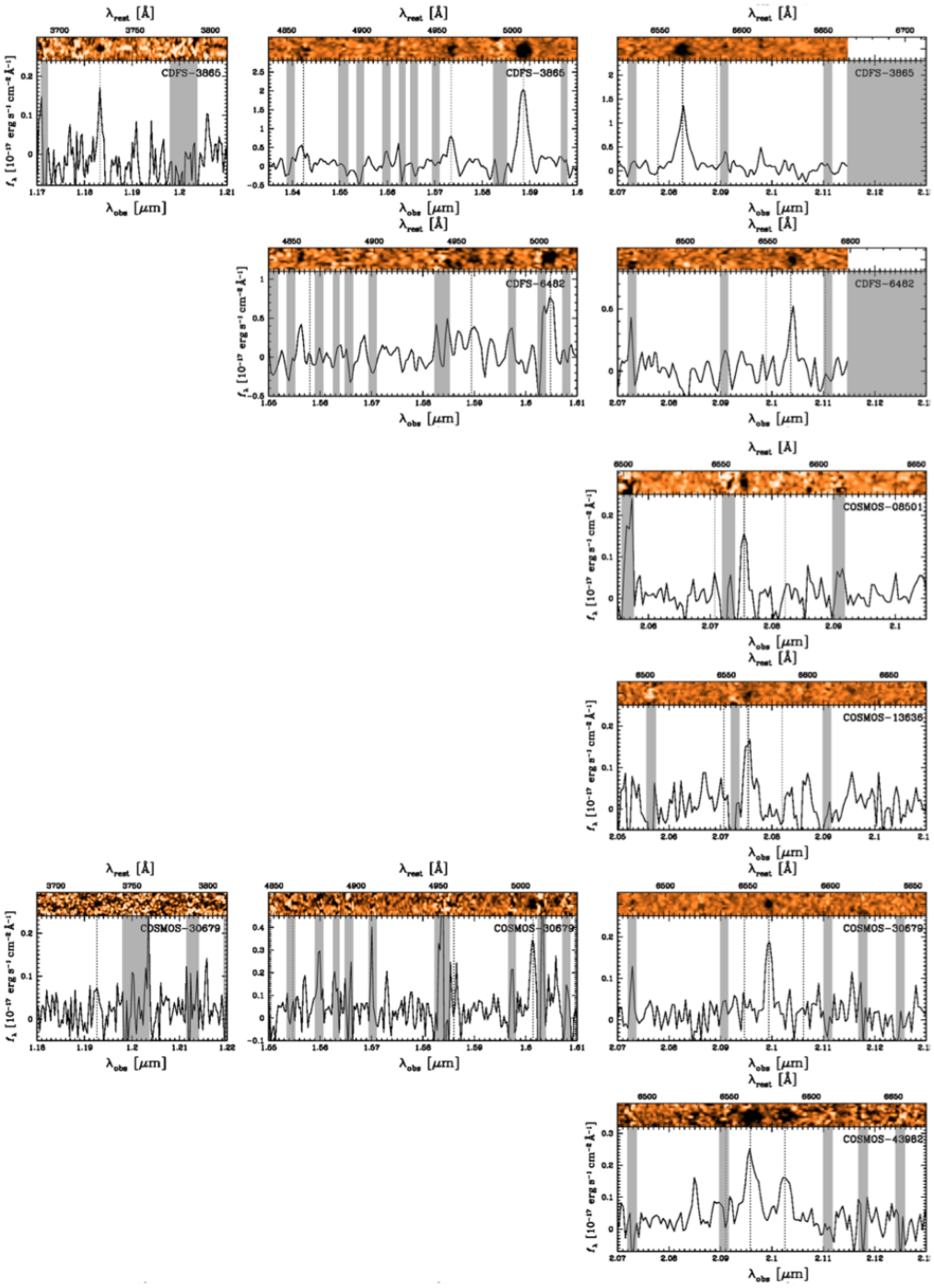

Figure 2.1. From left to right, J, H, and K band spectra of the LAEs. In each panel, the 2D and 1D spectra taken by MMIRS and NIRSPEC are shown. The Figure is quoted from Hashimoto *et al.* (2013) and Nakajima *et al.* (2013) and edited by T. Hashimoto.

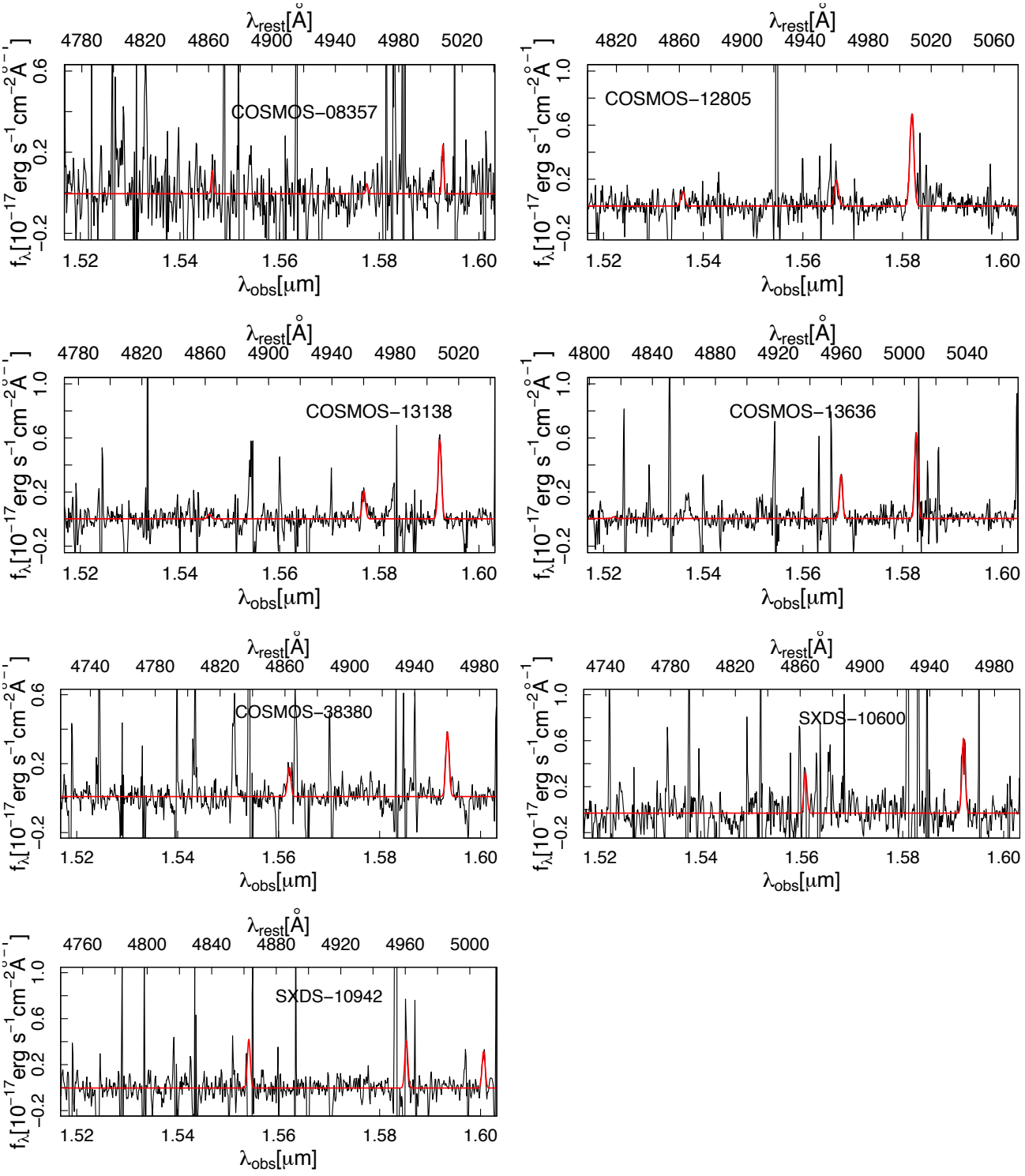

Figure 2.2. Reduced 1D spectra taken by FMOS. The red curve presents the best fit triplet Gaussian.

lutions for our observations were $R \sim 4100$ and ~ 1100 for MagE and LRIS, respectively. The slit was centered on the centroid of the NB387 image, i.e., the centroid of the Lyα light profile.

2.2.1 MagE Spectroscopy and Reduction

The MagE observations were carried out for the two CDFS objects and the four COSMOS objects, CDFS-3865, CDFS-6482, COSMOS-08501, COSMOS-13636, COSMOS-30679, and COSMOS-43982, during several observing runs between 2010 November and 2014 January. The slit width was $1.''0$ for the runs, corresponding to $R \sim 4100$. Spectroscopic standard stars, dome flats, and Xenon flash lamp flats, were obtained on each night for calibrations. On these nights, the typical seeing size was $1.''0$.

The spectra were reduced with `IDL` based pipeline, `MagE_REDUCE`, constructed by G. Becker (see also Kelson 2003). This pipeline processes the raw frames, performing the wavelength calibration, optimal sky subtraction, and extracts their 1D spectrum. Each of these reduced frames was then combined to form our final calibrated spectrum. We inspect one order of the echelle spectra ranging from 3520 Å to 4100 Å in the observed frame, which covers a Lyα line. From this, a Lyα line was identified above the 3 σ noise of the local continuum.

The calibrated 1D spectra are shown in Figure 2.3, where $y-$ axis is the relative flux. This is due to the fact that echelle spectra are notorious for flux-calibration.

2.2.2 LRIS Spectroscopy and Reduction

The four COSMOS objects and two SXDS objects, COSMOS-08357, COSMOS-12085, COSMOS-13138, COSMOS-38380, SXDS-10600, and SXDS-10942, were observed with LRIS on the Keck I telescope on 2012 March 19 – 21 and November 14 – 15. Details of the observation and data reduction procedures are presented in Shibuya *et al.* (2014a). Briefly, the objects were observed with the 600/500 gratings, whose spectral coverage and spectral resolution are 3300Å – 5880Å and $R \sim 1000$, respectively. The seeing size was $0.''7$ – $1.''6$.

We identified a Lyα line in all of the objects. In addition, we detected several metal absorption lines (e.g., Si II λ1260 and C IV λ1548 lines) in individual LRIS spectra of COSMOS-12805, COSMOS-13636, and SXDS-10600 (Shibuya *et al.* 2014a).

The flux-calibrated 1D spectra of the sample are shown in Figure 2.4. In each panel, a

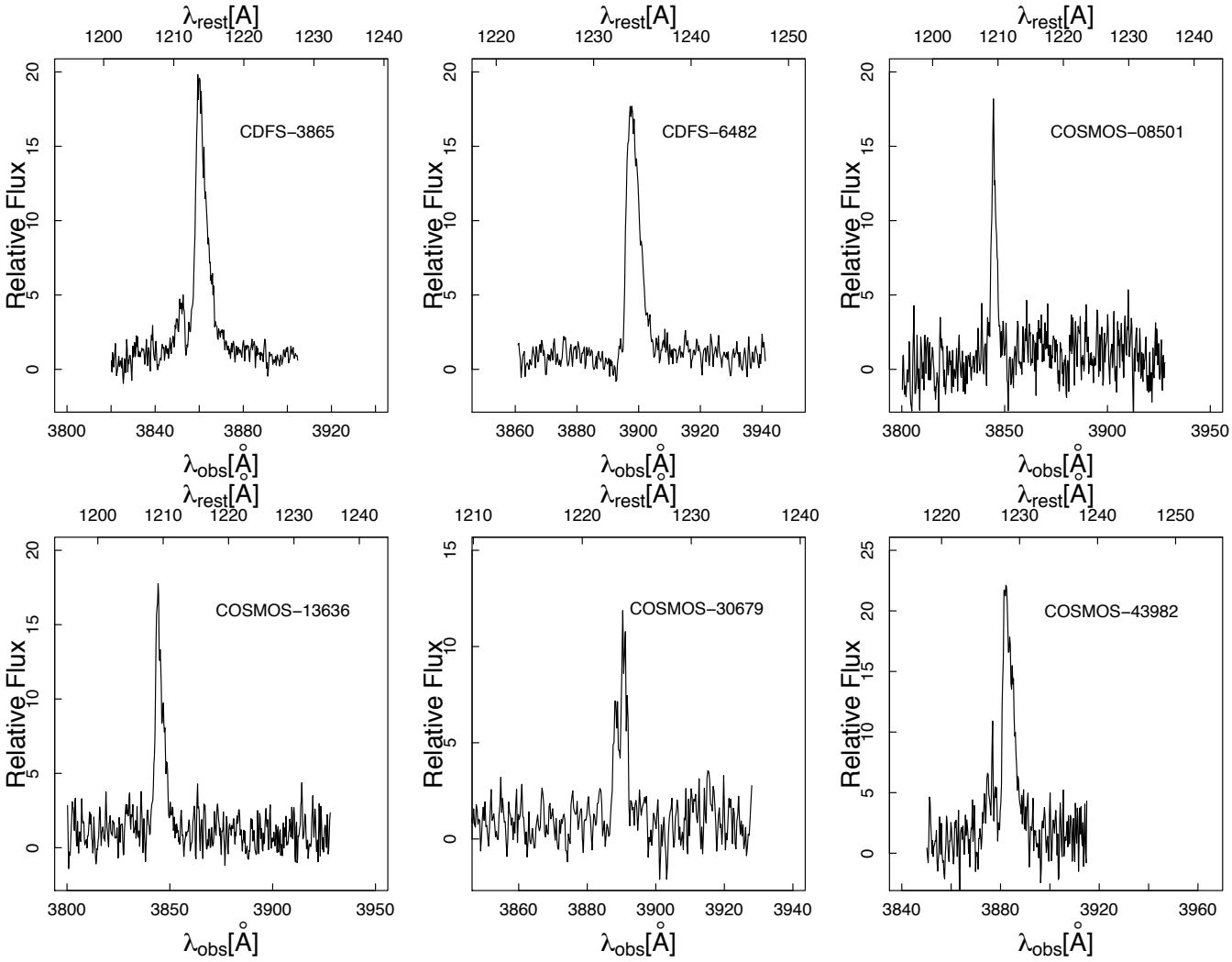

Figure 2.3. Reduced 1D spectra taken by MagE.

Lyα line is denoted by the red dotted line.

A summary of our observations is listed in Table 2.1.

2.3 The Presence of AGNs in the Sample

The presence of AGNs in the MagE objects has been examined in Hashimoto *et al.* (2013) and Nakajima *et al.* (2013), and those of the LRIS objects in Shibuya *et al.* (2014a).

In short, for the MagE objects, we inspected it in three ways. We first compared the sky coordinates of the objects with those in very deep archival X-ray and radio catalogs. Then we checked for the presence of high ionization state lines such as CIV λ 1549 and He II λ1640 lines in the spectra. Finally, we applied the BPT diagnostic diagram (Baldwin *et al.* 1981) to the objects. An AGN activity is not seen in the objects except for COSMOS-

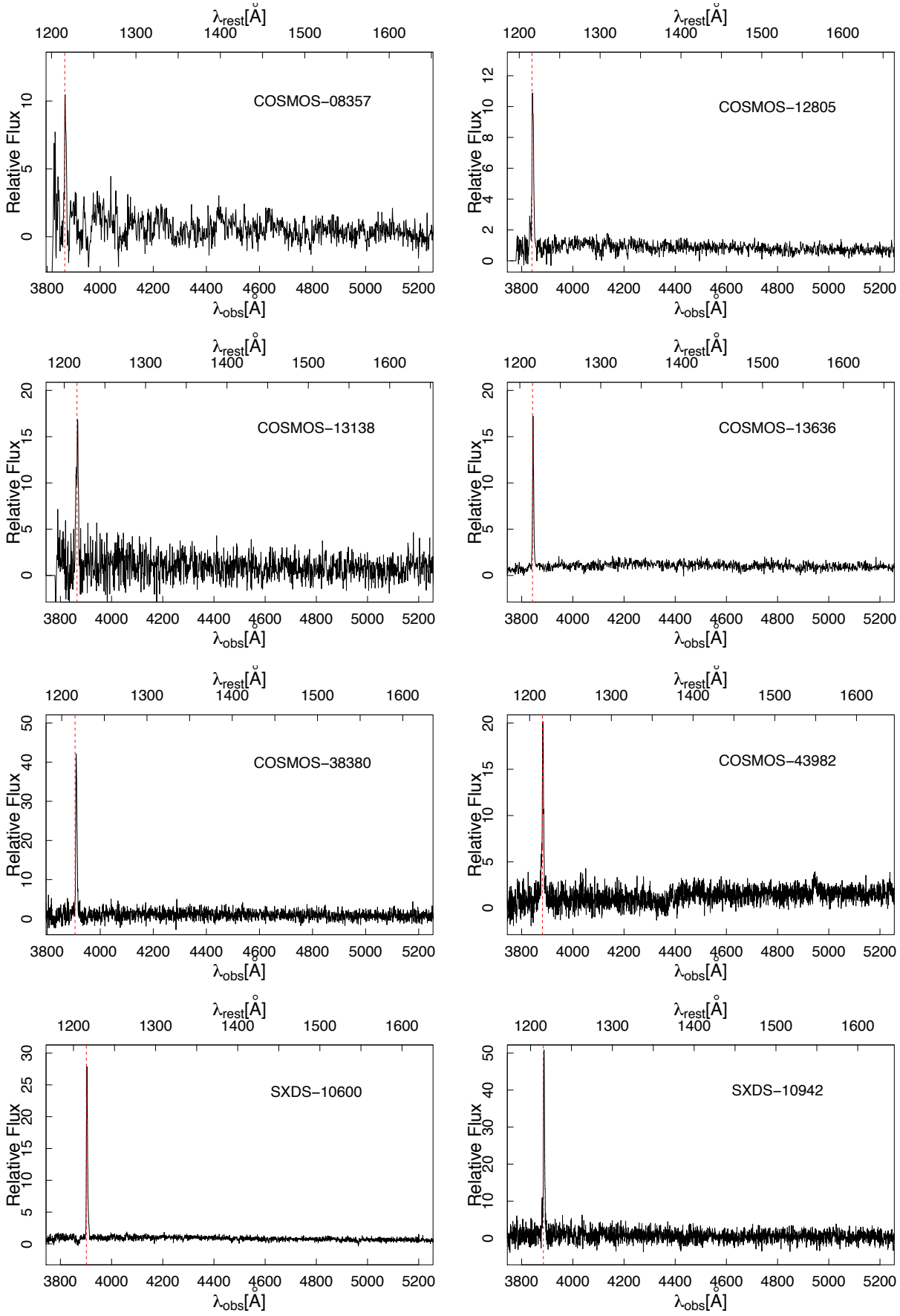

Figure 2.4. Reduced 1D spectra taken by LRIS. The red dotted line corresponds to the Lyα wavelength.

43982 whose high [NII] /Hα line ratio is consistent with that of an AGN.

On the other hand, due to a lack of Hα or [NII] λ6568 data, we were only able to use the two forms of investigation for the LRIS objects. Of these, only COSMOS-43982 showed clear detection of a CIV λ 1549 line in its optical spectrum.

In summary, we have ruled out AGN activity in all sample's objects, except for COSMOS-43982.

Table 2.1. Summary of our observations

Object	α(J2000)	δ(J2000)	EW(Lyα)$_{\rm photo}$ (Å)	$L(Ly\alpha)$ (10^{42} erg s^{-1})	NIR obs.	opt. obs.	Source[a] (1)
(2)	(3)	(4)	(5)	(6)	(7)	(8)	
CDFS-3865	03:32:32.31	-28:00:52.20	64 ± 29	29.8 ± 4.9	NIRSPEC (J) MMIRS (HK)	MagE	H13, N13
CDFS-6482	03:32:49.34	-27:59:52.35	76 ± 52	15.4 ± 8.1	MMIRS (HK)	MagE	H13, N13
COSMOS-08501	10:01:16.80	+02:05:36.26	280 ± 30	8.8 ± 1.1	NIRESPC (K)	MagE	N13
COSMOS-30679	10:00:29.81	+02:18:49.00	87 ± 7	8.5 ± 0.7	NIRSPEC (H and K)	MagE	H13, N13
COSMOS-13636	09:59:59.38	+02:08:38.36	73 ± 5	11.3 ± 0.5	FMOS (H) NIRSPEC (K)	MagE and LRIS	H13, N13, S14
COSMOS-43982[b]	09:59:54.39	+02:26:29.96	130 ± 12	11.0 ± 0.5	MMIRS (HK)	MagE and LRIS	H13, N13, S14
COSMOS-08357	09:59:59.07	+02:05:31.60	47 ± 8	0.5 ± 0.1	FMOS (H)	LRIS	S14, N14b
COSMOS-12805	10:00:15.29	+02:08:07.50	34 ± 6	2.6 ± 0.3	FMOS (H)	LRIS	S14, N14b
COSMOS-13138	10:00:02.61	+02:08:24.50	40 ± 10	0.4 ± 0.1	FMOS (H)	LRIS	S14, N14b
COSMOS-38380	09:59:40.94	+02:23:04.20	137 ± 15	2.6 ± 0.3	FMOS (H)	LRIS	S14, N14b
SXDS-10600	02:17:46.09	-06:57:05.00	58 ± 3	1.9 ± 0.1	FMOS (H)	LRIS	S14, N14b
SXDS-10942	02:17:59.54	-06:57:25.60	135 ± 10	0.3 ± 0.0	FMOS (H)	LRIS	S14, N14b

Notes.— (1) Object ID; (2)(3) Right ascension and Declination; (4)(5) rest-frame Lyα EW and luminosity derived from narrow- and broadband photometry; (6) Instruments and filters used for the NIR observations; (7) Instruments used for the optical observations; and (8) source of the information

a – H13: Hashimoto *et al.* (2013); N13: Nakajima *et al.* (2013); S14: Shibuya *et al.* (2014a); N14b: Nakajima et al (2014, in preparation) b – AGN-like object

Chapter 3

Observational Results

3.1 Spectroscopic Properties

3.1.1 Line Centroid and FWHM Measurements for Nebular Emission Lines

Line centroid (i.e., redshift) and FWHM measurements of nebular emission lines are crucial for a detailed modeling of the Lyα line, since they encode information on the intrinsic (i.e., before being affected by radiative transfer) Lyα redshift and FWHM. In order to obtain these parameters and their uncertainties, we apply a Monte Carlo technique as follows. First, for each object and for each line, we measure the 1σ noise of the local continuum. Then we create 10^3 fake spectra by perturbing the flux at each wavelength of the true spectrum by the measured 1σ error (Kulas *et al.* 2012; Chonis *et al.* 2013). For each fake spectrum, the wavelength at the highest flux peak is adopted as the line centroid, and the wavelength range encompassing half the maximum flux is adopted as the FWHM. The standard deviation of the distribution of measurements from the 10^3 artificial spectra is adopted as the error on the line centroid and FWHM. When multiple lines are detected, we adopt a weighted mean value of them. A summary of the measurements are listed in columns 2 and 3 of Table 3.1. All redshift (FWHM) values are corrected for the LSR motion (instrumental resolution). When the line is unresolved, the instrumental resolution is given as an upper limit. The mean FWHM value for the sample of 8 objects with a measurable velocity dispersion is FWHM(neb) $= 129 \pm 55$ km^{-1}, which is smaller than that of LBGs, FWHM(neb) $= 200 - 250$ km^{-1} (Pettini *et al.* 2001; Erb *et al.* 2006a; Kulas *et al.* 2012). This is consistent with the recent results of Erb *et al.* (2014), who have found that the median FWHM(neb) in 36 $z \sim 2$ LAEs is 127 km s^{-1}. These results indicate that LAEs have smaller dynamical mass than those of LBGs.

Table 3.1. Summary of the spectroscopic properties of the sample

Object	$z_{\rm sys}$	FWHM(neb) (km s^{-1})	Blue Bump	$S_{\rm w}$	$\Delta v_{{\rm Ly}\alpha,{\rm r}}$ (km s^{-1})	$\Delta v_{{\rm Ly}\alpha,{\rm b}}$ (km s^{-1})	$\Delta v_{\rm peak}$ (km s^{-1})	$\Delta v_{\rm abs}$ (km s^{-1})
(1)	(2)	(3)	(4)	(5)	(6)	(7)	(8)	(9)
CDFS-3865	2.17242 ± 0.00016	242 ± 31	yes	8.8 ± 0.3	245 ± 36	-352 ± 59	597 ± 67	(-102 ± 65)
CDFS-6482	2.20490 ± 0.00042	99^{+66}_{-99}	no	6.6 ± 1.7	118 ± 48	-	-	(-102 ± 65)
COSMOS-08501	2.16161 ± 0.00042	< 200	no	2.2 ± 2.7	82 ± 40	-	-	
COSMOS-30679	2.19725 ± 0.00020	92 ± 45	no	3.1 ± 1.0	290 ± 33	-	-	(-102 ± 65)
COSMOS-13636 (MagE)	2.16075 ± 0.00019	73 ± 5	no	5.3 ± 1.0	146 ± 25	-	-	(-102 ± 65)
COSMOS-13636 (LRIS)	2.16075 ± 0.00019	73 ± 5	no	6.2 ± 0.5	161 ± 18	-	-	-130±70
COSMOS-43982 (MagE)	2.19267 ± 0.00036	325 ± 36	yes	7.9 ± 1.3	117 ± 53	-297 ± 57	414 ± 78	-
COSMOS-43982 (LRIS)	2.19267 ± 0.00036	325 ± 36	yes	-4.2 ± 0.6	155 ± 40	-165 ± 90	320 ± 98	-
COSMOS-08357	2.18053 ± 0.00031	< 136	no	-4.2 ± 7.9	106 ± 71	-	-	-
COSMOS-12805	2.15887 ± 0.00024	110 ± 16	yes	8.9 ± 0.7	171 ± 25	-605 ± 114	776 ± 117	-170 ± 50
COSMOS-13138	2.17914 ± 0.00012	63 ± 6	yes	-1.6 ± 4.8	191 ± 59	-214 ± 87	405 ± 105	-
COSMOS-38380	2.21245 ± 0.00015	99 ± 9	no	2.5 ± 0.8	338 ± 21	-	-	-
SXDS-10600	2.20922 ± 0.00014	55 ± 28	no	11.7 ± 0.2	186 ± 13	-	-	-260 ± 60
SXDS-10942	2.19574 ± 0.00025	< 136	yes	1.3 ± 0.3	135 ± 10	-374 ± 41	556 ± 66	-

Notes.— The symbol "-" indicates we have no measurement. (1) Object ID; (2) Systemic redshift derived from the weighted mean of the nebular emission redshifts; (3) Weighted mean FWHM of nebular emission line; (4) Presence of the blue bump emission in the Lyα profile; (5) Weighted skewness of the Lyα line (Kashikawa *et al.* 2006); (6) Velocity offset of the Lyα main red peak with respect to the $z_{\rm sys}$; (7) Velocity offset of the Lyα blue-bump with respect to the $z_{\rm sys}$; (8) Peaks separation between $\Delta v_{{\rm Ly}\alpha,{\rm r}}$ and $\Delta v_{{\rm Ly}\alpha,{\rm b}}$; and (9) Mean velocity offset of LIS absorption lines with respect to the $z_{\rm sys}$ (Hashimoto *et al.* 2013; Shibuya *et al.* 2014a).

3.1.2 Lyα Profiles

While the majority of Lyα profiles are single-peaked (e.g., Shapley *et al.* 2003; Steidel *et al.* 2010), a fraction of Lyα profiles are known to be multiple-peaked (e.g., Yamada *et al.* 2012; Kulas *et al.* 2012). In particular, a secondary small peak blueward of the systemic redshift is called a "blue bump" (see the case 2 profile in Figure 12 in Verhamme *et al.* 2006). Theoretical studies have shown that the blue bump is a natural outcome of the radiative transfer in a low speed galactic outflow (e.g., Zheng & Miralda-Escudé 2002).

We determine a blue emission to be detected in our spectra if there exists an excess

emission blueward of the systemic redshift above 3σ noise of the local continuum. We detect blue emission in five objects and in six spectra; MagE ones of CDFS-3865 and COSMOS-43982, and LRIS ones of COSMOS-12805, COSMOS-13138, COSMOS-43982, and SXDS-10942. From the fact that these spectra show a main red peak with a secondary blue peak, we conclude that these spectra have a blue bump. The position of the blue bump is designated by a blue arrow in Figures 3.1 and 3.2, where both Lyα and nebular lines are converted into the velocity space. The velocity zero point in these figures is determined by the systemic redshift. The result is summarized in the column 4 of Table 3.1.

The frequency of blue bump objects in the sample is $\sim 40\%$ (5/12). There are four LAEs in the literature that have a blue bump: one among the two LAEs studied in McLinden *et al.* (2011) and all three LAEs studied in Chonis *et al.* (2013). For a total sample of 17 LAEs, the frequency is calculated to be $\sim 50\%$ (9/17). Note that this is a lower limit due to the limited spectral resolution. On the other hand, Kulas *et al.* (2012) have studied 18 $z \sim 2-3$ LBGs with $z_{\rm sys}$ measurements which are preselected to have a multiple-peaked Lyα profile. They have argued that $\sim 30\%$ of the parent sample are multiple-peaked and that 11 out of the 18 objects have a blue bump, indicating that the blue bump frequency in LBGs is $\sim 20\%$ ($\sim 30\% \times 11/18$). These results imply that the blue bump feature is slightly more common in LAEs than in LBGs. However, a larger sample, observed at a higher spectral resolution, is needed for a definite conclusion.

Observed Lyα lines usually have an asymmetric profile with a red tail and a sharp blue cut off. Some studies at high-z utilize the asymmetry of the Lyα line to distinguish it from interloper lines of foreground galaxies. Thanks to the simultaneous detection of Lyα and nebular emission lines, it is no doubt that our detected lines are Lyα lines. Still, it is useful to quantify the asymmetry of the Lyα line of our objects. We use the weighted skewness, S_w (Kashikawa *et al.*, 2006). Skewness is the third moment of the flux distribution, and the weighted skewness is defined as the product of the skewness and the line width. A positive S_w means that the Lyα profile has a red tail. The measured $S_{\rm w}$ values for the sample are listed in the column 5 of Table 3.1. While most spectra have a positive $S_{\rm w}$ value beyond the 1 σ uncertainty, four spectra, MagE-COSMOS-08501, LRIS-COSMOS-08357, LRIS-COSMOS-43982, and LRIS-COSMOS-13138, have $S_{\rm w} \sim 0$ within the 1 σ uncertainty. Taking a closer look at these spectra, the negative $S_{\rm w}$ of LRIS-COSMOS-43982 is due to its merged blue bump.

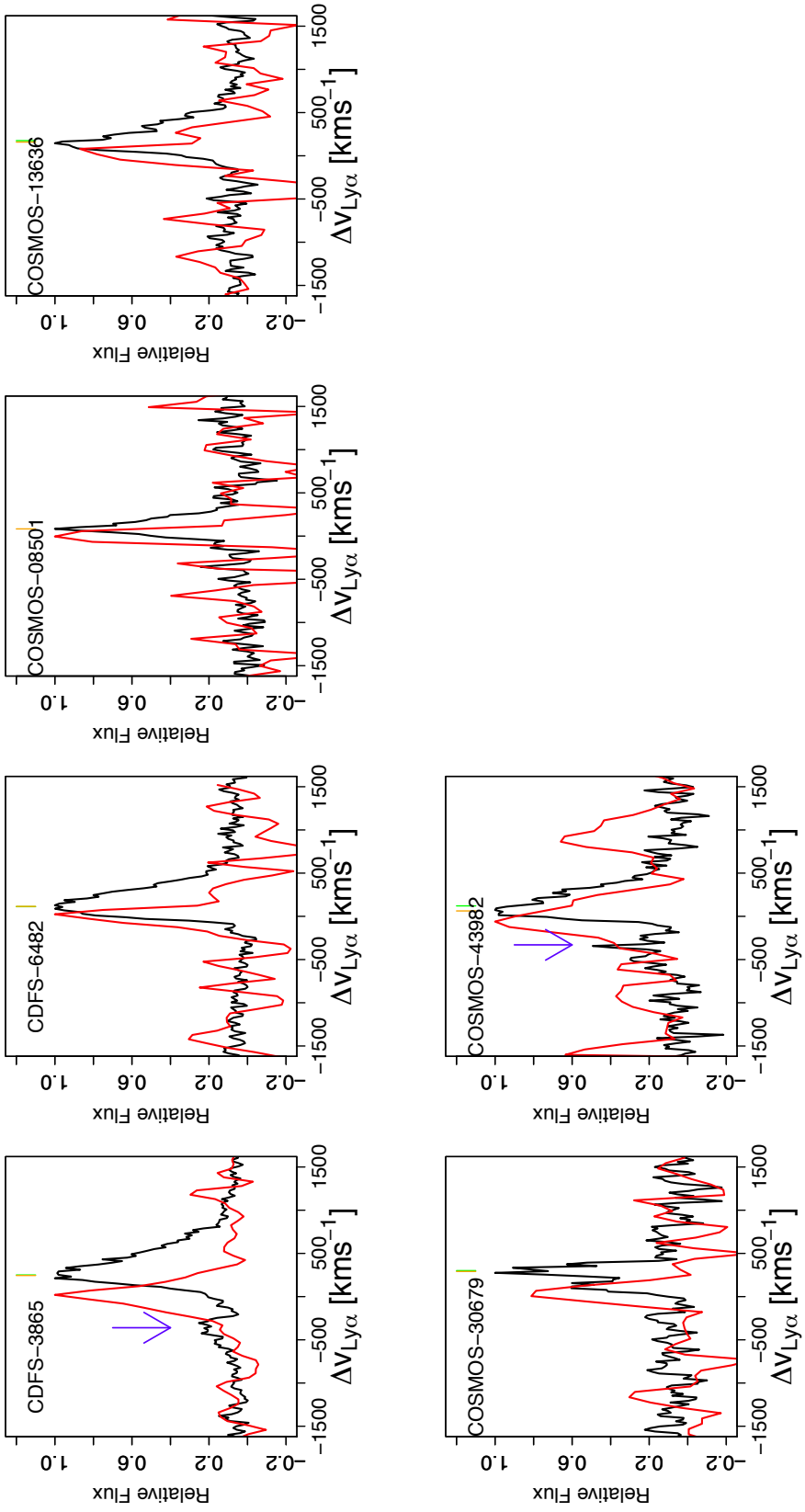

Figure 3.1. Lyα lines obtained by MagE (black) and Hα lines obtained by MMIRS or NIRSPEC (red), All spectra are scaled in the wavelength range from -1500 to $+1500$ km s^{-1}. Green and orange segments indicate the peak flux positions derived from a Gaussian and a Monte Carlo techniques, respectively.

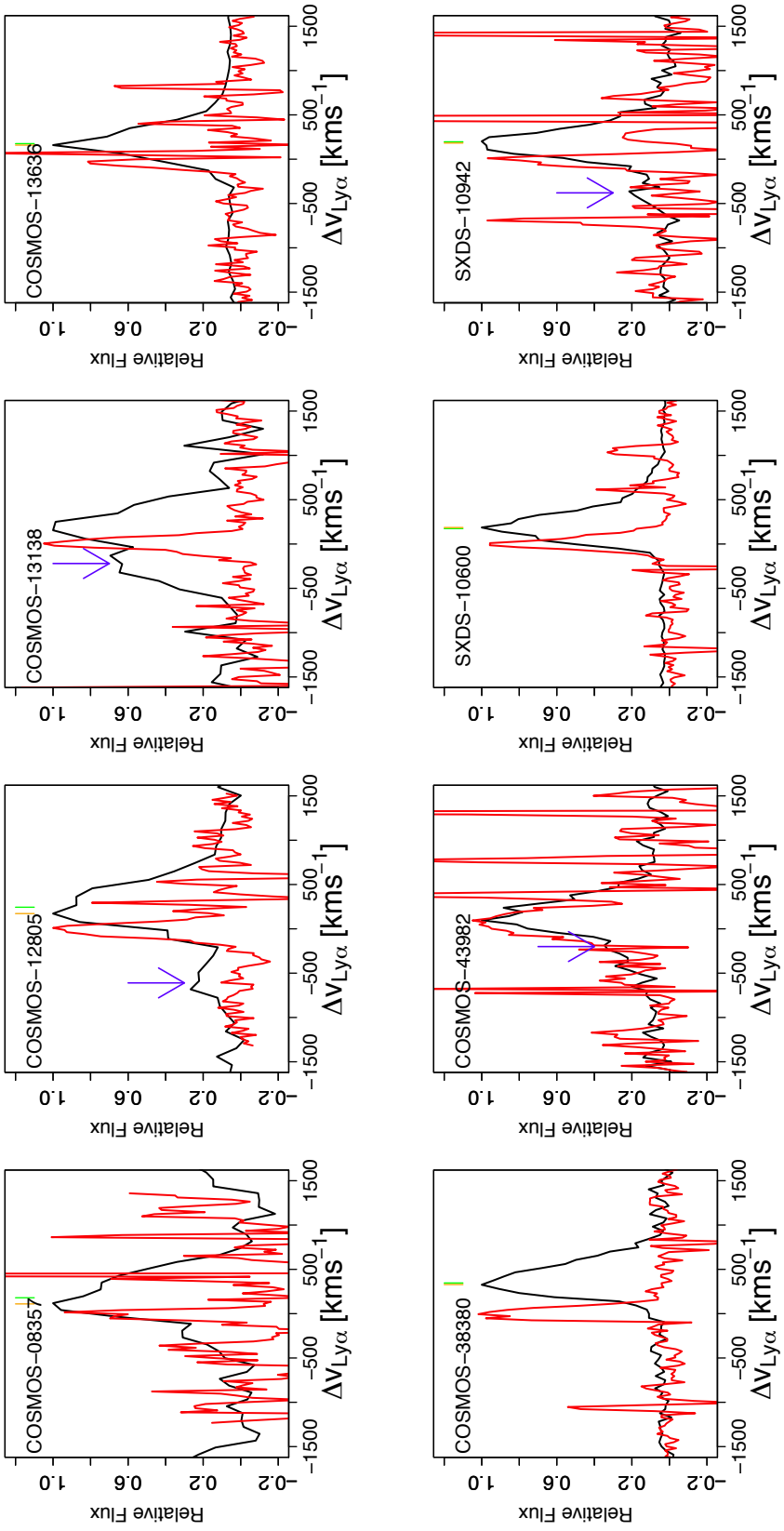

Figure 3.2. Lyα lines obtained by LRIS (black) and [OIII] lines by FMOS (red), All spectra are scaled in the wavelength range from -1500 to $+1500$ km s^{-1}. The meanings of the two segments are the same as those in Figure 3.1.2.

3.1.3 Lyα Velocity Properties

We derive three velocity offsets related to the Lyα line: the velocity offset of the main red peak of the Lyα line with respect to the systemic,

$$\Delta v_{\mathrm{Ly}\alpha,\mathrm{r}} = c\frac{z_{\mathrm{Ly}\alpha,\mathrm{r}} - z_{\mathrm{sys}}}{1+z_{\mathrm{sys}}}, \tag{3.1}$$

; that of the blue bump of a Lyα line with respect to the systemic, if any,

$$\Delta v_{\mathrm{Ly}\alpha,\mathrm{b}} = c\frac{z_{\mathrm{Ly}\alpha,\mathrm{b}} - z_{\mathrm{sys}}}{1+z_{\mathrm{sys}}}, \tag{3.2}$$

; and that of the two peaks,

$$\Delta v_{\mathrm{peak}} = \Delta v_{\mathrm{Ly}\alpha,\mathrm{r}} - \Delta v_{\mathrm{Ly}\alpha,\mathrm{b}}, \tag{3.3}$$

where z_{sys}, $z_{\mathrm{Ly}\alpha,\mathrm{r}}$, and $z_{\mathrm{Ly}\alpha,\mathrm{b}}$ represent the systemic redshift, the Lyα redshift of the main red peak, and that of the blue bump, respectively.

Lyα Main Red Peak Velocity Offsets, $\Delta v_{\mathrm{Ly}\alpha,\mathrm{r}}$

We estimate the $\Delta v_{\mathrm{Ly}\alpha,\mathrm{r}}$ value using a Monte Carlo technique in a similar manner to that in §3.1.1. First, for each object, we measure a 1σ error of the Lyα spectrum set by the continuum level at the wavelength longer than 1216Å. Then we create 10^3 fake spectra converted into the velocity space by simultaneously perturbing the flux at each wavelength and the systemic redshift listed in Table 3.1 by their 1σ errors. Finally, we measure the velocity at the highest flux peak. The mean and the standard deviation value of the distribution of 10^3 measurements is adopted as the $\Delta v_{\mathrm{Ly}\alpha,\mathrm{r}}$ and its error, respectively. The derived $\Delta v_{\mathrm{Ly}\alpha,\mathrm{r}}$ values are listed in the column 6 of Table 3.1, ranging from 82 km s^{-1} to 338 km s^{-1} with a mean value of 174 ± 19 km s^{-1}. In most cases, these values are consistent with those measured in Hashimoto *et al.* (2013) and Shibuya *et al.* (2014a) within 1σ, however, they are not for COSMOS-08357 and COSMOS-12805. This is due to the fact that these studies have applied a symmetric/asymmetric profile fit to the Lyα line. In Figures 3.1 and 3.2, we show the two $\Delta v_{\mathrm{Ly}\alpha,\mathrm{r}}$ values derived from the Monte Carlo and the profile fit technique as the green and orange line segments, respectively. For the sake of consistency in the definition of the $\Delta v_{\mathrm{Ly}\alpha,\mathrm{r}}$ in the shell model (Verhamme *et al.* 2006; Schaerer *et al.* 2011), we adopt these new measurements. We note that our discussions remain unchanged even if we adopt previous $\Delta v_{\mathrm{Ly}\alpha,\mathrm{r}}$ values.

The $\Delta v_{\mathrm{Ly}\alpha,\mathrm{r}}$ value has been measured in more than 60 LAEs (McLinden *et al.* 2011; Finkelstein *et al.* 2011; Hashimoto *et al.* 2013; Guaita *et al.* 2013; Chonis *et al.* 2013;

Shibuya *et al.* 2014a; Song *et al.* 2014; Erb *et al.* 2014). These studies have shown that LAEs at $z \sim 2-3$ have a mean $\Delta v_{\mathrm{Ly}\alpha,\mathrm{r}}$ of $\simeq 200$ km s^{-1}, which is significantly smaller than that of LBGs at a similar redshift, $\Delta v_{\mathrm{Ly}\alpha,\mathrm{r}} \simeq 400$ km s^{-1} (e.g., Steidel *et al.* 2010; Rakic *et al.* 2011; Kulas *et al.* 2012). The top panel of Figure 3.3 represents the histogram of $\Delta v_{\mathrm{Ly}\alpha,\mathrm{r}}$ for the 12 LAEs (14 spectra) studied in this study and 18 LBGs given by Kulas *et al.* (2012). We carry out the Kolmogorov-Smirnov (K-S) test for the two populations. The resultant probability is 10^{-6}, indicating that $\Delta v_{\mathrm{Ly}\alpha,\mathrm{r}}$ is definitively different between LAEs and LBGs.

This implies that objects with a high EW(Lyα) tend to have a small $\Delta v_{\mathrm{Ly}\alpha,\mathrm{r}}$ (Hashimoto-relation). Figure 3.4, quoted from Hashimoto *et al.* (2013), and the right panel of Figure 10 in Shibuya *et al.* (2014a) clearly demonstrate this trend. Figure 10 in Shibuya *et al.* (2014a) includes all the objects presented here except COSMOS-08501. This new object with an extremely large EW(Lyα) of $\sim 280 \pm 30$ Å has the smallest $\Delta v_{\mathrm{Ly}\alpha,\mathrm{r}}$ of 82 ± 40 km s^{-1}. Thus, this object is also consistent with the Hahsimoto-relation.

Lyα Blue Bump Velocity Offsets, $\Delta v_{\mathrm{Ly}\alpha,\mathrm{b}}$

For each detected blue bump in §3.1.2, we estimate the $\Delta v_{\mathrm{Ly}\alpha,\mathrm{b}}$ value in the same manner as that for the $\Delta v_{\mathrm{Ly}\alpha,\mathrm{r}}$. We obtain $\Delta v_{\mathrm{Ly}\alpha,\mathrm{b}} = -352 \pm 59$ km s^{-1} (CDFS-3865), -297 ± 57 km s^{-1} (MagE-COSMOS-43982), -605 ± 114 km s^{-1} (COSMOS-12805), -214 ± 87 km s^{-1} (COSMOS-13138), -165 ± 90 km s^{-1} (LRIS-COSMOS-43982), and -374 ± 41 km s^{-1} (SXDS-10942). The result is listed in the column 7 of Table 3.1. We combine our $\Delta v_{\mathrm{Ly}\alpha,\mathrm{b}}$ measurements with those in the four aforementioned LAEs with the blue bump, and construct a large sample of LAEs with the blue bump consisting of 9 objects (10 spectra): one from McLinden *et al.* (2011) with $\Delta v_{\mathrm{Ly}\alpha,\mathrm{b}} = -454$ km s^{-1} and three from Chonis *et al.* (2013) with $\Delta v_{\mathrm{Ly}\alpha,\mathrm{b}} = -127, -250$, and -236 km s^{-1}. The mean value of $\Delta v_{\mathrm{Ly}\alpha,\mathrm{b}}$ in the large sample is $\Delta v_{\mathrm{Ly}\alpha,\mathrm{b}} = -316 \pm 45$ km s^{-1}, which is consistent with that in the 11 LBGs with the blue bump, $\Delta v_{\mathrm{Ly}\alpha,\mathrm{b}} = -367 \pm 46$ km s^{-1} (Kulas *et al.* 2012). We calculate the K-S probability, to be 0.3901, indicating that LAEs have $\Delta v_{\mathrm{Ly}\alpha,\mathrm{b}}$ values comparable to those in LBGs. The middle panel of Figure 3.3 shows the trend.

We check if our result remains unchanged even if we take the spectral resolution effect into account. The sample in Kulas *et al.* (2012) has been observed with three settings; 300-line grating, 400-, and 600-line grisms, corresponding to the spectral resolution of $R \sim 600, 800$, and 1300, respectively. We compare the mean $\Delta v_{\mathrm{Ly}\alpha,\mathrm{b}}$ value of our four

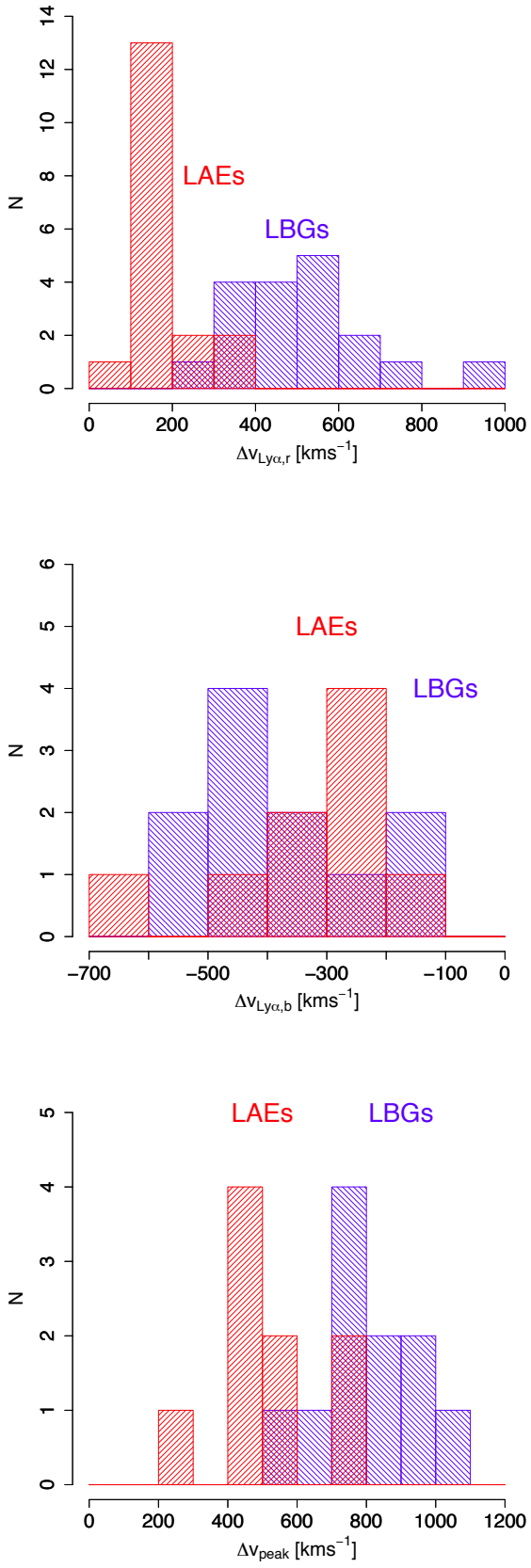

Figure 3.3. Histograms of $\Delta v_{\mathrm{Ly}\alpha,\mathrm{r}}$ (top panel), $\Delta v_{\mathrm{Ly}\alpha,\mathrm{b}}$ (middle), and Δv_{peak} (lower) for the LAEs studied in this paper and the literature (McLinden *et al.* 2011; Chonis *et al.* 2013) and LBGs given by Kulas *et al.* (2012).

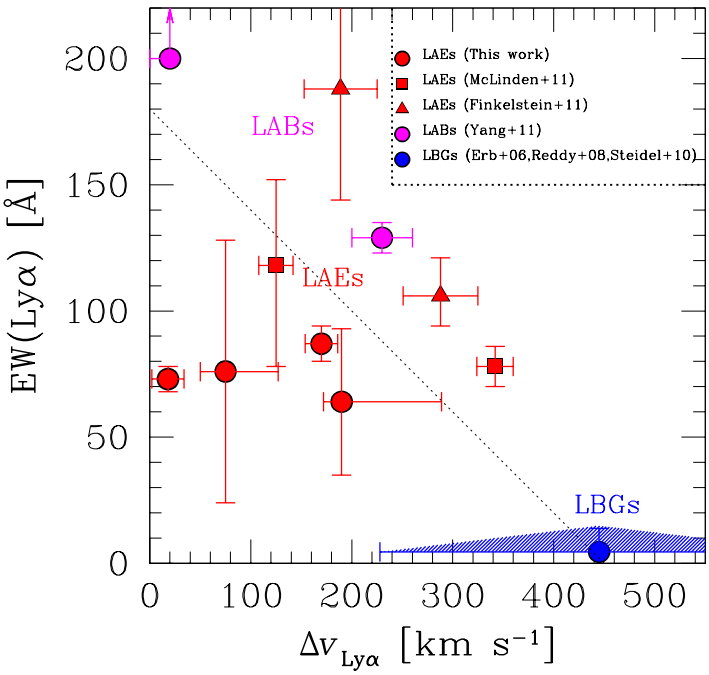

Figure 3.4. The figure is quoted from Hashimoto *et al.* (2013) (see also the right panel of Figure 10 in Shibuya *et al.* 2014a). Rest-frame EW(Lyα) plotted against $\Delta v_{\mathrm{Ly}\alpha,\mathrm{r}}$. The red circles are our LAEs. The red square and the red triangle show the LAEs by McLinden *et al.* (2011) and Finkelstein *et al.* (2011), respectively. The blue symbol indicates the average of 41 LBGs, with the error bars corresponding to the 68 percentiles of the $\Delta v_{\mathrm{Ly}\alpha}$ distribution (Steidel *et al.*, 2010) and the EW distribution (Reddy *et al.*, 2008). The magenta circles denote the LABs by Yang *et al.* (2011). The dotted line is the best-fit linear function to all the data points.

LAEs taken by LRIS ($R \sim 1100$) and that of six LBGs with the blue bump obtained at a similar resolution ($R \sim 1300$). The resultant mean $\Delta v_{\mathrm{Ly}\alpha,\mathrm{b}}$ values for LAEs and LBGs are -340 ± 99 and -356 ± 70 km s^{-1}, respectively, and the K-S probability is 0.9238. Thus, LAEs and LBGs have equivalent $\Delta v_{\mathrm{Ly}\alpha,\mathrm{b}}$ values even at the similar spectral resolution.

Velocity Offsets Between the Main Red Peak and the Blue Bump, Δv_{peak}

Finally, for each of the spectra that show the blue bump, we measure the peaks velocity offset, Δv_{peak}. We obtain $\Delta v_{\mathrm{peak}} = 597 \pm 67$ km s^{-1} (CDFS-3865), 414 ± 78 km s^{-1} (MagE-

COSMOS-43982), 776 ± 117 km s^{-1} (COSMOS-12805), 405 ± 105 km s^{-1} (COSMOS-13138), 320 ± 98 km s^{-1} (LRIS-COSMOS-43982), and 556 ± 66 km s^{-1} (SXDS-10942). The result is listed in the column 8 in Table 3.1. In order to make a large sample with the measured $\Delta v_{\rm peak}$ value, we utilize again the results in four LAEs with the blue bump from the literature: one LAE studied in McLinden *et al.* (2011) with $\Delta v_{\rm peak} = 796$ km s^{-1} and three LAEs studied in Chonis *et al.* (2013) with $\Delta v_{\rm peak} = 300, 425$, and 415 km s^{-1}. The mean value of the 9 objects (10 spectra) is $\Delta v_{\rm peak} = 500 \pm 56$ km s^{-1}, which is significantly smaller than that of the 11 LBGs with the blue bump, $\Delta v_{\rm peak} = 801 \pm 41$ km s^{-1} (Group I in Kulas *et al.* 2012). The K-S probability is calculated to be 0.00636, indicating that LAEs and LBGs have different $\Delta v_{\rm peak}$ values. The lower panel of 3.3 shows the trend.

We examine the spectral resolution effect exactly the same manner as that in §3.1.3. The mean $\Delta v_{\rm peak}$ value of the four LAEs taken by LRIS ($R \sim 1100$) and that of the six LBGs with the blue bump obtained at the similar spectral resolution ($R \sim 1300$) are $\Delta v_{\rm peak} = 514 \pm 100$ and 778 ± 59 km s^{-1}, respectively. In conjunction with the K-S probability, 0.09524, we conclude that LAEs have a significantly smaller $\Delta v_{\rm peak}$ value than that of LBG even at the same spectral resolution.

In summary, we have derived three Lyα velocity offsets, $\Delta v_{{\rm Ly}\alpha,{\rm r}}$, $\Delta v_{{\rm Ly}\alpha,{\rm b}}$, and $\Delta v_{\rm peak}$. While we need bigger samples with the blue bump for a definite conclusion, we find that LAEs have a smaller (comparable) value of the $\Delta v_{{\rm Ly}\alpha,{\rm r}}$ ($\Delta v_{{\rm Ly}\alpha,{\rm b}}$) than that of LBGs, which makes their $\Delta v_{\rm peak}$ value also smaller than that of LBGs.

3.1.4 LIS Absorption Lines and their Velocity Properties

Low ionization state (LIS) metal absorption lines encode information on cold neutral gas in galaxies. The mean blueshift of LIS absorption lines with respect to the systemic velocity, $\Delta v_{\rm abs}$, traces the average speed of a galactic outflow (e.g., Pettini *et al.* 2001; Shapley *et al.* 2003; Martin 2005).

Stacked Spectrum of the four MagE spectra

We examine LIS absorption lines using Magellan/MagE echellette spectrograph data. We inspect one order of the echelle spectra ranging from 3788 Å to 4419 Å in the observed frame. This wavelength range covers Si II λ1260, O I λ1302, Si II λ1304, and C II λ1335 lines.

Since none of these lines is identified in the individual spectra because of the too faint

continua, we make a composite spectrum of the four objects as follows. For each object, we shift individual spectral data from the observed to the rest frame using $z_{\rm sys}$ given in Table 3.1. Then, we stack the spectra of the four objects with statistical weights based on the S/N ratios at 1250–1340 Å.

Figure 3.5 presents the composite spectrum. An absorption feature is seen near each of the four lines' wavelengths. For each feature, we fit a Gaussian profile to obtain the rest-frame equivalent width, EW(LIS), and the velocity offset of the line center with respect to the systemic velocity, $\Delta v_{\rm abs}$. We securely detect the Si II λ1260 line and the blended O I λ1302 + Si II λ1304 lines at the 5.2 σ and 3.7 σ levels, respectively, and marginally detect the C II λ1335 line at the 2.0σ level. Note that all lines are blue-shifted with respect to the systemic velocity.

The weighted mean offset velocity of these absorption lines is $\Delta v_{\rm abs} = -102 \pm 65$ km s^{-1}, which is listed in the column 9 of Table 3.1. This value is comparable to with or lower than those of LBGs, which are typically $\Delta v_{\rm abs} \sim -150$ km s^{-1} (Shapley *et al.* 2003; Steidel *et al.* 2010). Thus, LAEs and LBGs have similar $\Delta v_{\rm abs}$ values, in contrast to the significant difference in $\Delta v_{{\rm Ly}\alpha,{\rm r}}$ and $\Delta v_{\rm peak}$.

Three Individual Spectra

Shibuya *et al.* (2014a) have detected several LIS absorption lines in four LAEs on the individual basis (see their Figure6). Among the four objects, COSMOS-13636, COSMOS12805, and SXDS-10600 are used in this study. The derived mean blue shifts are $\Delta v_{\rm abs} = -130 \pm 70$ km s^{-1} (COSMOS-13636), -170 ± 50 km s^{-1} (COSMOS-12805), and -260 ± 60 km s^{-1} (SXDS-10600), respectively. These values are also listed in the column 9 of Table 3.1.

3.1.5 Two Component [OIII] Profiles

Among the nebular emission lines we have obtained, while most objects show normal symmetric Gaussian profiles, two objects, COSMOS-13138 and SXDS-10600, show a non-Gaussian [OIII] λ5007 line. As demonstrated in Figure 3.6, the [OIII] λ5007 line of COSMOS-13138 and SXDS-10600 shows an asymmetric profile with a secondary blueshifted and redshifted component, respectively.

Such a profile has been reported in various objects: both local and high-z star-forming galaxies and ULIRGs (e.g., Shapiro *et al.* 2009; Genzel *et al.* 2011; Newman *et al.* 2012; Soto *et al.* 2012), a high-z Oxygen-Two Blob (OII blob) (Harikane *et al.*, 2014), and a

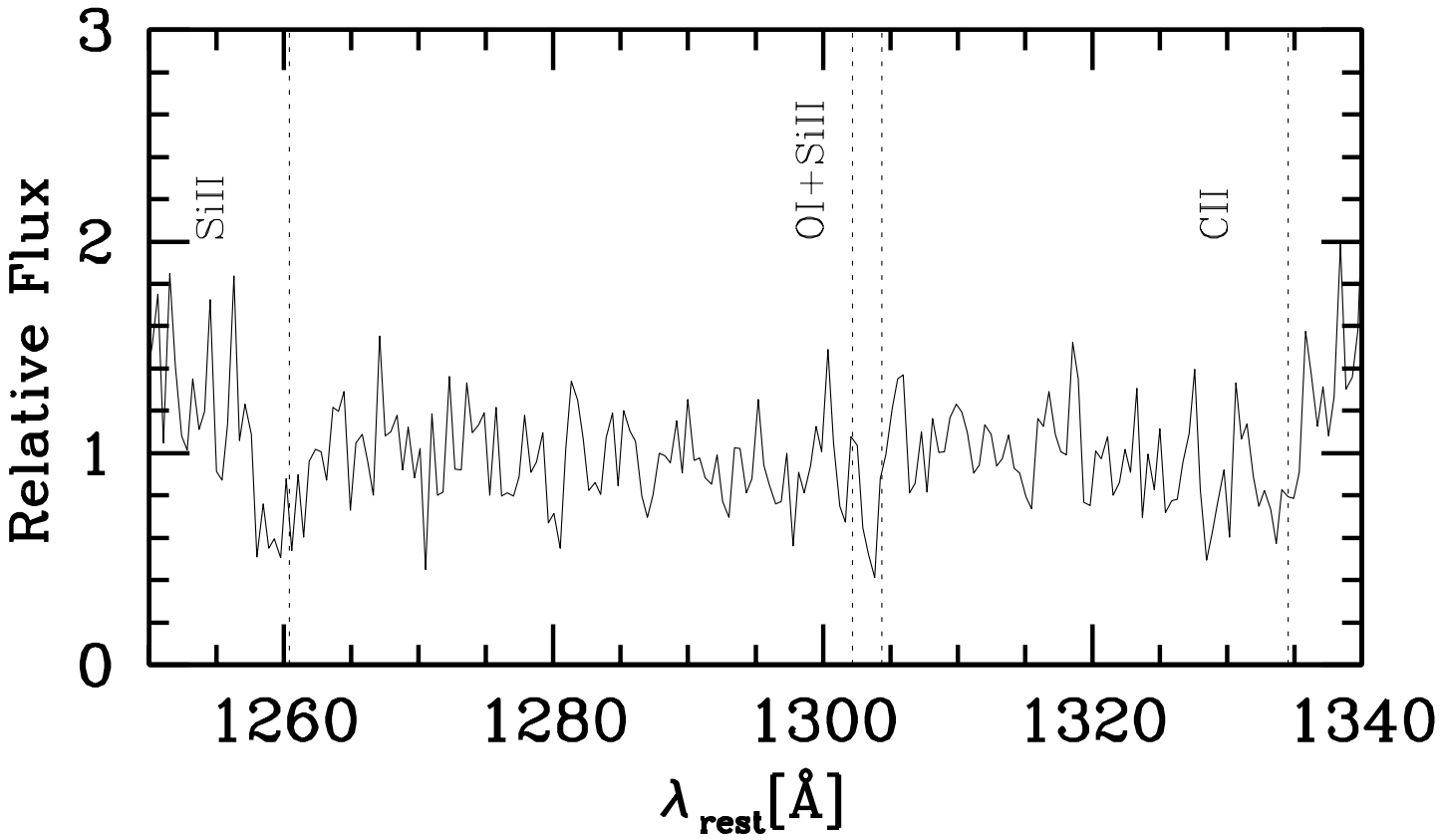

Figure 3.5. Composite FUV spectrum of the four LAEs. The spectrum has been normalized to unity in the continuum. The dotted lines indicate the rest-frame vacuum wavelengths of four LIS absorption lines. The spectrum is plotted with 0.5 Å pix^{-1} sampling so that the profile of the blended O I and Si II lines be clearly shown.

few Lyman-Alpha Blobs (LABs) (Yang *et al.*, 2014). However in LAEs, there has been no study which reports its presence.

Aforementioned studies apply a two Gaussian components fit, a narrow and a broad components fit, to the line. To examine the presence of two components, we also perform the two Gaussian components fit to the lines. We have six parameters: fluxes, line centroids, and FWHMs for the both components. We require that widths of both components are larger than the spectral resolution, and that the broad component has a larger FWHM than that of the narrow component. Best fit parameters are determined through

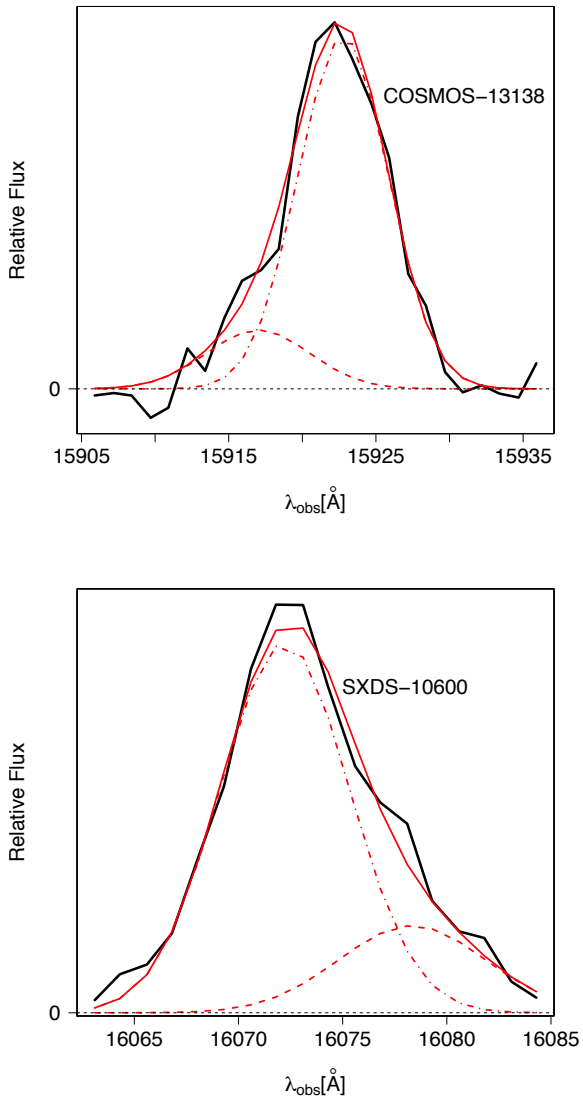

Figure 3.6. [OIII] λ5007 spectrum of COSMOS-13138 (left panel) and SXDS-10600 (right) taken by FMOS. The black solid lines are the observed spectra. There is a broad component in addition to a narrow component. The red solid lines denote the best-fit functions for the whole lines, and the red dashed lines represent those of the individual components.

minimum χ^2 realizations, and the parameter range satisfying $\chi^2 \lesssim \chi^2_{\rm min} + 1$ is adopted as an error, where $\chi^2_{\rm min}$ denotes the minimum χ^2 value. The results are listed in Table 3.2. Since both of the broad and narrow components are detected in $\gtrsim 4\sigma$, we conclude that we have detected two components in the profile.

The velocity offset of the two components are 104 ± 11 km s^{-1} (COSMOS-13138) and

115 ± 8 km s^{-1} (SXDS-10600), respectively.

Derived FWHM values of the broad component after the correction for the instrumental resolution are 70 ± 50 and 80 ± 30 km s^{-1}. These are much smaller than those of the star forming galaxies at $z \sim 2$ (FWHM $= 300 - 1000$ km s^{-1}, Genzel *et al.* 2011), and slightly smaller than those of the OII blob (FWHM $= 120 - 130$ km s^{-1}, Harikane *et al.* 2014) and the LABs (FWHM $= 100 - 280$ km s^{-1}, Yang *et al.* 2014). These small values exclude the possibility of the broad component in LAEs originating from an AGN activity (cf., Osterbrock & Ferland 2006) or a powerful outflow driven by a starburst (e.g., Shapiro *et al.* 2009; Genzel *et al.* 2011; Newman *et al.* 2012). In those cases, the FWHM of the broad component should be as large as $\sim 300 - 1000$ km s^{-1}. It is possible that the two component lines originate from two big star-forming regions (e.g., Harikane *et al.* 2014). As discussed in Harikane *et al.* (2014), the velocity offset of the two components, ~ 100 km s^{-1}, may be due to a rotation of the objects. We conclude that, while the origin of the two component [OIII] profile is not clear given the limited number of objects with these two component lines, we have demonstrated that LAEs have this feature.

Table 3.2. Summary of the Two Component Fit for [OIII] λ5007 Lines

Object	$f_{\rm narrow}$ (10^{-17} erg s^{-1} cm^{-2})	$f_{\rm broad}$ (10^{-17} erg s^{-1} cm^{-2})	$z_{\rm narrow}$	$z_{\rm broad}$	FWHM$_{\rm narrow}$ (km s^{-1})	FWHM$_{\rm broad}$ (km s^{-1})
(1)	(2)	(3)	(4)	(5)	(6)	(7)
COSMOS-13138	4.7 ± 0.2	0.9 ± 0.2	2.17931 ± 0.00002	2.17821 ± 0.00012	30 ± 20	70 ± 50
SXDS-10600	14.9 ± 0.6	4.2 ± 0.6	2.20915 ± 0.00002	2.21038 ± 0.00008	20 ± 30	80 ± 30

Notes.— (1) Object ID; (2)(3) Fluxes of the narrow ($f_{\rm narrow}$) and the broad ($f_{\rm broad}$) components. Note that the values are not corrected for the slit loss; (4)(5) Redshifts of the narrow ($z_{\rm narrow}$) and the broad ($z_{\rm broad}$) components; (6)(7) FWHM measurements of the narrow (FWHM$_{\rm narrow}$) and the broad (FWHM$_{\rm broad}$) components.

3.2 Stellar Population Derived from SED Fitting

In this study, we utilize SED fitting results of the sample, in particular, stellar dust extinction, $E(B-V)_*$, and stellar mass, M_*. In the following sections, we compare the $E(B-V)_*$ values with the results from Lyα radiation transfer fitting, and investigate the relationship between the Lyα profile trends and M_* (see §5.1). SED fitting results for the MagE (LRIS) objects have been presented in Hashimoto *et al.* (2013) and Nakajima *et al.*

(2013) (Shibuya *et al.* 2014a).

The procedure of the SED fitting in these papers is the same as that of Ono *et al.* (2010a). For the CDFS objects, we use 12 band passes: B, V, R, I, z, J, H, K data from the MUSYC public data release [*1] (Cardamone *et al.*, 2010), and *Spitzer*/IRAC 3.6, 4.5, 5.8, and 8.0 μm photometry from the *Spitzer* legacy survey of the UDS field. For the COSMOS and SXDS objects, we use 11 band passes: B, V, r', i', and z' data taken with Subaru/Suprime-Cam, J data taken with UKIRT/WFCAM, K_s data taken with CFHT/WIRCAM (McCracken *et al.*, 2010), and *Spitzer*/IRAC 3.6, 4.5, 5.8, and 8.0 μm photometry from the *Spitzer* legacy survey of the UDS field. We use neither u^*/U nor NB387-band data, since the photometry of these bands is contaminated by the IGM absorption and/or Lyα emission. Table 3.3 summarizes the broadband photometry of our objects. Basically, the uncertainties in the optical photometry include both photometric errors and systematic errors associated with aperture correction and photometric calibration.

We use the stellar population synthesis model of GALAXEV (Bruzual & Charlot, 2003) including nebular emission (Schaerer & de Barros, 2009), and adopt a Salpeter initial mass function (Salpeter, 1955). Because LAEs are metal poor star-forming galaxies, we choose constant star formation models with a metallicity of $Z/Z_\odot = 0.2$. We use Calzetti law (Calzetti *et al.* 2000) for the stellar continuum extinction, $E(B-V)_*$. We apply description in Madau (1995) to correct for the IGM attenuation; at $z \simeq 2.2$, continuum photons shortward of Lyα are absorbed by 18 %. Figure 3.7 shows the best-fit model spectra with the observed flux densities for individual objects. The physical quantities derived from SED fitting are summarized in Table 3.4. Because the continuum emission of COSMOS-30679 is blended with a foreground object, we deblend the source with GALFIT (Peng *et al.* 2002; see Nakajima *et al.* 2013 for details). While photometry data both before and after deblending are given in Table 3.3, we use the latter for SED fitting.

Here we note the derived $E(B-V)_*$ and M_* values. The former range from $E(B-V)_* =$ 0.04 to 0.40 with a mean value of $E(B-V)_* = 0.16$, and the latter from $\log M_* = 7.7$ to $10.8 M_\odot$ with a mean of $\log M_* = 9.3 M_\odot$.

[*1] http://www.astro.yale.edu/MUSYC/

Table 3.3. Broadband Photometry of Our Sample

CDFS sample	B	V	R	I	z	J	H	K	[3.6]	[4.5]	[5.8]	[8.0]	source[a]
CDFS-3865	23.01	22.94	22.92	23.14	22.93	22.73	22.27	22.38	22.82	22.82	22.51	23.00	H13, N13
CDFS-6482	23.93	23.87	23.78	23.95	23.67	23.50	23.36	23.07	22.88	22.83	23.34	99.99	H13, N13
	(28.32)	(27.85)	(27.82)	(26.14)	(25.64)	(24.57)	(24.57)	(23.97)	(26.23)	(25.68)	(23.66)	(23.43)	H13, N13
COSMOS sample	B	V	R	I	z	J	...	K_s	[3.6]	[4.5]	[5.8]	[8.0]	
COSMOS-08501	25.86	25.91	26.08	25.88	25.81	98.45	...	25.64	99.99	99.99	99.99	99.99	N13
COSMOS-13636	24.43	24.21	24.35	24.19	24.24	23.10	...	23.43	24.10	23.75	99.99	99.99	H13, N13, S14
COSMOS-30679	24.05	23.12	22.91	22.46	22.33	21.15	...	21.82	22.12	22.57	99.99	23.06	H13, N13
COSMOS-30679(†)	24.76	23.82	24.44	24.09	23.49	22.31	...	23.29					H13, N13
COSMOS-43982	25.00	24.38	24.48	23.99	23.73	21.89	...	21.62	21.20	21.02	20.69	20.75	H13, N13, S14
(limitmag)	(29.13)	(28.18)	(28.33)	(27.87)	(26.89)	(24.17)	...	(24.84)	(25.05)	(24.25)	(21.90)	(20.63)	H13, N13
(limitmag)(†)	(28.76)	(26.24)	(25.79)	(25.34)	(24.85)	(23.68)	...	(24.63)	...	...	...	...	H13, N13
COSMOS-08357	25.64	25.40	25.50	25.51	25.59	98.74	24.46	24.76	24.61	24.30	98.22	98.13	
COSMOS-12805	24.53	24.23	24.37	24.44	24.20	23.69	23.41	24.21	23.54	23.55	22.23	22.06	
COSMOS-13138	25.78	25.47	25.50	25.61	24.92	24.04	25.21	26.40	23.77	24.37	23.53	98.13	
COSMOS-38380	24.68	24.48	24.52	24.49	24.29	24.01	25.31	23.47	23.12	22.80	22.37	23.18	
(limitmag)	(29.14)	(28.18)	(28.31)	(27.95)	(26.85)	(24.44)	(25.11)	(24.84)	(25.09)	(24.35)	(21.83)	(20.65)	
SXDS sample	B	V	R	I	z	J	H	K_s	[3.6]	[4.5]	[5.8]	[8.0]	
SXDS-10600	23.71	23.76	23.79	23.79	23.88	23.65	23.10	23.41	23.18	23.35	22.78	98.14	
SXDS-10942	25.59	25.63	25.81	25.85	25.97	25.62	25.22	24.72	25.63	29.60	98.26	98.14	
(limit mag)	29.05	28.79	28.57	28.60	27.60	26.39	25.68	26.17	25.72	25.67	23.28	23.04	

Notes.— All magnitudes are total magnitude. 99.99 mag means negative flux densities. Magnitude in parentheses are 1σ uncertainties adopted in SED fitting.

a – H13: Hashimoto *et al.* (2013); N13: Nakajima *et al.* (2013); S14: Shibuya *et al.* (2014a).

Table 3.4. Results of SED fitting

Object	$\log(M_*)$ ($M_\odot$)	$E(B-V)$ (mag)	log(SFR) ($M_\odot$/yr)	χ^2	source
CDFS-3865	$9.50^{+0.01}_{0.03}$	$0.14^{+0.00}_{-0.00}$	$2.17^{+0.01}_{-0.01}$	32.170	H13, N13
CDFS-6482	$9.80^{+0.06}_{-0.05}$	$0.15^{+0.02}_{-0.02}$	$1.71^{+0.09}_{-0.09}$	12.374	H13, N13
COSMOS-08501	$7.84^{+1.21}_{-0.27}$	$0.08^{+0.04}_{-0.08}$	$1.68^{+1.24}_{-1.44}$	1.825	N13
COSMOS-13636	$9.12^{+0.13}_{-0.14}$	$0.18^{+0.01}_{-0.01}$	$1.80^{+0.08}_{-0.09}$	22.356	H13, N13, S14
COSMOS-30679	$10.34^{+0.00}_{-0.00}$	$0.40^{+0.00}_{-0.00}$	$3.10^{+0.00}_{-0.00}$	7062.297	H13, N13
COSMOS-30679(†)	$9.74^{+0.26}_{-0.52}$	$0.24^{+0.04}_{-0.04}$	$1.79^{+0.29}_{-0.19}$	32.068	H13, N13
COSMOS-43982	$10.80^{+0.01}_{-0.06}$	$0.40^{+0.02}_{-0.01}$	$2.37^{+0.08}_{-0.04}$	71.642	H13, N13, S14
COSMOS-08357	$9.21^{+0.28}_{-0.40}$	$0.14^{+0.05}_{-0.05}$	$0.98^{+0.28}_{-0.25}$	6.0	S14
COSMOS-12805	$9.44^{+0.13}_{-0.17}$	$0.16^{+0.02}_{-0.02}$	$1.49^{+0.12}_{-0.05}$	66	S14
COSMOS-13138	$9.48^{+0.22}_{-0.20}$	$0.19^{+0.04}_{-0.04}$	$1.06^{+0.22}_{-0.19}$	17	S14
COSMOS-38380	$10.06^{+0.06}_{-0.11}$	$0.13^{+0.02}_{-0.01}$	$1.30^{+0.08}_{-0.08}$	14	S14
SXDS-10600	$9.46^{+0.05}_{-0.04}$	$0.05^{+0.00}_{-0.01}$	$3.10^{+0.00}_{-0.00}$	47	S14
SXDS-10942	$7.73^{+0.10}_{-0.04}$	$0.04^{+0.02}_{-0.02}$	$3.10^{+0.00}_{-0.00}$	4	S14

Notes.— Physical Properties and their 1σ uncertainties of the sample from SED fitting.

a – H13: Hashimoto *et al.* (2013); N13: Nakajima *et al.* (2013); S14: Shibuya *et al.* (2014a).

3.3 Morphological Properties

In the following sections, we use the results of three morphological properties all of which are statistically studied for $z \sim 2.2$ LAEs in Shibuya *et al.* (2014b): the presence of a merger, the spatial offset between Lyα and stellar-continuum emission peaks, $\delta_{\mathrm{Ly}\alpha}$, and the ellipticity. Shibuya *et al.* (2014b) have utilized the I_{814} and H_{160} data taken with ACS and WFC3 on *HST* to examine the rest-frame UV and optical morphology, respectively. Among the objects presented in this study, the rest-frame UV images of the eight COSMOS objects have been investigated in Shibuya *et al.* (2014b).

The presence of a merger has been examined by two methods: the close-pair method(e.g., Le Fèvre *et al.* 2000; Law *et al.* 2012) and the morphological index method, especially *CAS* system (Abraham *et al.* 1996; Conselice *et al.* 2000). In Shibuya *et al.* (2014b), the former method has been applied to the objects with $I_{814} < 26.5$, which is the case for all the COSMOS objects presented in this study except for COSMOS-13138. The result is that two objects, COSMOS-13636 and COSMOS-12805, have a merger, while the rest of the seven objects do not have a merger. On the other hand, the latter one has been done for the objects with $I_{814} < 25.0$ and half light radii, r_{e}, larger than $0.''09$. The reason why we have limited the sample for the latter method is to obtain

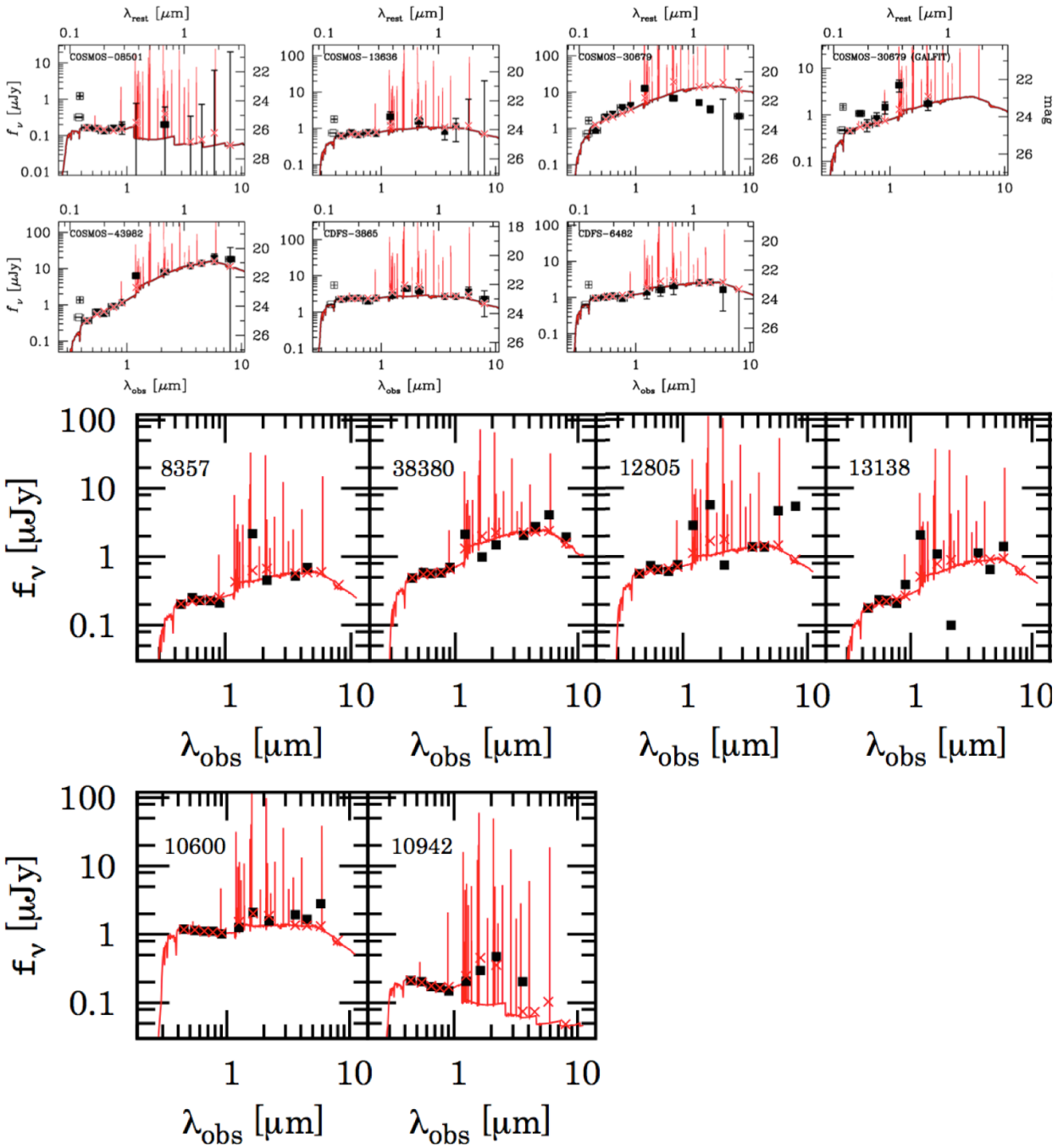

Figure 3.7. Results of SED fitting. The upper two panels are drawn from Hashimoto *et al.* (2013), while the lower two panels are from Shibuya *et al.* (2014a).

reliable values of the indices. This is the case for three COSMOS objects presented in this study, COSMOS-13636, COSMOS-43982, and COSMOS-38380. The result is that none of the three objects has a merger. The two results for COSMOS-13636 are not consistent with each other because we have used two different methods. Thus, among the eight COSMOS objects, a merger may present in COSMOS-13636 and COSMOS-12805, and it does not in the rest of the COSMOS objects (Table 3.5).

The Lyα spatial offset, $\delta_{\mathrm{Ly}\alpha}$, has been examined by performing source detections with `SExtractor` for both of Subaru NB387 and *HST* I_{814} images. While compact objects with symmetric UV light profiles tend to have small $\delta_{\mathrm{Ly}\alpha}$ values, objects with asymmetric, disturbed UV light profiles likely to have large $\delta_{\mathrm{Ly}\alpha}$ values (e.g., Jiang *et al.* 2013; Shibuya *et al.* 2014b). Thus, this quantity could be a useful tracer of the HI gas stability around a galaxy. The value is reliably obtained for the objects with $I_{814} < 26.5$ and NB387 < 24.5, where the typical positional error in I_{814} (NB387) is less than $0.''02$ ($0.''3$). For the eight COSMOS objects in this study, none has a significant Lyα spatial offset larger than the typical error of the $\delta_{\mathrm{Ly}\alpha}$, $\sim 0.''36$.

The ellipticity, $\epsilon = 1 - a/b$, where a and b are the major and minor axis, is a useful indicator of the galactic disk inclination. In Shibuya *et al.* (2014b), this has been measured using `GALFIT` software (Peng *et al.* 2002) for objects with $I_{814} < 25.0$ and half light radii, r_{e}, larger than the typical PSF size. The former criterion, corresponding to the $S/N = 30$ detection, is needed for the reliable ellipticity measurements (e.g.,Mosleh *et al.* 2012; Ono *et al.* 2013). Among the sample, this is the case for the only three objects, COSMOS-30679, COSMOS-38380, and COSMOS-43982. The resultant ellipticity values are $\epsilon = 0.24$ (COSMOS-30679), 0.34 (COSMOS-38380), and 0.49 (AGN-COSMOS-43982), respectively (Table 3.5).

Table 3.5. Summary of Morphological Properties

Object	merger (pair, CAS)	ϵ
CDFS-3865	-, -	-
CDFS-6482	-, -	-
COSMOS-08501	no, -	-
COSMOS-30679	no, -	0.24
COSMOS-13636	yes, no	-
COSMOS-43982	no, no	0.49
COSMOS-08357	no, -	-
COSMOS-12805	yes, -	-
COSMOS-13138	no, -	-
COSMOS-38380	no, no	0.34
SXDS-10600	-, -	-
SXDS-10942	-, -	-

Notes.— Morphological properties of the sample.

Chapter 4

Close Comparison between Observed and Modeled Lyα Lines

Due to the resonant nature of Lyα, the observed Lyα line of a galaxy has a complicated profile depending on the kinematics and geometry of the ISM. A Lyα source in a simple static gas cloud produces a symmetric double-peaked profile centered at 1216 Å due to significant resonant scattering at 1216 Å (Harrington, 1973; Neufeld, 1990; Dijkstra *et al.*, 2006). If the bluer peak is heavily absorbed by the intervening IGM along the line of sight, only the redder peak will be observed. In the case of outflow, the Lyα emission line should show an asymmetric profile similar to a P Cygni profile. Verhamme *et al.* (2006) have explained some of observed Lyα profiles with a strong red peak and a weak blue peak with models of an expanding shell that absorbs Lyα photons at around 1216 Å, although the surface brightness distribution may not be explained by such wind shells (see, e.g., Barnes & Haehnelt 2009). In short, when an outflow exists, the observed Lyα line should show an asymmetric profile with a strong peak redshifted with respect to the systemic velocity.

We have demonstrated in §3.1.2 that most spectrum has a positive $S_{\rm w}$ value, indicating that most of our Lyα line is asymmetric with a red tail. The spectra of LRIS-COSMOS-13138 is a symmetric double-peaked profile centered at 1216 Å which is a characteristic profile of a static cloud in the ISM. As found in §3.1.3, 12 of the 14 spectra have a positive $\Delta v_{\rm Ly\alpha,r}$ beyond the 2σ uncertainty. In addition, the LIS absorption lines are blue-shifted

with respect to the systemic velocities when they are detected.

These results lead us to a conclusion that the Lyα emission of our objects is mostly originated from outflowing gas. Motivated by the results, we try to compare our observed Lyα profiles with a Lyα radiative transfer model of an expanding shell.

4.1 Lyα Radiative Transfer Model and Fitting Procedure

4.1.1 A Library of Synthetic Spectra

The library of synthetic Lyα spectra used to compare with the observed Lyα spectra of our 12 $z \sim 2.2$ LAEs has been described in Schaerer *et al.* (2011). Lyα radiation transfer has been computed with McLya (Verhamme *et al.*, 2006) through spherically symmetric expanding shells of homogeneous and isothermal neutral hydrogen gas. The shell is describe by 4 parameters:

- the radial expansion velocity, $V_{\rm exp}$,
- the neutral hydrogen column density along any line of sight, $N_{\rm HI}$,
- the Doppler parameter b, describing the thermal and turbulent motion in the shell,
- and the dust absorption optical depth at the Lyα wavelength, $\tau_{\rm a}$, related to the gas dust extinction by $E(B-V)_{\rm gas} \approx (0.06...0.11)\tau_{\rm a}$, where the lower and higher values in the parenthesis correspond to the attenuation law for starbursts (Calzetti *et al.* 2000) and the Galactic extinction law (Seaton 1979), respectively.

The Lyα source is located at the center of the shell. The intrinsic (i.e., before being affected by the radiative transfer effect) spectrum is a Gaussian Lyα line plus a flat continuum, and is characterized by 2 parameters :

- the Lyα equivalent width, EW$_{\rm int}$(Lyα),
- and the full width at half maximum, FWHM$_{\rm int}$(Lyα).

The parameter ranges examined are listed in Table 4.1. For a comparison with the observed data, each rest-frame model has been shifted using the systemic redshift $z_{\rm sys}$ values listed in Table 3.1. To reflect the $z_{\rm sys}$ uncertainty, we have allowed the observed Lyα spectra to shift relative to the velocity zero point within the error. Thus, combinations of 6 free parameters are fitted to the data.

Table 4.1. Model Parameter Values

Model parameter	Values												
$V_{\rm exp}$ [km s^{-1}]	0.,	20.,	50.,	100.,	150.,	200.,	250.,	300.,	400.,	500.,	600.,	700.	
$\log(N_{\rm HI})$ [cm^{-2}]	16.0,	18.0,	18.5,	19.0,	19.3,	19.6,	19.9,	20.2,	20.5,	20.8,	21.1,	21.4,	21.7
b [km s^{-1}]	10.,	20.,	40.,	80.,	160.								
$\tau_{\rm a}$	0.,	0.2,	0.5,	1.0,	1.5,	2.0,	3.0,	4.0					
EW$_{\rm int}$(Lyα) [Å]	0.,	100.,	200.,	300.,	400.,	500.,	600.,	700.,	800.,	900.,	1000.	(a)	
FWHM$_{\rm int}$(Lyα) [km s^{-1}]	0.,	100.,	200.,	300.,	400.,	500.,	600.,	700.,	800.,	900.,	1000.	(a)	

Notes.— (a) The two parameters characterizing the input Lyα spectrum, EW$_{\rm int}$(Lyα) and FWHM$_{\rm int}$(Lyα), can also be fixed with the arbitrary number between 0 and 1000.

In §3.1.5, we have shown that two objects, COSMOS-13138 and SXDS-10600, have a non-Gaussian [OIII] λ5007 line profile. We assume that the intrinsic Lyα profile of these objects is a Gaussian in this section, and mention the results with the input profile exactly the same as that of non-Gaussian [OIII] λ5007 line in §5.1.2.

This library of Lyα spectra has been successfully used to reproduce various observed Lyα line profiles of $z > 3$ LBGs, from strong emission to broad absorption (Verhamme *et al.*, 2008; Schaerer & Verhamme, 2008; Dessauges-Zavadsky *et al.*, 2010; Vanzella *et al.*, 2010; Lidman *et al.*, 2012).

4.1.2 Fitting to Observed Spectra

To perform a statistical comparison between the observed and modeled Lyα line profiles, we calculate the χ^2 values for each of the possible combinations of the parameters for each galaxy (cf., Chonis *et al.* 2013). Since model spectra are normalized and at an infinite spectral resolution, two steps are needed before the χ^2 calculation. First, we normalize the observed spectra using the continuum level estimated at wavelengths longer than 1216Å. Second, each model Lyα spectrum has been convolved with a Gaussian whose FWHM is related to the spectral resolutions used for the observations:

$$\mathrm{FWHM} = c/R, \tag{4.1}$$

where c is the speed of light.

We note that our fitting techniques gives exactly the same statistical weight to all data points, in the continuum or in the line. Finally for the sake of consistency, for each object, we calculate the χ^2 values in the wavelength range from $-3 \times \mathrm{FWHM_{obs}}(\mathrm{Ly}\alpha)$ to

$+3 \times \mathrm{FWHM_{obs}(Ly}\alpha)$ around the Lyα line center.

In Figure 4.1, we demonstrate how the best fit, and its associated errors, are found using χ^2 values. To do this an example of the fit to the $V_{\rm exp}$ for both a well and poorly constrained objects are shown. In the left panels of this figure, one can see the broad range of $V_{\rm exp}$ values with low reduced χ^2 for COSMOS-08357 in comparison to CDFS-3865, which have Lyα ratios of ~ 11 and ~ 98, respectively. To measure median and 1σ values, we convert χ^2 values into probabilities using the formula, $p \propto \exp(-\chi^2/2)$ for each five 2D parameter set ($V_{\rm exp}$ vs. $N_{\rm HI}$, $V_{\rm exp}$ vs. $\tau_{\rm a}$, $V_{\rm exp}$ vs. b, $V_{\rm exp}$ vs. $\mathrm{FWHM_{int}(Ly}\alpha)$, and $V_{\rm exp}$ vs. $\mathrm{EW_{int}(Ly}\alpha)$). After normalizing them so that the total probability is unity, we draw a probability (PDF) and a cumulative density function (CDF) as shown in the middle and the right panels, respectively. Finally, we adopt the values where the CDF value satisfying CDF $= 0.50, 0.16$, and 0.84 as the mean and $\pm1\sigma$, respectively. Performing these for each five 2D parameter set results in five mean and $\pm1\sigma$ values. As can be seen, all the five mean and $\pm1\sigma$ values are consistent with each other for CDFS-3865, whereas those are not for COSMOS-08357. In the latter case, we adopt the mean value of the five mean and $\pm1\sigma$ values.

4.2 Results

We show the reproduced Lyα profiles (§4.2.1), describe the derived parameters (§4.2.2), and examine the influence of spectral resolutions on the results (§4.2.3).

4.2.1 Fitted Profiles

Figure 4.2 shows the best fit model spectra with the observed ones. All the Lyα profiles are quite well reproduced by the model, which seems to differ from the previous studies, Kulas *et al.* (2012) and Chonis *et al.* (2013). They had difficulty reproducing their Lyα profiles, especially the position and the flux of the blue bump. This might be due to model differences. These two studies have utilized the uniform expanding shell model constructed by Zheng & Miralda-Escudé (2002) and Kollmeier *et al.* (2010). There are three major differences between the models (c.f., Chonis *et al.* 2013). First, in addition to the three common parameters, $V_{\rm exp}$, $N_{\rm HI}$, and b, the model used in this study also includes an additional one for dust absorption. Second, the grid number and the physical range of parameters are different. The model constructed by Zheng & Miralda-Escudé (2002) and Kollmeier *et al.* (2010) have four grids of each parameter with physical ranges; $V_{\rm exp} = 50$,

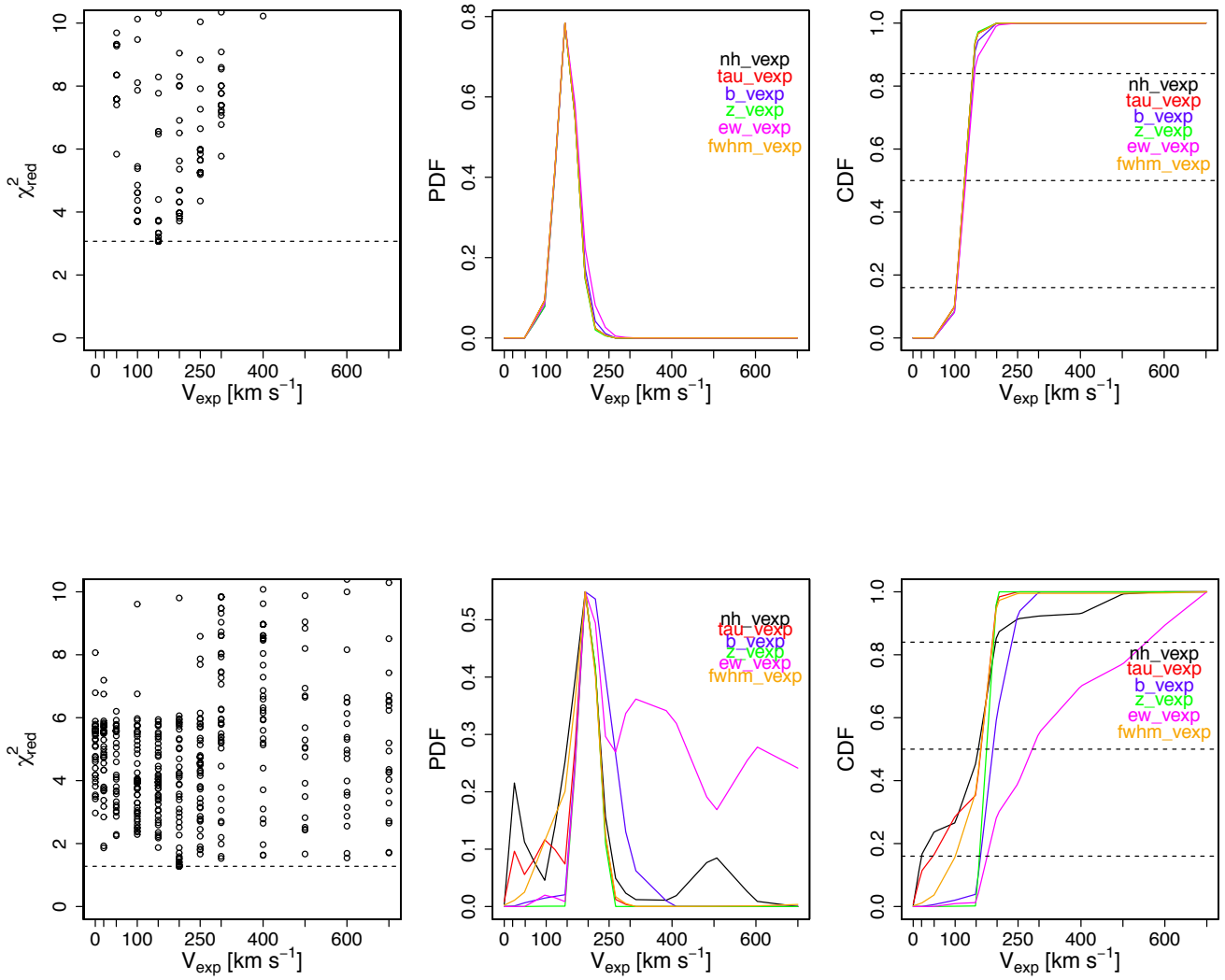

Figure 4.1. Examples of reduced χ^2 values (left panels), converted probability density function (PDF) (middle panels), and the cumulative density function (CDF) (right panels), for the parameter $V_{\rm exp}$. The upper (lower) panels are for CDFS-3865 (COSMOS-08357).

100, 200, 300 km s^{-1}, log ($N_{\rm HI}$) = 17, 18, 19, 20.3 cm^{-2}, and b = 20, 40, 80, 120 km s^{-1}, whereas the model used in this study has 12 $V_{\rm exp}$, 13 $N_{\rm HI}$, and 5 b grids spanning a wider physical range (Table 4.1). Finally, the intrinsic spectrum of these models is assumed to be a monochromatic Lyα line, while we model a Gaussian plus a continuum. As we show in §4.2.2 and later sections, we infer that the key to better reproduce the blue bump is to transfer a whole line of a Gaussian and a continuum.

4.2.2 Derived Parameters

The best fit parameters are summarized in Table 4.2. We describe the mean values of the derived parameters, and systematically compare them with those of LBGs modeled by the same code (Verhamme *et al.* 2008; Schaerer & Verhamme 2008; Dessauges-Zavadsky *et al.* 2010). For the parameter FWHM$_{\rm int}$(Lyα), we examine the mean values of two subsamples, objects with the blue bump and those without. This is in order to demonstrate that FWHM$_{\rm int}$(Lyα) is the key parameter to better reproduce the blue bump. We have checked that there is no significant difference between the two subsamples for the other parameters.

The mean $V_{\rm exp}$ value in the LAEs is 148 km s^{-1}, which is comparable to that of LBGs, $\sim$ 130 km s^{-1}. This strongly disfavors the hypothesis that the small $\Delta v_{\rm Ly\alpha}$ in LAEs is due to their large outflow velocity.

The most interesting parameter, $N_{\rm HI}$, ranges from log($N_{\rm HI}$) = 16.0 to 19.7 cm^{-2}. The mean value is 18.3 cm^{-2}, which is more than one order of magnitude smaller than the typical log($N_{\rm HI}$) value in LBGs, $\sim$ 20.0 cm^{-2}.

The mean values of $\tau_{\rm a}$ and b are 0.9 and 38 km s^{-1}, respectively, both of which are consistent with those in LBGs, $\sim$ 0.8 and $\sim$ 30 km s^{-1}.

FWHM$_{\rm int}$(Lyα) values range from FWHM$_{\rm int}$(Lyα) = 50 to 847 km s^{-1}. The mean values for the whole sample, the non blue bump sample, and the blue bump sample, are 354, 169, and 602 km s^{-1}, respectively. This shows that the blue bump objects have significantly larger FWHM$_{\rm int}$(Lyα) values than those of the non blue bump objects. This trend is similar to the results in Verhamme *et al.* (2008). They have found that most LBGs with a single peaked Lyα profile are best fitted with moderate values of FWHM$_{\rm int}$(Lyα), $\sim$ 200 km s^{-1}, whereas the best fit FWHM$_{\rm int}$(Lyα) values for the two LBGs with the blue bump, FDF4691 and FDF5215, are greater than 500 km s^{-1}. These results support our claims that a large FWHM$_{\rm int}$(Lyα) value helps fitting the blue bump. We investigate if there are any observational trends for the blue bump objects, and discuss possible

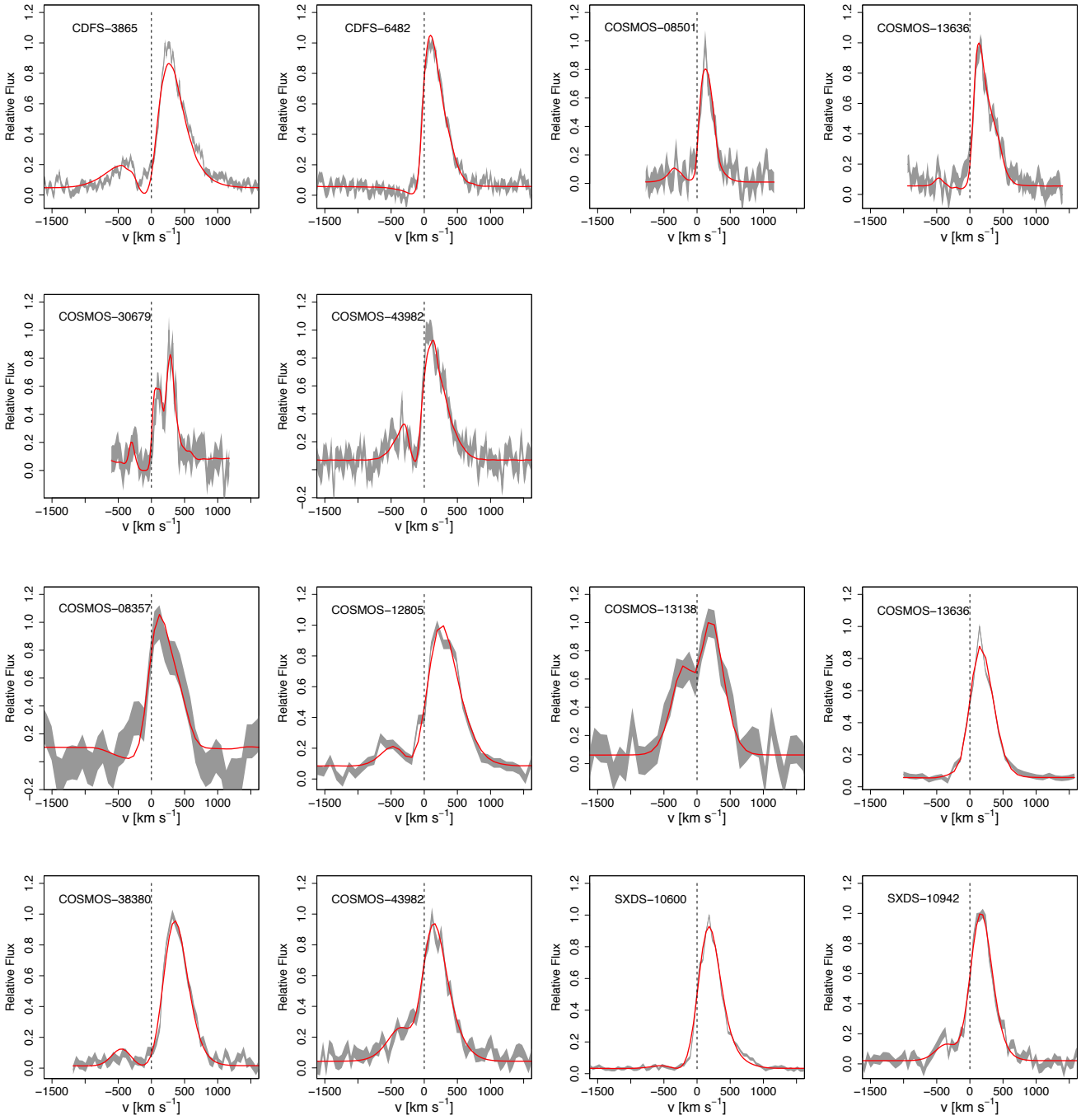

Figure 4.2. The upper two panels show the reproduced Lyα line profiles (red) on top of the observed ones (grey) for MagE, while the lower ones are for LRIS. The gray region denotes the 1σ range of the observed spectrum. All spectra are scaled in the wavelength range from -1500 to $+1500$ km s^{-1}.

mechanisms for the blue bump objects to have a large FWHM$_{\rm int}$(Lyα) value in §5.1.

Since starburst activities which produce Lyα photons should be similar within LAEs and LBGs, we expect comparable mean EW$_{\rm int}$(Lyα) values for these two kinds of galaxies. The result is that the mean EW$_{\rm int}$(Lyα) value in LAEs, 65 Å, is somewhat smaller than that in LBGs, 108 Å.

Table 4.2. Summary of the Lyα Fitting for the Sample

Object	$\chi^2_{\rm red}$	$V_{\rm exp}$ (km s^{-1})	$\log(N_{\rm HI})$ (cm^{-2})	τ_a	b (km s^{-1})	FWHM(Lyα)$_{\rm int.}$ (km s^{-1})	EW(Lyα)$_{\rm int.}$ (Å)
(1)	(2)	(3)	(4)	(5)	(6)	(7)	(8)
CDFS-3865	3.1	120^{+21}_{-14}	$19.5^{+0.1}_{-0.1}$	$0.0^{+0.0}_{-0.0}$	15^{+13}_{-5}	846^{+106}_{-97}	35^{+7}_{-7}
CDFS-6482	1.3	177^{+18}_{-18}	$19.2^{+0.1}_{-0.1}$	$0.12^{+0.04}_{-0.08}$	10^{+8}_{-0}	271^{+38}_{-29}	28^{+0}_{-7}
COSMOS-08501	1.3	167^{+286}_{-106}	$18.7^{+0.5}_{-1.1}$	$1.56^{+1.54}_{-1.07}$	13^{+14}_{-3}	252^{+240}_{-134}	14^{+7}_{-7}
COSMOS-30679	1.0	127^{+14}_{-21}	$19.5^{+0.1}_{-0.1}$	$1.43^{+1.03}_{-0.53}$	29^{+8}_{-8}	50^{+38}_{-0}	39^{+1}_{-11}
COSMOS-13636 (MagE)	1.1	226^{+14}_{-21}	$16.0^{+0.0}_{-0.0}$	$0.12^{+0.14}_{-0.08}$	121^{+27}_{-27}	256^{+101}_{-58}	28^{+0}_{-7}
COSMOS-13636 (LIRS)	6.2	127^{+14}_{-21}	$18.8^{+0.2}_{-0.2}$	$0.08^{+0.08}_{-0.04}$	30^{+8}_{-6}	127^{+19}_{-19}	28^{+0}_{-7}
COSMOS-43982 (MagE)	1.0	141^{+88}_{-57}	$18.2^{+0.6}_{-1.6}$	$1.15^{+1.54}_{-0.89}$	12^{+11}_{-2}	544^{+120}_{-134}	28^{+7}_{-11}
COSMOS-43982 (LRIS)	1.4	138^{+85}_{-71}	$18.1^{+0.4}_{-1.5}$	$0.02^{+0.22}_{-0.02}$	13^{+8}_{-3}	621^{+53}_{-86}	42^{+7}_{-7}
COSMOS-08357	1.3	170^{+25}_{-42}	$19.7^{+0.1}_{-0.6}$	$2.24^{+1.25}_{-0.95}$	19^{+14}_{-9}	74^{+82}_{-24}	85^{+42}_{-35}
COSMOS-12805	3.1	177^{+18}_{-21}	$19.2^{+0.1}_{-0.1}$	$1.73^{+0.71}_{-0.38}$	10^{+18}_{-0}	645^{+38}_{-38}	42^{+7}_{-0}
COSMOS-13138	1.5	21^{+481}_{-21}	$18.8^{+0.4}_{-0.7}$	$1.13^{+1.45}_{-0.89}$	15^{+14}_{-5}	501^{+144}_{-144}	64^{+11}_{-11}
COSMOS-38380	2.1	127^{+14}_{-21}	$19.7^{+0.1}_{-0.1}$	$0.69^{+0.28}_{-0.32}$	60^{+14}_{-14}	99^{+9}_{-9}	276^{+14}_{-21}
SXDS-10600	6.2	226^{+14}_{-21}	$16.0^{+0.0}_{-0.0}$	$1.74^{+0.20}_{-0.16}$	121^{+27}_{-27}	223^{+19}_{-19}	113^{+7}_{-7}
SXDS-10942	1.6	131^{+32}_{-35}	$16.0^{+0.0}_{-0.0}$	$0.12^{+0.08}_{-0.08}$	60^{+14}_{-14}	453^{+82}_{-67}	85^{+14}_{-7}

Notes.— (1) Object ID; (2) Reduced χ^2 value of the fitting calculated as $\chi^2_{\rm red} = \chi^2/(N-M)$, where N and M denote the number of data points and the degree of freedom, respectively; (3)(4)(5)(6)(7) and (8) Derived best fit parameter of the radial expansion velocity, the column density of the neutral Hydrogen, the dust absorption optical depth, the Doppler parameter, the intrinsic Lyα FWHM, and the intrinsic Lyα EW, respectively.

4.2.3 Influence of Spectral Resolution on the Fitting Procedure

To investigate the influence of spectral resolution on the fitting results, we compare the best fit parameters of the two objects observed with the two spectrographs, COSMOS-13636 and COSMOS-43982. As can be seen in Table 4.2, the two fitting results of COSMOS-43982, MagE-COSMOS-43982 and LRIS-COSMOS-43982, are consistent with each other, whereas those of MagE-COSMOS-13636 and LRIS-COSMOS-13636 are not. The latter would be due to the fact that MagE-COSMOS-13636 and LRIS-COSMOS-

13636 have two very different reduced χ^2 values, 1.1 and 6.2, respectively.

Taking a closer look into these two fits, we see that the extremely small 1 σ noise in the flux of LRIS-COSMOS-13636 could be a key reason for its high χ^2 value. On the other hand, the modeled spectrum seems to be over-smoothed, leading us to infer its Lyα line resolution were under-estimated. Indeed, it is known that the spectral resolution for the line can be higher than the canonical value. A combination of these factors would naturally cause the large resultant χ^2 value, and the discrepancy between the different best-fit parameters at two resolutions.

4.3 Degeneracy among Parameters

In this subsection, we investigate degeneracies among the model parameters to understand how they affect our determination of the best fit parameters. First we describe possible degeneracies, then statistically examine them using 2D χ^2 values.

It is possible that parameters τ and $\mathrm{EW_{int}(Ly\alpha)}$ are degenerated as an observed profile can be reproduced equivalently well either assuming a weak intrinsic line with low dust extinction, or a strong intrinsic line with a high dust content. There would also be a degeneracy between b and $\mathrm{FWHM_{int}(Ly\alpha)}$ in the sense that both broaden the line profile. Furthermore, when there is a blue bump in the profile, we need either high b or low V_{exp} values to reproduce it.

Figures 4.3 - 4.5 are 2D parameter grid maps for CDFS-3865 with the grey dots showing the entire grids. We use these maps and χ^2 values to examine the actual degeneracies among the parameters. If there is a degeneracy between two parameters, a χ^2 contour would be tilted and elongated. The blue grids in these figures show those satisfying $\Delta\chi^2 \leq 6.17$ above the raw minimum χ^2 designated by the white dots, i.e., the 3 σ uncertainty of the parameters (Press *et al.* 1992). Thanks to the number of data points given by high spectral resolutions, and the relatively coarse grids, even the 3 σ uncertainty is converged into the one grid. This indicates that there is no degeneracy which affects our determination of the best fit. We have checked that this is also true for the rest of the sample in this study. Thus, we conclude that the systematic uncertainty among the parameters due to the degeneracies is small, and it does not affect our discussions.

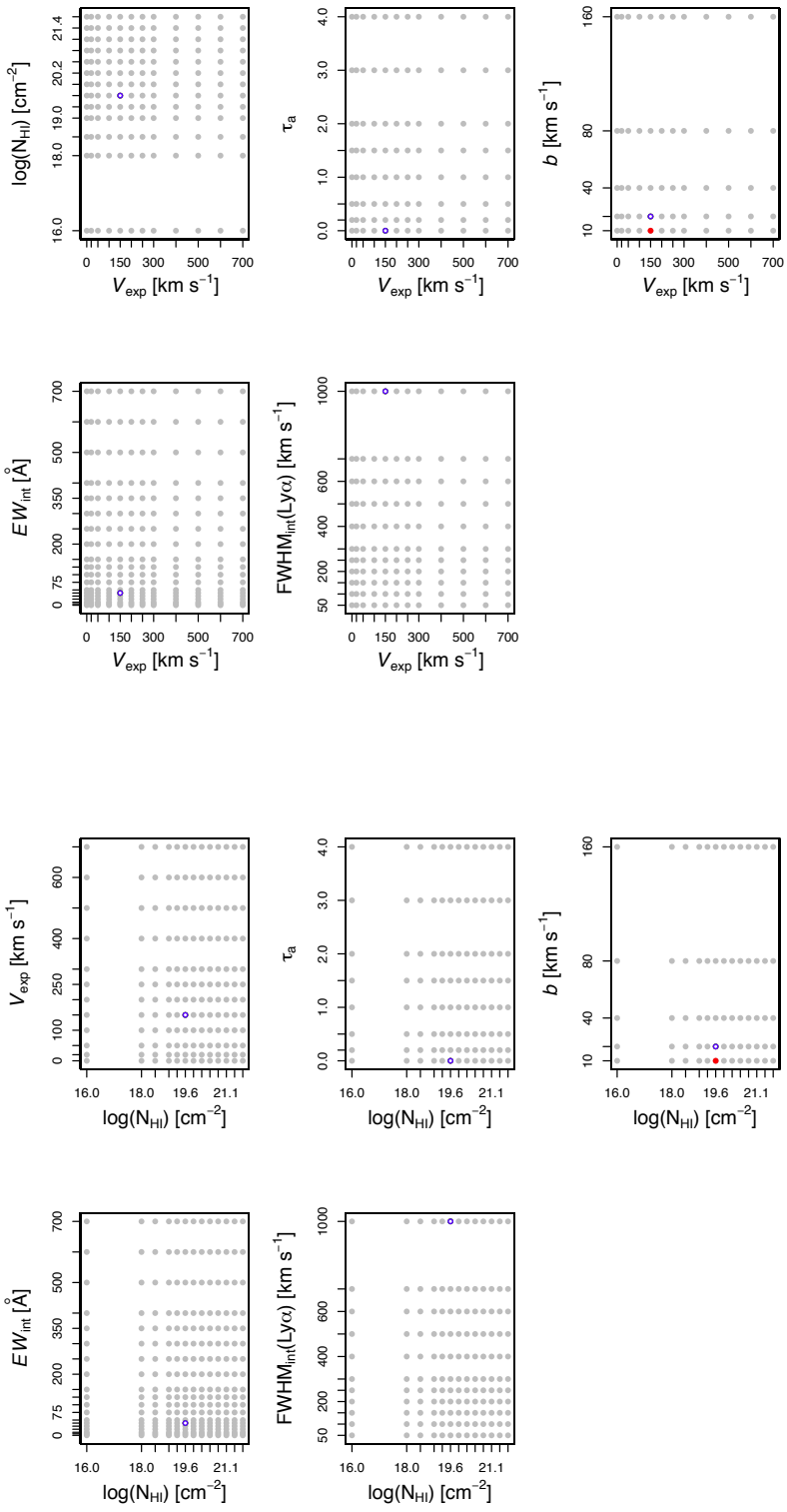

Figure 4.3. Upper and lower five panels show 2D χ^2 contours for $V_{\rm exp}$ and $\log(N_{\rm HI})$, respectively, for CDFS-3865. The blue (red) grids in these figures show those satisfying $\Delta\chi^2 \leq 6.17$ ($6.17 \leq \Delta\chi^2 \leq 9.21$) above the raw minimum χ^2 designated by the white dots, i.e., the 3 σ (4 σ) uncertainty of the parameters (Press *et al.* 1992).

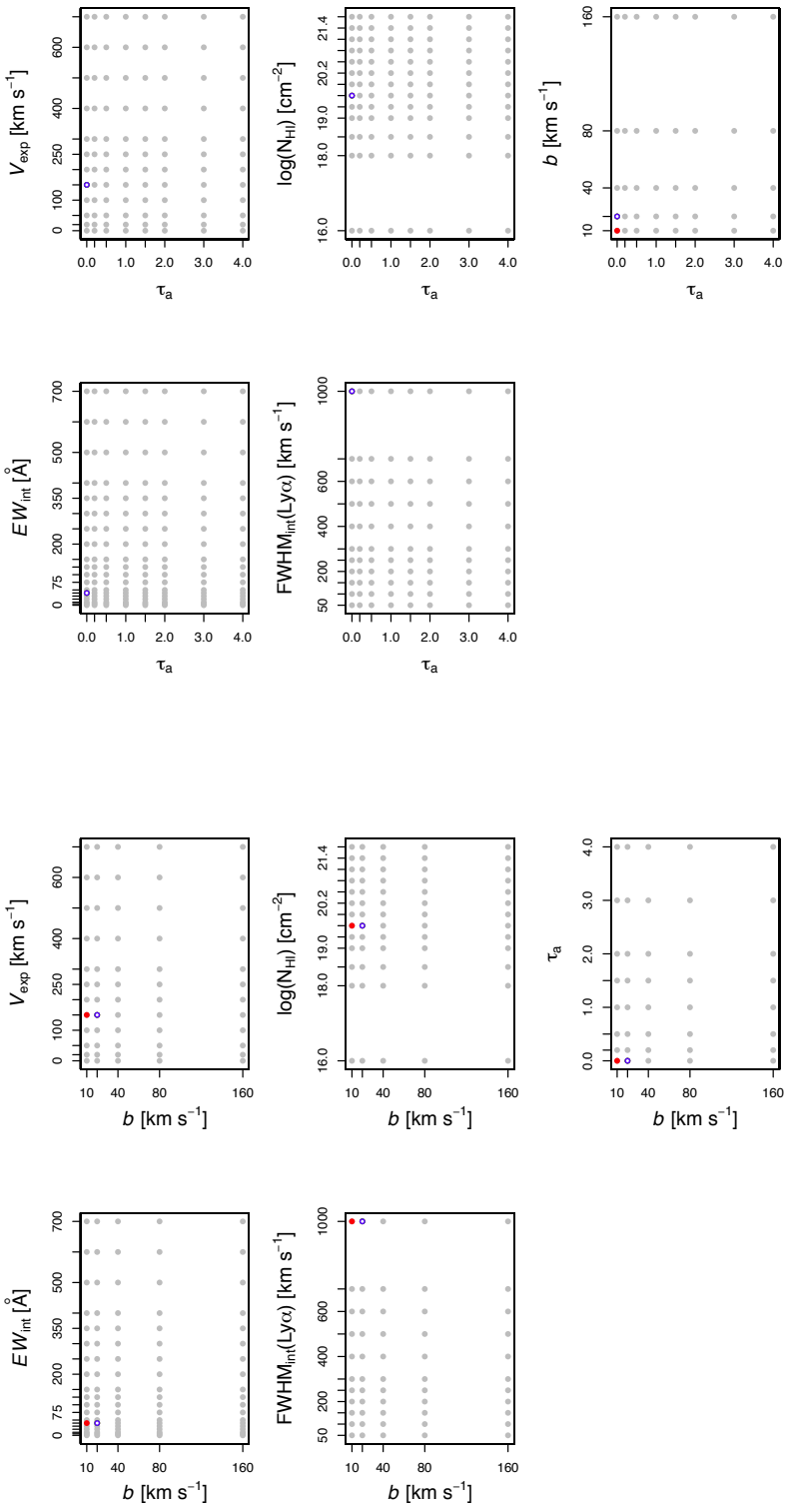

Figure 4.4. Upper and lower five panels show 2D χ^2 contours for τ_a and b, respectively, for CDFS-3865. The meaning of the colors are the same as those in Figure 4.3.

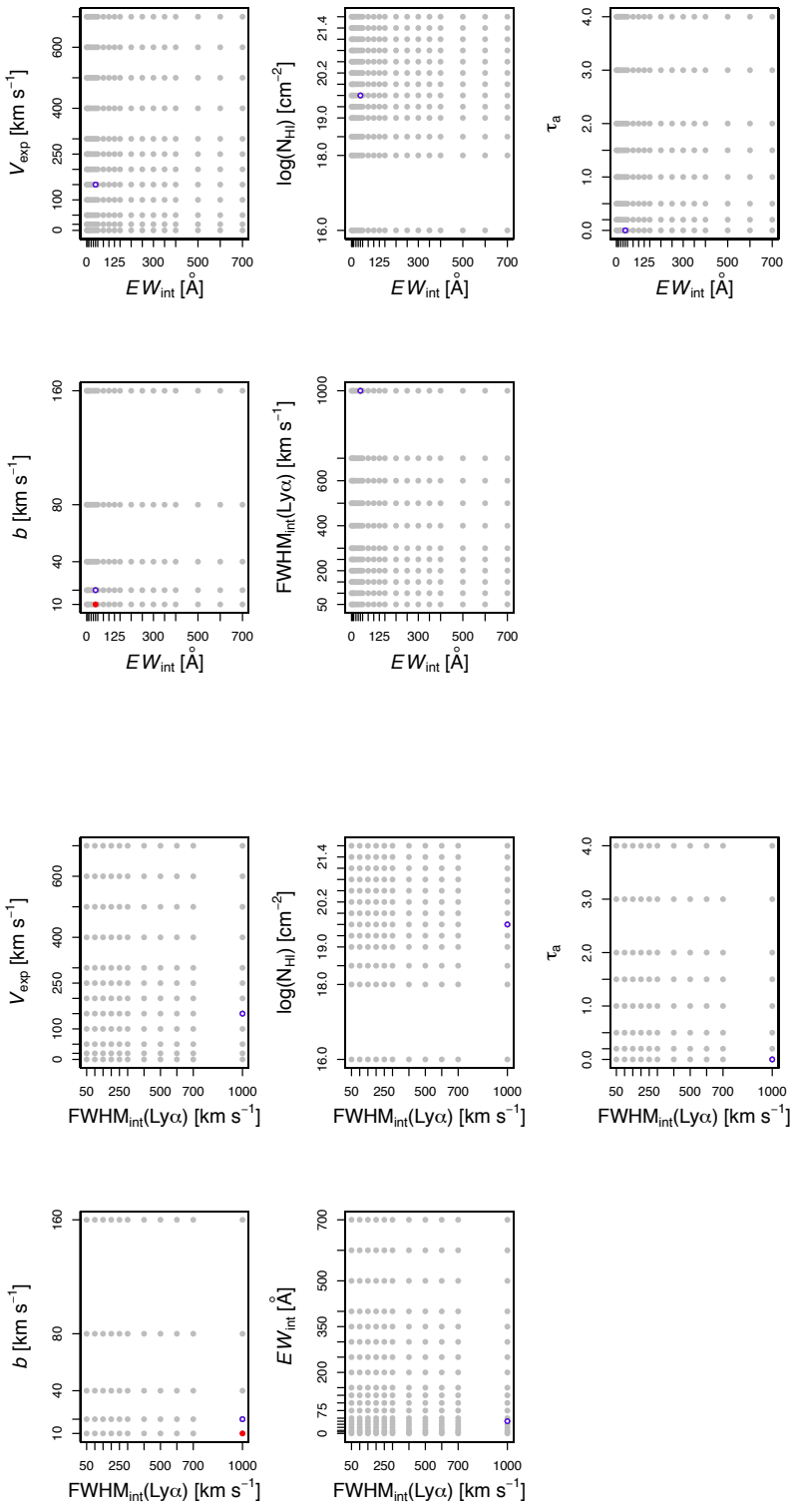

Figure 4.5. Upper and lower five panels show 2D χ^2 contours for $\mathrm{EW_{int}(Ly\alpha)}$ and $\mathrm{FWHM_{int}(Ly\alpha)}$, respectively, for CDFS-3865. The meaning of the colors are the same as those in Figure 4.3.

4.4 Comparison between Observables and Model Parameters

In order to examine if our best fit parameters are reasonable, we compare the derived parameters with the observables.

4.4.1 Galactic Outflow Velocity: $|\Delta v_{\rm abs}|$ vs. $V_{\rm exp}$

As stated in §3.1.4, several LIS absorption lines have been detected in the three individual spectra of COSMOS-12805, COSMOS-13636, and SXDS-10600 (Shibuya *et al.* 2014a), and in the stacked spectrum of the four LAEs, CDFS-3865, CDFS-6482, COSMOS-13636, and COSMOS-30679 (Hashimoto *et al.* 2013). The measured blueshift of LIS absorption lines with respect to the systemic $\Delta v_{\rm abs}$, a useful tracer of the average speed of a galactic outflow, is listed in Table 3.1. Figure 4.6 shows the comparison between $|\Delta v_{\rm abs}|$ and the best fit parameter of the shell expansion velocity, $V_{\rm exp}$. For the stacked spectrum, we plot the mean $V_{\rm exp}$ value of the four LAEs, 163 ± 25 km s^{-1}. While there are only four data points, $|\Delta v_{\rm abs}|$ and $V_{\rm exp}$ are quite well consistent with each other.

4.4.2 Dust Extinction: $E(B-V)_*$ vs. $\tau_{\rm a}$

The stellar dust extinction values, $E(B-V)_*$, for the sample have been derived in previous studies (Hashimoto *et al.* 2013; Nakajima *et al.* 2013; Shibuya *et al.* 2014a) (see §3.1.4). Figure 4.7 compares stellar dust extinction values, $E(B-V)_*$, with gas dust extinction values, $E(B-V)_{\rm gas}$. $E(B-V)_{\rm gas}$ values are derived assuming the relation:

$$E(B-V)_{\rm gas} \approx 0.10\tau_{\rm a} \tag{4.2}$$

Dotted and dashed lines correspond to empirical relations $E(B-V)_* = E(B-V)_{\rm gas}$ (Erb *et al.* 2006a) and $E(B-V)_* = 0.44E(B-V)_{\rm gas}$ (Calzetti *et al.* 2000), respectively. As Kashino *et al.* (2013) have shown, the difference between the two dust extinction values becomes small in high-z galaxies compared to local galaxies.

The figure shows that half of the sample roughly lie between the two lines, while the rest of the sample show low $E(B-V)_{\rm gas}$ values. A similar trend has been found in Figure 12 of Verhamme *et al.* (2008) who have compared the two dust extinction values for $z \sim 3$ LBGs. They have assumed two different star formation histories (SFHs) in deriving $E(B-V)_*$: a constant SFH indicated by red triangles and an exponentially decreasing SFH indicated by blue open circles, the former of which is the same as that

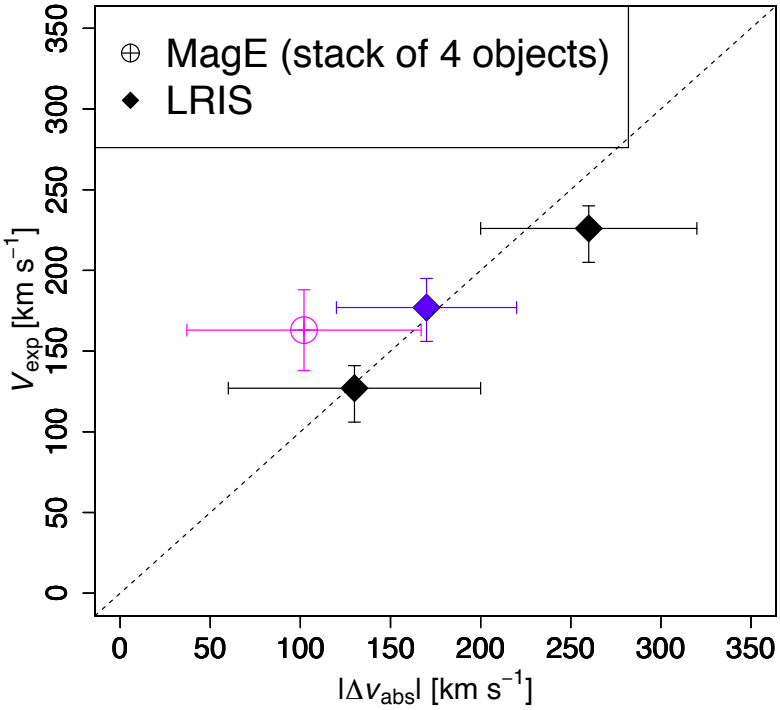

Figure 4.6. $V_{\rm exp}$ plotted against $|\Delta v_{\rm abs}|$. The diamonds are the three LRIS objects whose LIS absorption lines are detected in the individual spectrum (Shibuya *et al.* 2014a). The blue point shows the object with the blue bump in the Lyα profile, while the two black ones are those without. The magenta circle is the stacked spectrum of the four MagE LAEs, CDFS-3865, CDFS-6482, COSMOS-13636, and COSMOS-30679 (Hashimoto *et al.* 2013).

assumed in this study. Both our data and the red triangles in Verhamme *et al.* (2006) are similarly distributed in the sense that half of the sample has comparable extinction values and the rest has low $E(B-V)_{\rm gas}$ values. Taking into account the systematic uncertainty of dust extinction measurements, due to the SFH assumption, we conclude that the two dust extinction values are not inconsistent.

4.4.3 Full Width at Half Maximum of Lines: FWHM(neb) vs. FWHM$_{\rm int}$(Lyα)

Figure 4.8 plots the observed FWHM of nebular emission lines, FWHM(neb), versus modeled FWHM of the intrinsic (i.e., before being affected by the radiative transfer effect) Lyα line, FWHM$_{\rm int}$(Lyα). Assuming that both Lyα and nebular emission lines originate

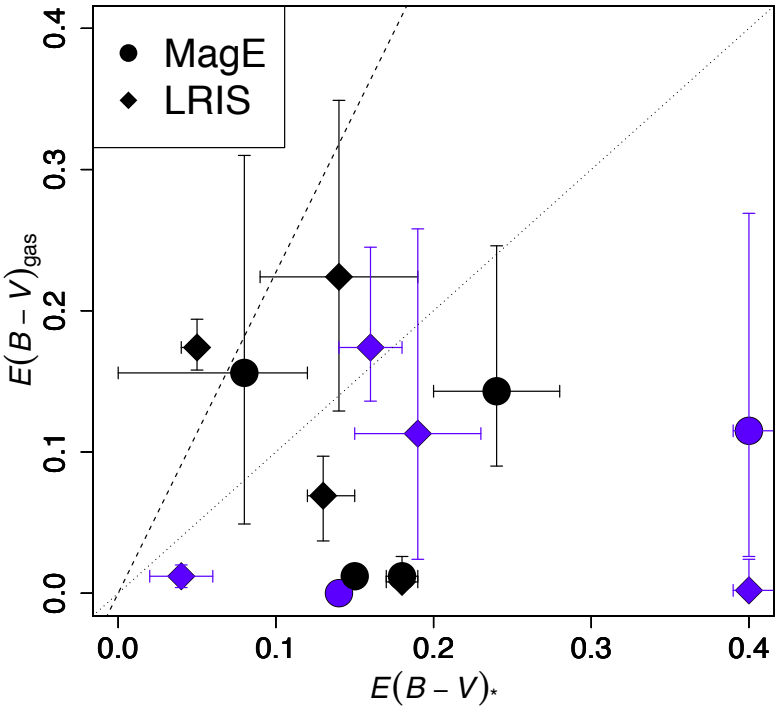

Figure 4.7. $E(B-V)_{\rm gas}$ plotted against $E(B-V)_*$ for all the sample. The circles show the MagE objects, while the diamonds are the LRIS objects. The blue points are the objects with the blue bump in the Lyα profile, while the black ones are those without. The dotted and dashed lines correspond to $E(B-V)_* = E(B-V)_{\rm gas}$ (Erb *et al.* 2006b) and $E(B-V)_* = 0.44E(B-V)_{\rm gas}$ (Calzetti *et al.* 2000), respectively.

from an HII region, the two FWHMs should be similar. However, $\mathrm{FWHM_{int}(Ly\alpha)}$ is systematically larger than FWHM(neb), $\mathrm{FWHM_{int}(Ly\alpha)} \gtrsim$ FWHM(neb). Additional scattering of Lyα photons in an $\mathrm{H_{II}}$ region due to residual $\mathrm{H_I}$ atoms in it may be at work. Assuming a static $\mathrm{H_{II}}$ region with a neutral hydrogen column density of $\log(\mathrm{N_{HI}}) \lesssim 17.0$, corresponding to the unity optical depth for ionizing photons, $\tau_{\rm ion} \lesssim 1$ (cf., Verhamme *et al.* 2014), $\mathrm{FWHM_{int}(Ly\alpha)}$ can be broadened by 200 km s^{-1} compared to FWHM(neb). As can be seen from Figure 4.8, while this additional broadening would help explain the discrepancy of the one-to-one relation for the non blue bump objects, it is still not enough for the blue bump objects. We discuss some interpretations for the huge $\mathrm{FWHM_{int}(Ly\alpha)}$ in the blue bump objects in §5.1.

In §4.2.2, we have argued that transferring a whole line of a Gaussian and a continuum

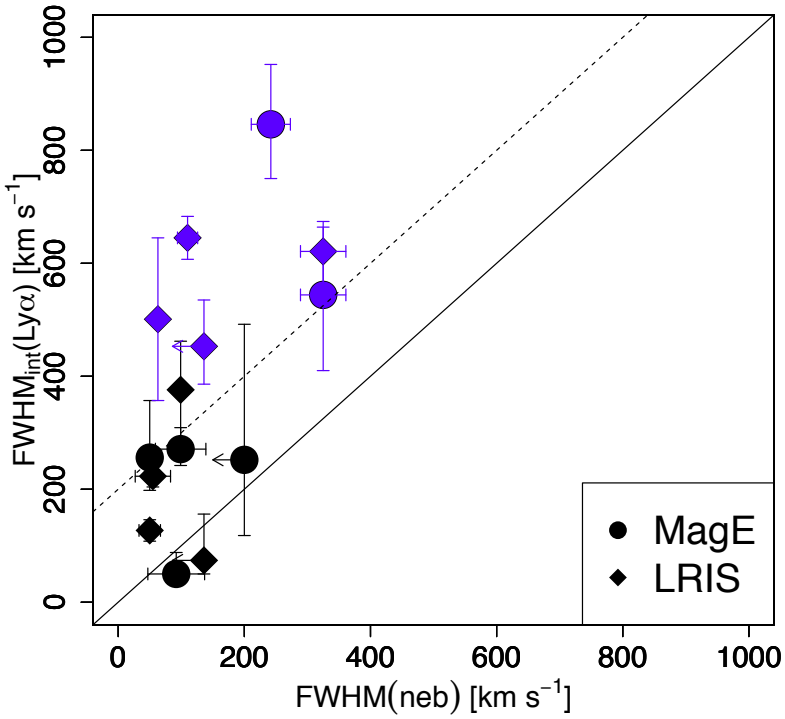

Figure 4.8. FWHM$_{\rm int}$(Lyα) plotted against FWHM(neb) for all the sample. The meaning of the symbol and the color is the same as those in Figure 4.7. The solid line shows the one-to-one relation between the two FWHMs, while the dotted line is a relation between the two after taking into account the additional scattering of Lyα photons by residual H$_{\rm I}$ atoms in an H$_{\rm II}$ region, FWHM$_{\rm int}$(Lyα) = FWHM(neb) + 200.

instead of a chromatic line is important to reproduce the blue bump. To demonstrate this, we perform Lyα profile fitting of the blue bump objects with fixing FWHM$_{\rm int}$(Lyα) = FWHM(neb). The blue bump is poorly reproduced as shown in Figure 4.9, indicating that the flux and position of the blue bump can not be reproduced well if fitted with a monochromatic line. We examine if the derived best-fit model parameters differ between the free and fixed FWHM$_{\rm int}$(Lyα) cases. While there is no systematic difference in the two cases for $V_{\rm exp}$ and $N_{\rm HI}$, we find that b ($\tau_{\rm a}$) becomes large (small) in the fixed FWHM$_{\rm int}$(Lyα) case. This would be related to the intrinsic degeneracy between them discussed in §4.3.

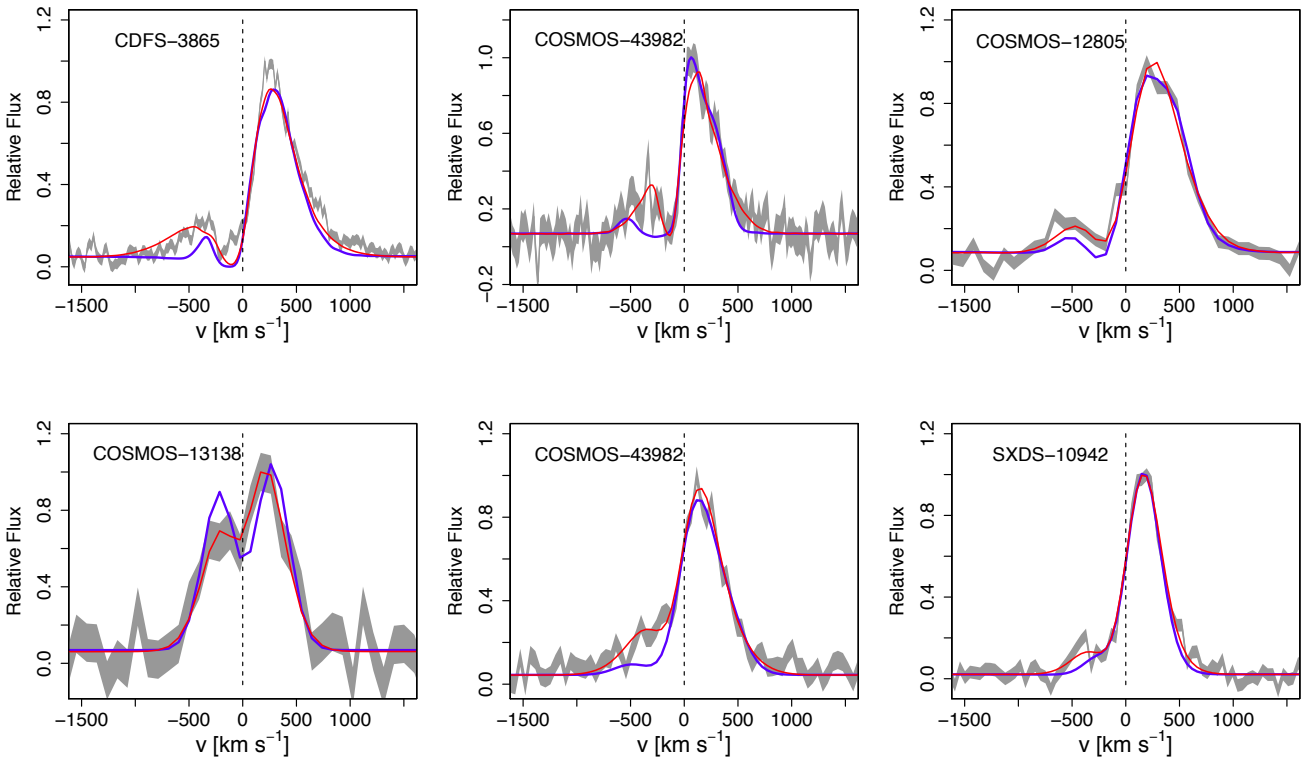

Figure 4.9. The same as Figure 4.2, but for the blue bump with fixing $\mathrm{FWHM_{int}(Ly\alpha)}$ = FWHM(neb). Blue lines are reproduced Lyα lines with a fixed $\mathrm{FWHM_{int}(Ly\alpha)}$, while red lines are those with a free $\mathrm{FWHM_{int}(Ly\alpha)}$.

4.4.4 Equivalent Width: EW(Lyα) vs. $\mathrm{EW_{int}(Ly\alpha)}$

Figure 4.10 plots the observed EW(Lyα) against the best fit intrinsic EW(Lyα) obtained from the Lyα fitting, $\mathrm{EW_{int}(Ly\alpha)}$. Since we have modeled Lyα emission lines that entered through the slit, we use EW(Lyα) values measured from spectra as the observed EW(Lyα). All the data points are expected to lie above the one-to-one relation, $\mathrm{EW_{int}(Ly\alpha)} \gtrsim \mathrm{EW(Ly\alpha)_{spec}}$. This is because we have used the uniform shell model which does not cause a EW(Lyα) boost unlike clumpy shell models (cf., Neufeld 1991; Laursen *et al.* 2013; Duval *et al.* 2014). As can be seen, all the data points satisfy the criteria within the 1σ uncertainty.

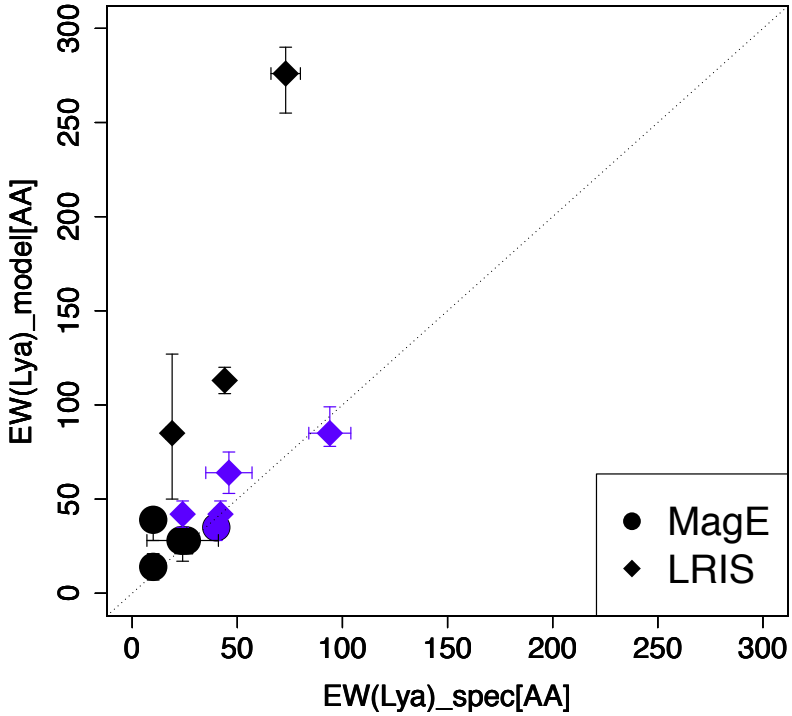

Figure 4.10. $EW_{int}(Ly\alpha)$ plotted against $EW(Ly\alpha)$ obtained from spectroscopy. The meaning of the symbol and the color is the same as those in Figure 4.7. Since we have assumed the uniform shell model which does not cause a $EW(Ly\alpha)$ boost, the data points are expected to lie above the one-to-one relation.

Chapter 5

Discussion

5.1 Mystery of the Blue Bump Objects

As described in previous sections, $\mathrm{FWHM_{int}(Ly\alpha)}$ significantly larger than FWHM(neb) is required to well reproduce Lyα profiles with the blue bump. As seen in Figure 4.9, the position and the flux of the blue bump is poorly reproduced if we fix $\mathrm{FWHM_{int}(Ly\alpha)}$ = FWHM(neb).

In this section, we first examine if there are any characteristic properties for the blue bump objects, then discuss the origin of the large discrepancy between $\mathrm{FWHM_{int}(Ly\alpha)}$ and FWHM(neb).

5.1.1 Any Difference in Properties between the Blue Bump and the Non Blue Bump Objects ?

In §4.2.2, we have shown that $\mathrm{FWHM_{int}(Ly\alpha)}$ is the only significant difference in model parameters between the two subsamples. Here we also examine the difference between them in observational properties such as stellar mass, Lyα luminosity, morphological ellipticity, and the presence of a merger.

First, it is possible that all objects intrinsically have the blue bump but we have lost them in objects with a faint Lyα luminosity and/or small stellar mass. Lyα luminosity, L(Lyα), of the blue bump sample ranges $\mathrm{L(Ly\alpha)} = 0.3 - 29.8$ (10^{42} erg s^{-1}) with a mean value of 8.8 ± 5.6 (10^{42} erg s^{-1}), whereas that of the non-blue bump sample ranges $\mathrm{L(Ly\alpha)}$ $= 0.5 - 15.4$ (10^{42} erg s^{-1}) with a mean 7.0 ± 2.1 (10^{42} erg s^{-1}). This indicates that the two subsamples have similar Lyα luminosities. Likewise, stellar mass, M_*, of the blue bump sample ranges $\log(M_*) = 7.73 - 10.80$ ($M_\odot$), with a mean value of 9.4 ± 0.5 ($M_\odot$),

whereas that of the non-blue bump sample ranges $\log(M_*) = 7.84 - 10.06$ $(M_\odot)$, with a mean value of 9.3 ± 0.3 $(M_\odot)$. Thus, stellar masses in these subsamples are identical to with each other.

Second, objects with the blue bump would more likely to be seen edge-on than those without. Recent theoretical studies (Verhamme *et al.* 2012; Zheng & Wallace 2014) have investigated the inclination effects to the Lyα emissivity and profile. These studies have shown that the blue bump flux relative to the total Lyα flux is enhanced with an increasing ellipticity. Indeed, the Lyα profile seen edge-on is similar to the one reproduced in the static gas cloud in the uniform shell. This is because outflowing gas is more likely to be blown out perpendicular to the galaxy disk, reducing the relative outflow velocity toward the disk direction. As seen in Table 3.5, there are three objects whose ellipticity has been measured. Due to the small number of objects, we cannot determine if there is any difference between the two subsamples.

And finally, as discussed in Kulas *et al.* (2012) and Chonis *et al.* (2013), a galaxy merger can be the origin of the blue bump. In this case, both the redder and bluer Lyα emission components correspond to those from two objects, respectively (see also Cooke *et al.* 2010; Rauch *et al.* 2011). As described in §3.3 (Table 3.5), the presence of a merger has been examined in seven out of the eight COSMOS objects. The result that merger rate is quite low among the sample imply that this scenario is unlikely, at least for the present sample.

We note here the observational results of Erb *et al.* (2010) and Heckman *et al.* (2011). These studies have found that objects with the blue bump in a Lyα line tend to have a low covering fraction of the neutral gas measured by LIS absorption lines. Among the sample, due to the small number of objects whose LIS absorption lines have been detected, we cannot investigate this.

We conclude that there is no significant difference in Lyα luminosity, stellar mass, morphological ellipticity, and the presence of a merger between the two subsamples.

In the future, to understand the origin of the blue bump, the sample whose Lyα and absorption line velocity properties as well as the morphological ones are simultaneously examined should be increased.

5.1.2 Possible Explanations for Large $\mathrm{FWHM_{int}}$ in Blue Bunp Objects

In this subsection, we explore some possible explanations of the large discrepancy between the two FWHMs in the blue bump objects.

First, it is possible that the observed Lyα photons are produced not only from recombination of hydrogen gas ionized in HII regions, but also from e.g., shock heating, fluorescence (e.g., Cantalupo *et al.* 2012, 2014), and/or gravitational cooling (e.g., Dijkstra *et al.* 2006). If these are taken into account, the huge FWHM$_{\rm int}$(Lyα) in the blue bump objects could be explained. Especially, fluorescence caused by QSO would ionize the outer layer of the neutral gas in the ISM, and produce the large FWHM$_{\rm int}$(Lyα). However, we have checked that there are no QSO around the sample. Gravitational cooling can also lead the large FWHM$_{\rm int}$(Lyα) because it is occurred at both the inner and outer regions of a galaxy. The flux ratio between Lyα and Hα lines produced by cooling radiation is F(Lyα)/F(Hα) $\sim$ 100, which is significantly larger than that in Case-B recombination, $\sim$ 8.7 (Dijkstra 2014). Furthermore, gravitational cooling can enhance the observed blue bump flux (e.g., Dijkstra *et al.* 2006). Thus, the large FWHM$_{\rm int}$(Lyα) in the blue bump objects could be due to gravitational cooling. One might think that, if this scenario is the case, the observed flux ratio between Ly and Hα should be F(Lyα)/F(Hα) $\sim$ 100. Two objects with a blue bump, CDFS-3865 and COSMOS-43982, have both Lyα and Hα measurements (Hashimoto *et al.* 2013; Nakajima *et al.* 2013). We calculate the flux ratio to be $\sim$ 2 (CDFS-3865) and $\sim$ 5 (COSMOS-43982), which are too low at first glance. However, as we describe below, this is not true. Yajima *et al.* (2012) have theoretically examined the Lyα flux ratio between that generated from photoionization and gravitational cooling for progenitors of a local L^* galaxy. They have shown that the ratio at $z \sim 2$ is $F(\mathrm{Ly}\alpha)_{\rm photo}/F(\mathrm{Ly}\alpha)_{\rm cooling} = 2/3$. Assuming this ratio, one can obtain the intrinsic Lyα/Hα flux ratio to be F(Lyα)/F(Hα) = ($F(\mathrm{Ly}\alpha)_{\rm photo}$ + $F(\mathrm{Ly}\alpha)_{\rm cooling}$) / ($F(\mathrm{H}\alpha)_{\rm photo}$ + $F(\mathrm{H}\alpha)_{\rm cooling}$) = ($F(\mathrm{Ly}\alpha)_{\rm photo}$ + 3/2 $\times$F($Ly\alpha$)$_{\rm photo}$) / ($F(\mathrm{Ly}\alpha)_{\rm photo}$/8.7 + 3/2 $\times$F($Ly\alpha$)$_{\rm photo}$/100) $\sim$ 20. Thus, the dust extinction and/or geometry effect could reproduce the observed line ratio of $\sim$ 2 and $\sim$ 5 if we assume Lyα escape fraction of $\sim 10-25\%$.

Second, throughout the paper, we have assumed the expanding shell model with a single point Lyα source centered at the shell. The more realistic configuration would be the extended Lyα source, e.g., an uniform Lyα emissivity in the shell. In this case, the blue bump photons can more easily escape from the galaxy without a large FWHM$_{\rm int}$(Lyα) (e.g., Verhamme *et al.* 2006). This is one of the mechanism which can fulfill the first situation: a combination of photoionization and gravitational cooling would result in the more extended Lyα source. In addition, the Lyα surface brightness profile, which can not be reproduced by the expanding shell model with a point Lyα source, can be well

reproduced in the extended Lyα source case (Rauch *et al.* 2011; Barnes *et al.* 2011). Thus, this could be another explanation for the large discrepancy.

Finally, in previous sections, we have assumed that the intrinsic Lyα profile is a Gaussian. However, as described in §3.1.5, COSMOS-13138 and SXDS-10600 show the [OIII] line with the secondary blueshifted and redshifted component, respectively. It is possible that a Lyα line also have a non Gaussian profile. This could help reproducing the profile without a large $\mathrm{FWHM_{int}}$(Lyα). To address this point, we perform a Lyα radiative transfer calculation for COSMOS-13138 assuming that the intrinsic Lyα profile has exactly the same profile as that of the two component [OIII] line. The resultant profile is poorly reproduced.

While the exact origin of the discrepancy is not clear, the first two explanations could be tested by very deep IFU spectroscopy observations in the future.

5.2 Origin of Small $\Delta v_{\mathrm{Ly}\alpha,\mathrm{r}}$

As described in §3.1.3, the mean $\Delta v_{\mathrm{Ly}\alpha,\mathrm{r}}$ value in LAEs is $\simeq 200$ km s^{-1}, significantly smaller than that of LBGs, $\Delta v_{\mathrm{Ly}\alpha,\mathrm{r}} \simeq 400$ km s^{-1} (LBGs; e.g., Steidel *et al.* 2010; Rakic *et al.* 2011; Kulas *et al.* 2012; Schenker *et al.* 2013, LAEs; e.g., McLinden *et al.* 2011; Hashimoto *et al.* 2013; Chonis *et al.* 2013; Shibuya *et al.* 2014a; Erb *et al.* 2014). We have also demonstrated that some LAEs have an extremely small $\Delta v_{\mathrm{Ly}\alpha,\mathrm{r}}$ value $\lesssim 100$ km s^{-1}.

Hashimoto *et al.* (2013) have examined the relation between $\Delta v_{\mathrm{Ly}\alpha,\mathrm{r}}$ and two observables, SFR and velocity dispersion, for a small sample of LAEs. They have argued that $\Delta v_{\mathrm{Ly}\alpha,\mathrm{r}}$ weakly correlates with both quantities. Based on a larger sample, Shibuya *et al.* (2014a) have also examined the relation between $\Delta v_{\mathrm{Ly}\alpha,\mathrm{r}}$ and three quantities, SFR, stellar mass, specific SFR, and dust extinction. Thanks to the large number of objects, they find that $\Delta v_{\mathrm{Ly}\alpha,\mathrm{r}}$ strongly correlates with SFR and stellar mass. In addition, Erb *et al.* (2014) have recently found that $\Delta v_{\mathrm{Ly}\alpha,\mathrm{r}}$ correlates with velocity dispersion. Furthermore, they have found that objects with a small $\Delta v_{\mathrm{Ly}\alpha,\mathrm{r}}$ value have a large fraction of emission blueward of the systemic velocity, while the red wing of the Lyα profile and the outflow velocity traced by absorption lines remain unchanged. Following these findings, they have argued that the small $\Delta v_{\mathrm{Ly}\alpha,\mathrm{r}}$ in LAEs is consistent with a scenario where opacity to Lyα photons is reduced by the bulk motion and/or covering fraction of the gas near the systemic velocity (see also Steidel *et al.* 2010). These results suggest that $\Delta v_{\mathrm{Ly}\alpha,\mathrm{r}}$ is closely related with the physical size of the galaxy system. However, discussion in these studies

remains qualitative, and that no definitive conclusions have been obtained.

In this section, using the largest sample of LAEs whose high-quality spectroscopy data and several properties have been obtained, we explore the origin of the small $\Delta v_{\mathrm{Ly}\alpha,\mathrm{r}}$ in LAEs based on comparisons with the results of radiative transfer models. The theoretical expectation is that four hypothesis are possible for the $\Delta v_{\mathrm{Ly}\alpha,\mathrm{r}}$ as small as $0 - 200$ km s^{-1}: a high-speed galactic outflow in a galaxy (e.g., Verhamme *et al.* 2006), a peculiar clumpy ISM with an unity covering fraction, $CF = 1$ (e.g., Neufeld 1991; Laursen *et al.* 2013; Duval *et al.* 2014), an inhomogeneous ISM with holes/cavities, i.e., $CF < 1$, (e.g., Behrens *et al.* 2014; Verhamme *et al.* 2014), and an ISM with an extremely low neutral hydrogen column density (e.g., Verhamme *et al.* 2006, 2014).

5.2.1 High Outflow Velocity

An outflow velocity larger than $V_{\mathrm{exp}} \sim 300$ km s^{-1} can reduce $\Delta v_{\mathrm{Ly}\alpha,\mathrm{r}}$ because Lyα photons would drop out of resonance with HI atoms in outflowing gas (e.g., Verhamme *et al.* 2006, 2014). However, our results of Lyα radiative transfer fitting in §4.2.2 show that all of the sample have small V_{exp} values of $100 - 200$ km s^{-1}. Combined with the findings in §4.4.1 that these V_{exp} are consistent with observables for the three individual spectra and the stacked spectrum, we conclude that the high outflow velocity hypothesis is unlikely. The result is summarized in the column 2 in Table 5.1.

5.2.2 Special Inhomogeneous ISM Condition

It is possible that the gas distribution in LAEs is inhomogeneous. Duval *et al.* (2014) have theoretically shown that if a galaxy has a peculiar inhomogeneous ISM with $CF = 1$, $\Delta v_{\mathrm{Ly}\alpha,\mathrm{r}}$ can be as small as ~ 0 km s^{-1}. They have studied the radiative transfer of Lyα and UV photons in an inhomogeneous clumpy ISM to understand the physical condition under which the observed EW(Lyα) being enhanced compared to the intrinsic EW(Lyα) (e.g., Neufeld 1991). In Duval *et al.* (2014), a revised geometry has been applied to the code constructed by Verhamme *et al.* (2006) and Schaerer *et al.* (2011), and is characterized by additional three parameters: clump volume filling factor, density contrast in HI between clumps and the interclump medium, $n_{\mathrm{IC}}/n_{\mathrm{C}}$, and covering factor of the gas, CF. The geometry of the clumps and inter clump medium in the code is illustrated in Figures 1, 5, and 8 in Duval *et al.* (2014). They have shown that if the ISM with $CF = 1$ is almost static ($V_{\mathrm{exp}} \lesssim 200$ km s^{-1}), extremely clumpy with a high density contrast in HI between clumps

and interclump medium ($n_{\rm IC}/n_{\rm C} \sim 0-0.01$), and very dusty ($E(B-V)_{\rm gas} > 0.30$), a Ly$\alpha$ profile becomes a symmetric Gaussian with $\Delta v_{{\rm Ly}\alpha,{\rm r}} \sim 0$ km s^{-1} (see the right bottom panel of Figure 15 in Duval *et al.* 2014). In addition, if these conditions are fulfilled, the EW(Lyα) boost, ${\rm EW_{obs}(Ly}\alpha) > {\rm EW_{int}(Ly}\alpha)$, can be achieved. This is because Lyα photons can be resonantly scattered on the surface of clouds without being absorbed by dust grains shielded by HI gas, whereas optically thin continuum photons are absorbed by dust (cf., Hansen & Oh 2006; Laursen *et al.* 2013).

We examine this hypothesis using the weighted skewness, $S_{\rm w}$ calculated in §3.1.2 (see also the column 5 in Table 3.1). A symmetric line as is the case of the peculiar ISM has $S_{\rm w} \sim 0$. MagE-COSMOS-08501, LRIS-COSMOS-08357, LRIS-COSMOS-43982, and LRIS-COSMOS-13138 have $S_{\rm w} \sim 0$ within the 1 σ uncertainty. The negative $S_{\rm w}$ of LRIS-COSMOS-43982 is due to its merged blue bump, as described in §3.1.2. As can be seen in Figure 3.1.2, the Lyα profile of LRIS-COSMOS-13138 is not a Gaussian but a symmetric double-peaked profile centered at 1216Å, which is a characteristic of a static gas cloud in the uniform shell. Thus, the peculiar inhomogeneous ISM hypothesis is unlikely for this object. On the other hand, the Lyα profiles of MagE-COSMOS-08501 and LRIS-COSMOS-08357 are single peaked with a very small $\Delta v_{{\rm Ly}\alpha,{\rm r}}$ value of 82 ± 40 and 106 ± 71 km s^{-1}, respectively. The hypothesis could be possible for these two objects.

For a further discussion, we use the results from the SED fitting (Table 3.4). Stellar dust extinction values are $E(B-V)_* = 0.08^{+0.04}_{-0.08}$ (COSMOS-08501) and $0.14^{+0.05}_{-0.05}$ (COSMOS-08357), both of which are too low for the peculiar inhomogeneous ISM hypothesis. While the dust extinction values may exclude the peculiar ISM hypothesis, we note here that an extremely high ${\rm EW(Ly}\alpha)_{\rm photo}$ in COSMOS-08501, ${\rm EW(Ly}\alpha)_{\rm photo} = 280 \pm 30$ Å, could be due to the EW(Lyα) boost in the peculiar ISM. To summarize, none of the sample satisfies the peculiar ISM hypothesis well. However, we find that the small $\Delta v_{{\rm Ly}\alpha,{\rm r}}$ in the two objects, MagE-COSMOS-08501 and LRIS-COSMOS-08357, might be explained by this hypothesis. The result is summarized in the column 3 in Table 5.1.

5.2.3 Covering Fraction below Unity or ISM Gas with Holes

Recently, Jones *et al.* (2013) have found that the neutral gas covering fraction is lower for LBGs with strong Lyα emission. If this is also the case for LAEs, the gas distribution in LAEs may be patchy, i.e., $CF < 1$. In this case, Lyα photons can directly escape from a galaxy. This would dramatically increase the Lyα flux at the line center, and

Table 5.1. Summary of the origin of the small $\Delta v_{\mathrm{Ly}\alpha,\mathrm{r}}$ in LAEs

Object	High outflow velocity	Peculiar ISM with $CF = 1$	Patchy ISM with $CF < 1$	Uniform ISM with low N_{HI}
(1)	(2)	(3)	(4)	(5)
CDFS-3865	no	no	no	possible
CDFS-6482	no	no	no	possible
COSMOS-08501	no	might be possible	no	possible
COSMOS-30679	no	no	no	possible
COSMOS-43982	no	no	possible	possible
COSMOS-08357	no	might be possible	possible	possible
COSMOS-12805	no	no	no	possible
COSMOS-13138	no	no	no	possible
COSMOS-38380	no	no	no	possible
SXDS-10600	no	no	no	possible
SXDS-10942	no	no	no	possible

Notes.—

decrease the $\Delta v_{\mathrm{Ly}\alpha,\mathrm{r}}$ as we describe below. The neutral gas CF in Jones *et al.* (2013) has been inferred from EW of LIS absorption lines obtained at a high spectral resolution (FWHM$\simeq$ 70 km s^{-1}). Among the sample, three objects, COSMOS-12805, COSMOS-13636, and SXDS-10600, have LIS absorption lines obtained by LRIS. CF of these objects have been measured in Shibuya *et al.* (2014a), all of which are calculated to be below unity. However, some studies point out that CF measurements strongly depend on the spectral resolution (e.g., Prochaska 2006 and private communication with M. Dessauges-Zavadsky).

Therefore, we instead use the results of radiative transfer models to examine the low CF hypothesis. Recently, Behrens *et al.* (2014) and Verhamme *et al.* (2014) have investigated the Lyα radiative transfer in a neutral gas with holes and/or cavities, i.e., $CF < 1$. The aim of these studies is to examine if there is a characteristic Lyα profile of objects with ionizing photons leaking. These studies have shown that, if a galaxy has the ISM with holes, Lyα photons escape from a galaxy either (1) directly from holes in the neutral gas and/or (2) after being diffused in the ISM. The first results in a main symmetric Gaussian profile with $\Delta v_{\mathrm{Ly}\alpha,\mathrm{r}} = 0$ km s^{-1}, whereas the second results in a secondary asymmetric redshifted (and blue-shifted) profile. At an infinite spectral resolution as is the case for the simulations, the hole gas hypothesis can be examined by the presence of the main peak at $v = 0$ km s^{-1}. However, at a finite resolution as is the case for the observations, the main peak could not be distinguished from the secondary peak.

We test the hypothesis as follows. First, we calculate a typical $\Delta v_{\mathrm{Ly}\alpha,\mathrm{r}}$ for the patchy ISM utilizing the code constructed by Verhamme *et al.* (2014). Figure 5.1 plots $\Delta v_{\mathrm{Ly}\alpha,\mathrm{r}}$ against CF for various spectral resolutions. The model parameters used are $V_{\mathrm{exp}} = 150$ km s^{-1}, $\log(N_{\mathrm{HI}}) = 20.0$ cm^{-2}, $\tau_{\mathrm{a}} = 1.0$, $b = 20$ km s^{-1}, $\mathrm{EW}_{\mathrm{int}}(\mathrm{Ly}\alpha) = 100$ Å, and $\mathrm{FWHM}_{\mathrm{int}}(\mathrm{Ly}\alpha) = 200$ km s^{-1}. As can be seen, $\Delta v_{\mathrm{Ly}\alpha,\mathrm{r}}$ suddenly drops at $CF < 1.00$, and becomes smaller than $\Delta v_{\mathrm{Ly}\alpha,\mathrm{r}} \sim 50$ (150) km s^{-1} for the MagE (LRIS) resolution at $CF < 0.90$. Although the result is obtained for one particular parameter set, it would not be changed even if we choose different model parameters. For example, as shown in the right panel of Figure 5 in Verhamme *et al.* (2014), the $\Delta v_{\mathrm{Ly}\alpha,\mathrm{r}}$ value is not sensitive to V_{exp}. Furthermore, due to the fact that Lyα photons tend to escape directly from holes instead of after being diffused in the ISM, increasing N_{HI} does not increase $\Delta v_{\mathrm{Ly}\alpha,\mathrm{r}}$. Thus, we infer that the objects with $\Delta v_{\mathrm{Ly}\alpha,\mathrm{r}} \lesssim 50$ (150) km s^{-1} could be explained by the patchy ISM hypothesis. Among the sample, nine spectra, MagE-CDFS-6482, MagE-COSMOS-08501, MagE-COSMOS-43982, LRIS-COSMOS-08357, LRIS-COSMOS-12805, LRIS-COSMOS-13138, LRIS-COSMOS-13636, LRIS-COSMOS-43982, and LRIS-SXDS-10942 satisfy the criterion.

Second, we compare the Lyα profile with those of nebular emission lines. In the case of the patchy ISM with $CF < 0.90$, the profile of the observed Lyα line would be indistinguishable from that of nebular emission lines. This is because the main Lyα component is not affected by the radiative transfer effect very much. As can be seen in Figures 3.1.2 and 3.1.2, among the nine spectra above, COSMOS-08357 and COSMOS-43982 satisfy the criterion.

Thus, we conclude that the small $\Delta v_{\mathrm{Ly}\alpha,\mathrm{r}}$ in the two objects, COSMOS-08357 and COSMOS-43982, could be explained by the low covering fraction hypothesis. The result is summarized in the column 4 in Table 5.1.

5.2.4 Low N_{HI}

Finally, we examine the low N_{HI} hypothesis. Although it is difficult to directly measure N_{HI} in LAEs from observations, we have inferred them using Lyα radiative transfer model (§4.2.2). If we exclude the blue bump objects from the sample, modeled Lyα profiles and parameters are all consistent with the observed Lyα profiles and observables. Thus, we assume that N_{HI} is also of reliable. Figure 5.2 is a plot of $\Delta v_{\mathrm{Ly}\alpha,\mathrm{r}}$ against $\log(N_{\mathrm{HI}})$ for the non-blue bump objects. We add results from the literature, Verhamme *et al.* (2008);

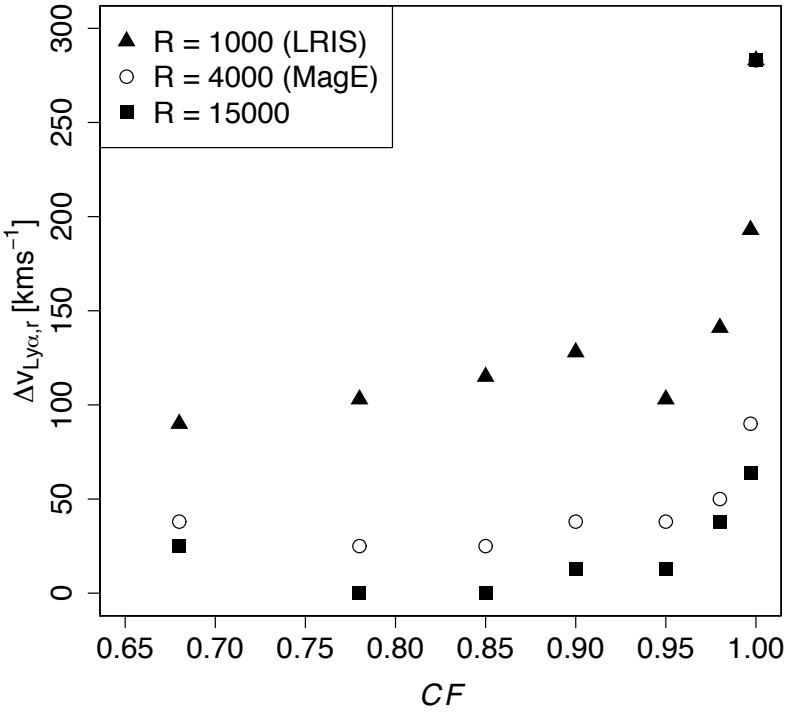

Figure 5.1. $\Delta v_{\mathrm{Ly}\alpha,\mathrm{r}}$ plotted against the covering fraction of the neutral gas, CF, for the three spectral resolutions. The result is obtained for a particular parameter set, V_{exp} = 150 km s^{-1}, $\log(N_{\mathrm{HI}})$ = 20.0 cm^{-2}, τ_{a} = 1.0, b = 20 km s^{-1}, $\mathrm{EW_{int}(Ly}\alpha)$ = 100 Å, and $\mathrm{FWHM_{int}(Ly}\alpha)$ = 200 km s^{-1}.

Vanzella *et al.* (2010); Dessauges-Zavadsky *et al.* (2010). These authors have also utilized the model used in this study for $z \sim 3$ LBGs with various EW(Lyα) (Verhamme *et al.* 2008), a strongly lensed LBG with Lyα absorption at $z \sim 2.73$ (MS 1512-cB58) (Schaerer & Verhamme 2008), a peculiar $z = 5.56$ [NIV emitter with EW(Lyα) = 89Å(Vanzella *et al.* 2010), and a lensed LBG with Lyα absorption, "the 8 o'clock arc" (Dessauges-Zavadsky *et al.* 2010). We also add the results of Kulas *et al.* 2012 and Chonis *et al.* (2013), although the models used in these studies are different from the ones used in the studies above. In the figure, motivated by their properties not by their selection, we have colored objects with EW(Lyα) $\gtrsim$ 30 Å in red and have labeled them as LAEs.

The figure shows a clear correlation between $\log(N_{\mathrm{HI}})$ and $\Delta v_{\mathrm{Ly}\alpha,\mathrm{r}}$. As described in §4.2.2, the mean $\log(N_{\mathrm{HI}})$ in $z \sim 2$ LAEs is $\log(N_{\mathrm{HI}})$= 18.3, which is more than one order of magnitude lower than those of $z \gtrsim 3$ LBGs, $\sim$ 20.0. Although we have excluded the blue bump objects in Figure 5.2 for the secure discussion, we note that they also have

comparable $N_{\rm HI}$ values, and are consistent with the correlation. We conclude that the small $\Delta v_{{\rm Ly}\alpha,{\rm r}}$ in the LAEs can be well explained by the low $N_{\rm HI}$ hypothesis.

The results are summarized in the column 5 in Table 5.1 We note that the second and third hypotheses are examined only qualitatively, while the first and fourth are both qualitatively and quantitatively. A future detailed Lyα modeling with clumpy shell models and/or patchy ISM models as well as the high resolution Lyα data would help the definitive conclusion.

5.3 Interpretation of Low $N_{\rm HI}$

As described in §5.2, the small $\Delta v_{{\rm Ly}\alpha,{\rm r}}$ in the sample can be well explained by the low $N_{\rm HI}$ hypothesis. In this section, we present three possible scenarios for LAEs to have a low $N_{\rm HI}$.

First, it is possible that LAEs have a small amount of HI gas mass. Indeed, Pardy *et al.* (2014) have detected an HI 21cm line for 14 local galaxies with Lyα emission (Lyman Alpha Reference Sample; Östlin *et al.* 2014), to find that the derived HI gas mass tentatively anti-correlates with EW(Lyα). The trend is also consistent with theoretical predictions (private communications with T. Garel and C. Lagos).

Second, if a galaxy has a high gas ionization state, ionizing photons would efficiently ionize the neutral gas in the ISM. This would decrease the thickness of the HI gas in the shell, and lower their $N_{\rm HI}$. This picture is consistent with the recent findings of Nakajima & Ouchi (2014), who have demonstrated that LAEs have a significantly higher ionization state than those of LBGs at a given redshift. The high ionization state in LAEs would be due to their young stellar populations (e.g., Pirzkal *et al.* 2007; Ono *et al.* 2010a,b). Young O- and B type stars in LAEs would efficiently produce ionizing photons, and lower their $N_{\rm HI}$.

Finally, it is possible that LAEs tend to be face-on galaxy. Theoretical studies have shown that an apparent $N_{\rm HI}$ is decreased when a galaxy is seen face-on (e.g., Verhamme *et al.* 2012; Zheng & Wallace 2014). This is because Lyα photons transversing perpendicular to a galaxy disk would suffer less number of scattering. Indeed, Shibuya *et al.* (2014b) have statistically examined the ellipticity, a useful tracer of the inclination of a galaxy, for $z \sim 2$ LAEs using *HST* data. A weak trend has been found that high EW(Lyα) objects tend to have a small ellipticity, suggesting that LAEs tend to be face-on galaxies.

A combination of these effects would result in a small number of Lyα photon scattering.

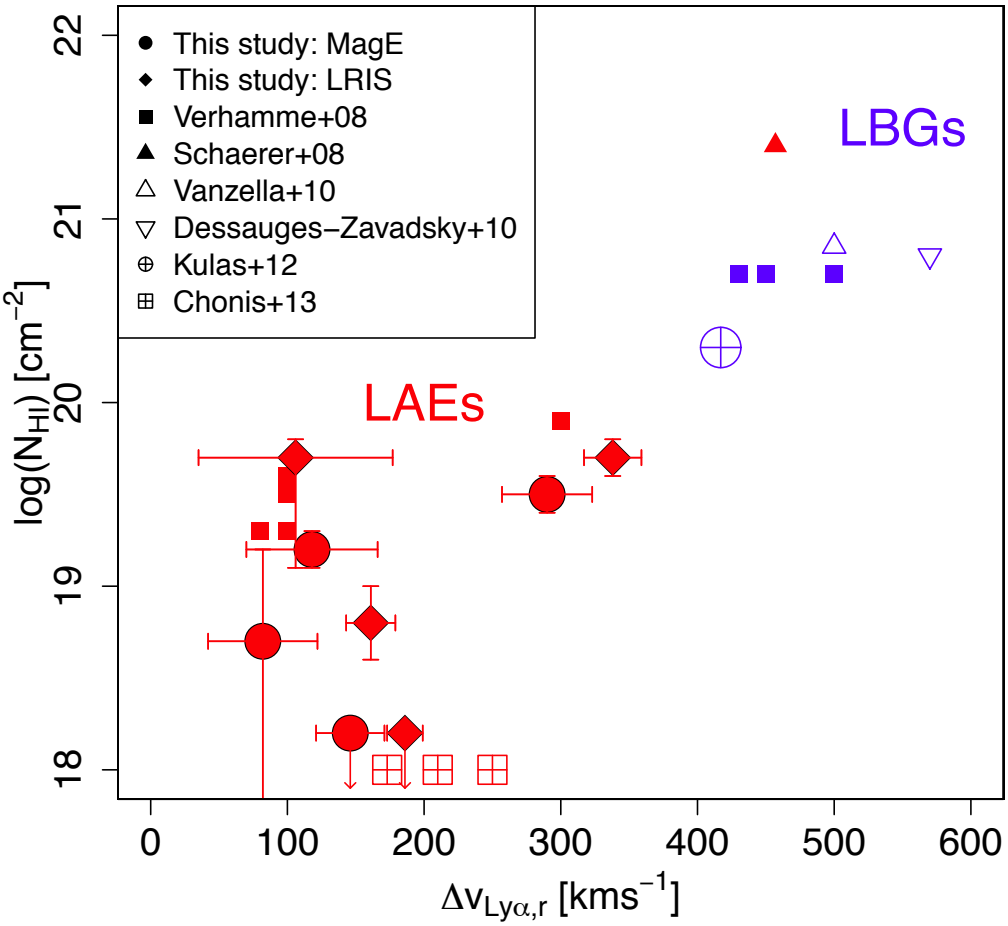

Figure 5.2. log($N_{\rm HI}$) plotted against $\Delta v_{\rm Ly\alpha,r}$. Red (blue) symbols corresponds to objects with EW(Lyα)$_{\rm photo}$ larger (lower) than 30 Å. Filled circles and diamonds are the non blue bump LAEs obtained by MagE and LIRS, respectively. Filled squares show $z \sim 3$ objects given by Verhamme *et al.* (2008). A filled triangle denotes a $z = 5.56$ [NIV emitter with EW(Lyα) = 89Å(Vanzella *et al.* 2010). An open triangle is a lensed LBG with Lyα absorption, cB58 (Schaerer & Verhamme 2008), while an inverted triangle is a lensed LBG with Lyα absorption, "the 8 o'clock arc" (Dessauges-Zavadsky *et al.* 2010). In addition, the objects studied in kulas2012 and Chonis *et al.* (2013) are denoted as a circle and three squares with a cross inside.

This would in turn decrease the Lyα velocity offset, $\Delta v_{\mathrm{Ly}\alpha,\mathrm{r}}$ (e.g., McLinden *et al.* 2011; Hashimoto *et al.* 2013; Erb *et al.* 2014) and the Lyα spatial offset, $\delta_{\mathrm{Ly}\alpha}$ (Jiang *et al.* 2013; Shibuya *et al.* 2014b).

5.4 Implications for Reionization Studies

5.4.1 An Implication for Epoch of Reionization

We have demonstrated that the average $\Delta v_{\mathrm{Ly}\alpha}$ in LAEs is $\sim$ 200 km s^{-1}, which is significantly smaller than that in LBGs (§3.1.3). This result is important not only for understanding the physical origin of Lyα emission in galaxies, but also for probing cosmic reionization with LAEs. If LAEs at $z > 6$ have similarly small $\Delta v_{\mathrm{Ly}\alpha,\mathrm{r}}$ values, the amount of Lyα photons scattered by the IGM, as used to constrain the epoch of reionization, may be in need of revision. For example, Santos (2004) has examined the transmission through the IGM of Lyα photons emitted from a galaxy for two cases, $\Delta v_{\mathrm{Ly}\alpha,\mathrm{r}} = 0$ and 360 km s^{-1}, the latter of which is comparable to the average $\Delta v_{\mathrm{Ly}\alpha,\mathrm{r}}$ of $z \sim 2$ – 3 LBGs. Some recent reionization studies using LAEs assume the latter case to estimate the neutral hydrogen fraction of the IGM, x_{HI}, at $z > 6$ (e.g., Kashikawa *et al.* 2006; Ota *et al.* 2008; Ouchi *et al.* 2010; Kashikawa *et al.* 2011). However, if $z > 6$ LAEs have $\Delta v_{\mathrm{Ly}\alpha,\mathrm{r}}$ as small as $\simeq$ 200 km s^{-1}, these studies may be overestimating x_{HI}. Similarly, Ono *et al.* (2012), Schenker *et al.* (2012), and Pentericci *et al.* (2011) have derived x_{HI} as large as $\sim$ 40 – 60% from a significant drop in the fraction of large-EW(Lyα) galaxies from $z \sim 6$ to 7. If such a high value were correct, reionization would take place very late, which cannot easily be reconciled with constraints from the Lyman alpha forest opacity (Becker *et al.*, 2007) or the large value of the Thomson optical depth, $\tau = 0.09$, obtained by WMAP observations (Dunkley *et al.*, 2009; Komatsu *et al.*, 2011). Future Lyα emission models for reionization studies would need to use our result of a small average $\Delta v_{\mathrm{Ly}\alpha,\mathrm{r}}$ value if $\Delta v_{\mathrm{Ly}\alpha,\mathrm{r}}$ does not significantly evolve over cosmic time.

5.4.2 An Implication for Ionization Sources

Related to the discussion in §5.2.3, recent patchy ISM radiative transfer models (Behrens *et al.* 2014; Verhamme *et al.* 2014) have proposed that the Lyα line profile can be used as a probe of Lyman continuum (LyC; $\lambda < 912$Å) leaking galaxies (LyC leakers). LyC

leakers are thought to have contributed ionizing the neutral intergalactic medium in the reionization epoch. Observationally, LyC emission is detected in LAEs and LBGs both spectroscopically (e.g., Shapley *et al.* 2006) and photometrically (e.g., Iwata *et al.* 2009 and Nestor *et al.* 2013). However, the success rate is very low possibly because LyC leakers are extremely faint objects (e.g., Ouchi *et al.* 2008).

Verhamme *et al.* (2014) have investigated two scenarios for ionizing photon escape: (1) the density bounded HII regions with an extremely low $N_{\rm HI}$ value, $\log(N_{\rm HI}) \lesssim 17.0$, corresponding to the unity optical depth for the ionizing photons, (2) or the partial covering fraction of the neutral gas in the ISM. They have shown that the $\Delta v_{{\rm Ly}\alpha,{\rm r}}$ ($\Delta v_{\rm peak}$, if the blue bump exists) value is extremely small in these cases, $\Delta v_{{\rm Ly}\alpha,{\rm r}} \lesssim 100$ km s^{-1} ($\Delta v_{\rm peak} \lesssim 150$ km s^{-1}).

On the other hand, as described in §3.1.3 and §5.4, objects with a large EW(Lyα) value tend to have a small $\Delta v_{{\rm Ly}\alpha,{\rm r}}$ ($\Delta v_{\rm peak}$) value, implying that they are good candidates of LyC leakers. If an ionizing photon escape fraction, $f_{\rm esc}$, is high, the recombination Lyα line might be weaken. However, as Nakajima & Ouchi (2014) have shown, EW(Lyα) can be as high as 100 Å even at $f_{\rm esc} \sim 0.5$.

Thus, we propose that objects with EW(Lyα) as large as 100Å are good LyC leaker targets. The merit of this candidate selection is that it does not require any spectroscopy data.

Chapter 6

Conclusion

6.1 Summary of The Thesis

In this thesis, we tackled three problems: (1) examining if LAEs have outflows, (2) testing a popular expanding shell model and understanding the Lyα escape mechanism in LAEs, (3) and discussing two implications for reionization studies.

6.1.1 The Presence of Outflows

Examining the incidence of outflows in LAEs, high-z low mass galaxies, is important for understanding the galaxy formation and mass-metallicity relation of low mass galaxies. The presence of outflows can be examined by measuring the blue-shift of absorption lines with respect to the systemic redshift. However, due to faintness in FUV continua of LAEs, absorption lines have been undetected. An alternative method to probe outflows is to examine Lyα line. Theoretical studies have shown that outflowing gas leads to an asymmetric Lyα profile with a positive $\Delta v_{\mathrm{Ly}\alpha,\mathrm{r}}$. However, due to the fact that the number of LAEs whose Lyα and nebular emission lines have simultaneously obtained is only four, there has not been a statistical discussion of the gas motion of LAEs.

To address this question, we utilized 12 Lyman Alpha Emitters (LAEs) which are initially taken from the largest LAE samples at $z \sim 2.2$ constructed by Nakajima *et al.* (2012, 2013). Several spectroscopic follow up observations have been conducted, and high spectral resolution Lyα data for the sample has been taken by Magellan/MagE ($R \sim 4000$) and Keck/LRIS ($R \sim 1100$), and nebular emission lines by Magellan/MMIRS, Keck/NIRSPEC, and Subaru/FMOS. We have successfully detected both Lyα and nebular emission lines in the all 12 objects. For the sample, we have derived their stellar

populations and their morphological properties in §3.2 and §3.3, respectively. In particular, stellar mass of the sample ranges from $\log(M_*) = 7.7$ to 10.8 $M_\odot$ with a mean of $\log(M_*) = 9.3$ $M_\odot$. This is smaller than the typical stellar mass of LBGs, $\log(M_*) \sim 10$ - 11 $M_\odot$, but is comparable to the typical stellar mass of LAEs, $\log(M_*) \lesssim 9$ $M_\odot$. The color-magnitude diagram also shows that the distribution of the sample among the whole LAEs is not biased (see the PhD thesis of K. Nakajima).

In order to examine the presence of outflows in the sample, we inspected velocity properties of absorption lines and Lyα lines. Our main results are as follows.

- Metal absorption lines have not been detected in the individual MagE spectra. To achieve a higher S/N ratio, using the systemic redshift determined by nebular emission lines, we stacked the four MagE spectra of CDFS-3865, CDFS-6482, COSMOS-13636, and COSMOS-30679. As a result, we successfully detected metal absorption lines in LAEs for the first time. The average blueshift with respect to the systemic redshift is $\Delta v_{\rm abs} = -102 \pm 65$ km s^{-1} (Hashimoto *et al.* 2013). In addition, metal absorption lines in three objects, COSMOS-12805, COSMOS-13636, and SXDS-10600, have been detected in Shibuya *et al.* (2014a) on an individual basis. The result is all the absorption lines are blue-shifted with respect to $z_{\rm sys}$ by -204 ± 27 km s^{-1}. These outflow velocities are consistent with the average outflow velocities of LBGs, $\Delta v_{\rm abs} = -227$ km s^{-1} (Steidel *et al.* 2010; Kulas *et al.* 2012).
- To measure the degree of Lyα asymmetry of the sample, we used the weighted skewness of the Lyα lines ($S_{\rm w}$; Kashikawa *et al.* 2006). This results in a positive $S_{\rm w}$ in most (8/12) objects at $> 3\sigma$, indicating that most Lyα profiles have a red tail and a blue sharp cut off. In addition, using the systemic redshift, $z_{\rm sys}$, we find that all the 12 galaxies have a main peak redward of the systemic, and 5 out of the 12 have an additional weak Lyα emission blueward of the systemic (blue bump). For the main peak, we find that 7/12 (5/12) have a positive $\Delta v_{{\rm Ly}\alpha,{\rm r}}$ at $> 3\sigma$ $(1 - 3\sigma)$,

Thus, we have confirmed the presence of outflows in LAEs using several methods with a large sample. While we did not discuss properties of outflows, e.g., a comparison of outflow velocities with escape velocities of galaxies and a measurement of the outflow rate, the presence of outflow itself and the outflow speed in LAEs is an important first step.

We have also obtained relevant observational results as follows.

- Using nebular emission lines, we have measured the FWHM of the sample. The mean FWHM value for the sample of 8 objects with a measurable velocity dispersion is FWHM(neb) $= 129 \pm 55$ km s^{-1}, which is smaller than those of LBGs, FWHM $= 200 - 250$ km s^{-1} (Pettini *et al.* 2001; Erb *et al.* 2006a; Kulas *et al.* 2012). The result implies that LAEs studied in this thesis have smaller dynamical masses than those of typical LBGs.
- For a sample of 17 objects from our study and the literature with a resolved Lyα line as well as a systemic redshift (McLinden *et al.* 2011; Chonis *et al.* 2013), we have measured three velocity offsets related to the Lyα line and systematically compared them with those of LBGs (Kulas *et al.* 2012): the velocity offset of the main red peak, $\Delta v_{\mathrm{Ly}\alpha,\mathrm{r}}$, that of the blue bump, $\Delta v_{\mathrm{Ly}\alpha,\mathrm{b}}$, if any, and that of the two peaks, Δv_{peak}. The mean $\Delta v_{\mathrm{Ly}\alpha,\mathrm{r}}$ ($\Delta v_{\mathrm{Ly}\alpha,\mathrm{b}}$) is 174 ± 19 km s^{-1} (-316 ± 45 km s^{-1}), which is smaller than (comparable to) that in LBGs, $\Delta v_{\mathrm{Ly}\alpha,\mathrm{r}} \simeq 400$ km s^{-1} ($\Delta v_{\mathrm{Ly}\alpha,\mathrm{b}} = -367 \pm 46$ km s^{-1}). These two velocity offsets naturally lead to a small average Δv_{peak} in LAEs, $\Delta v_{\mathrm{peak}} \sim 500 \pm 56$ km s^{-1}, compared to that in LBGs, $\Delta v_{\mathrm{peak}} \sim 801 \pm 41$ km s^{-1}. These results mean that the key difference in Lyα velocity properties between LAEs and LBGs is $\Delta v_{\mathrm{Ly}\alpha,\mathrm{r}}$. While $\Delta v_{\mathrm{Ly}\alpha,\mathrm{r}}$ has been statistically examined in LAEs (e.g., McLinden *et al.* 2011; Hashimoto *et al.* 2013; Shibuya *et al.* 2014a; Erb *et al.* 2014), we stress that we provide the first statistical measurements of $\Delta v_{\mathrm{Ly}\alpha,\mathrm{b}}$ and Δv_{peak} in LAEs.
- With the high spectral resolution near-infrared spectroscopy data, we have demonstrated that some LAEs have a two component nebular emission profile for the first time. For the two objects with a two component [OIII] profile, we find that the FWHM of the broad component is $70 - 80$ km s^{-1}. This would exclude the possibility of its origin being AGN activity or powerful hot outflows. The velocity offset between the two components is measured to be ~ 100 km s^{-1}, which is consistent with its origin being a galactic rotation.

6.1.2 The Lyα Escape Mechanism

Motivated by the finding that LAEs have outflows, we have applied a Lyα radiative transfer code constructed by Verhamme *et al.* (2006) and Schaerer *et al.* (2011) to our data. The aim is to understand the Lyα escape mechanism through the detailed comparison of observed the Lyα profiles with the radiative transfer model.

The radiation transfer has been computed using a Monte Carlo technique through idealized spherically symmetric shells of homogeneous and isothermal neutral hydrogen gas. While expanding shell models have been applied (e.g., Verhamme *et al.* 2008; Kulas *et al.* 2012; Chonis *et al.* 2013), results differ with each other. On one hand, Verhamme *et al.* (2008) have applied their model (Verhamme *et al.* 2006) to 11 $z \sim 3$ LBGs on an individual basis. They have successfully reproduced Lyα profiles as well as dust extinction values. On the other hand, Kulas *et al.* (2012) Chonis *et al.* (2013) have applied the expanding shell model constructed by Zheng & Miralda-Escudé (2002) and Kollmeier *et al.* (2010) to a stacked spectrum of 12 $z \sim 2-3$ LBGs and 3 individual LAEs, respectively. These authors have shown that the expanding shell model can not well reproduce observed Lyα profiles, especially a secondary emission blue-ward of the systemic velocity. In addition, there are some problems in these previous studies. There are, however, some problems to be solved in these studies. First, the best fit parameters in Verhamme *et al.* (2008) have been determined by eye, not by the statistics. This prevent us from determining the best-fit parameters and its associated errors, as well as the degeneracy among the parameters. Second, Kulas *et al.* (2012) have compared a stacked spectrum of 12 LBGs with modeled Lyα lines. As recently pointed out by several authors (e.g., Vargas *et al.* 2014), stacking analysis provides a poor representation of individual objects. This would cause a discrepancy between observed and modeled Lyα lines. Chonis *et al.* (2013) have compared observed and modeled Lyα lines on the individual basis for three objects. However, as described in Chonis *et al.* (2013), these three objects have very similar Lyα profiles and Lyα luminosities. Thus, prior to examining the Lyα escape mechanism, we need to first understand how well the expanding shell model can reproduce observed Lyα profiles and observables.

As stated, our sample has a wide variety of Lyα profiles and Lyα luminosities, as well as various observables such as dust extinction and outflow velocities. With the best fit parameters and their associated errors determined from the χ^2 statistics, we can statistically examine the validity of the model. The results of the close comparison between observed and modeled Lyα lines are as follows.

- We have run the code fixing $z_{\rm sys}$. The best-fit parameters and their associate errors are determined through the minimum χ^2 realization. This technique tells us how well the derived parameters are obtained, unlike previous studies which only show the best-fit parameters (e.g., Verhamme *et al.* 2006; Kulas *et al.* 2012; Chonis *et al.*

2013). This technique also tells us if model parameters are degenerate or not. We find that all the Lyα profiles are well reproduced by the model. Concerning degeneracies, we conclude that the systematic uncertainty among the parameters due to the degeneracies is small, and it does not affect our discussions.

- For the objects without a blue bump, all the model parameters including the galactic outflow velocity, the amount of dust extinction, and the intrinsic (i.e., before being affected by radiative transfer) FWHM of the Lyα line are broadly consistent with the observables, the outflow velocity inferred from LIS lines, the dust extinction derived from SED fitting, and the FWHM of nebular emission lines. However, for the objects with a blue bump, we find that the intrinsic FWHM of Lyα is significantly larger than the FWHM of nebular emission lines. For the blue bump objects, we have tried another fit fixing the intrinsic FWHM of Lyα as that of nebular emission lines. The result is that the position and the flux of blue bump are poorly reproduced.
- To understand the huge $\mathrm{FWHM_{int}}$(Lyα), we propose that if we introduce an additional source of Lyα emission such as gravitational cooling, the large $\mathrm{FWHM_{int}}$(Lyα) and the existence of the blue bump can be simultaneously explained. The former is because gravitational cooling could occur in the outer region of galaxies, and the latter is because it can enhance the blue bump emission.

Thus, we have statistically examined how well the expanding shell model can reproduce observed Lyα profiles and observables. The result is that the expanding shell model is a good one at least for the non-blue bump objects. For the blue bump objects also, taking into account the fact that the ratio of the blue bump flux to the total Lyα flux is small, the discrepancy could be modified. We have also shown that the model constructed by Kulas *et al.* (2012); Chonis *et al.* (2013) Cannot well reproduce the observed profiles because they transfer monochromatic Lyα lines. These results are important since many observational studies make use of the expanding shell model to interpret observed Lyα profiles.

After examining the validity of the model, we have inspected the Lyα escape mechanism. Due to the resonant nature of Lyα photons, Lyα photons would be easily absorbed by dust grains after their long light paths. However, LAEs have strong Lyα emission, suggesting that they have low dust extinction and/or some mechanisms that make light paths of Lyα photons short. While there are some observational studies which tried to understand this,

no decisive conclusions have been obtained. Thus, it is important to derive a parameter which cannot be directly obtained from observations, e.g., $N_{\rm HI}$. The fitting results show that the only parameter which differ above 1σ between LAEs and LBGs is $N_{\rm HI}$.

From observational results above, we have shown that the key difference in Lyα and absorption velocity properties between LAEs and LBGs is $\Delta v_{{\rm Ly}\alpha,{\rm r}}$. Thus, understanding the origin of the small $\Delta v_{{\rm Ly}\alpha,{\rm r}}$ through the detailed Lyα modeling should shed light on the Lyα RT and escape in LAEs. The result is as follows.

- We have examined four possibilities of the origin of the small $\Delta v_{{\rm Ly}\alpha,{\rm r}}$ in LAEs: a large galactic outflow velocity, the presence of a peculiar ISM with a unity covering fraction, $CF = 1$, a patchy ISM with a neutral gas covering fraction below unity, $CF < 1$, and a low neutral hydrogen column density of the outflowing gas. We find that the small $\Delta v_{{\rm Ly}\alpha,{\rm r}}$ can be well explained by the low neutral hydrogen column density scenario. Their typical neutral hydrogen column density is as low as 10^{19} cm^{-2}, which is more than one order of magnitude lower than that in LBGs. Such a low column density is consistent with the recent findings of LAEs having high ionization parameter of gas (Nakajima *et al.* 2013; Nakajima & Ouchi 2014) or low HI gas mass (Pardy *et al.* 2014).

We stress that we have examined the whole hypotheses of the small $\Delta v_{{\rm Ly}\alpha,{\rm r}}$ in LAEs quantitatively than previous studies. The impact of this study is that for the first time we have derived $N_{\rm HI}$ in LAEs and have shown that the low $N_{\rm HI}$ is the key for the small $\Delta v_{{\rm Ly}\alpha,{\rm r}}$ as well as the Lyα escape mechanism.

6.1.3 Implications for Reionization Studies

We have discussed two implications for reionization studies as follows.

- In estimating the neutral fraction of the IGM from Lyα emissivity, $\Delta v_{{\rm Ly}\alpha}$ is assumed to be 400 km s^{-1}. If LAEs at $z > 6$ have similarly small $\Delta v_{{\rm Ly}\alpha,{\rm r}}$ values as derived in this study, the amount of Lyα photons scattered by the IGM, as used to constrain the epoch of reionization, may be in need of revision.
- From our finding that high EW(Lyα) objects tend to have small $\Delta v_{{\rm Ly}\alpha,{\rm r}}$ and the finding in Verhamme *et al.* (2014) that objects with ionizing photon leaking should have small $\Delta v_{{\rm Ly}\alpha,{\rm r}}$, we propose that targeting high EW(Lyα) objects would be an efficient way to search for Lyman Continuum leaking galaxy candidates from

photometry alone.

6.2 LAE Images Obtained in This Thesis and Future Prospects

6.2.1 LAE Images Obtained in This Thesis

Previous stellar population and morphology studies have revealed that LAEs are young and small size objects. In this thesis, we have also demonstrated that LAEs have smaller stellar and dynamical mass than those in LBGs. These results suggest that LAEs are indeed small systems.

Concerning their kinematics, we have shown that LAEs have comparable outflow velocities to those of LBGs, indicating that LAEs have higher outflow velocities at a given stellar mass. Recently, e.g., Nakajima *et al.* (2013) have shown that LAEs do not obey to the well established mass-metallicity relation. They tend to have lower metallicity and higher ionization parameter than those of LBGs even at the same stellar mass. On the other hand, Lyα velocity properties have revealed that LAEs have significantly smaller $\Delta v_{\mathrm{Ly}\alpha,\mathrm{r}}$ compared to those in LBGs. As shown in Hashimoto *et al.* (2013), this is not simply due to their stellar mass or dynamical mass: even at a given physical quantities, LAEs have smaller $\Delta v_{\mathrm{Ly}\alpha,\mathrm{r}}$ than those in LBGs.

These results and our discussions combined, the key difference between LAEs and LBGs is N_{HI} and accompanying ionization state. In order for the definitive conclusion if LAEs and LBGs are different populations or not, we need a larger sample whose stellar population, morphology, kinematics, metallicity, gas ionization state, and N_{HI} can be simultaneously obtained. However, from this thesis, we can at least argue that LAEs are not a simple scale down version of LBGs.

6.2.2 Future Prospects

We did not discuss outflow properties of LAEs. In general, outflow is driven by either momentum or kinematic energy (e.g., Murray *et al.* 2005; Choi & Nagamine 2011). In order to understand the mechanism driving outflows, many observational results make use of stellar mass - outflow velocity relation (e.g., Martin 2005; Kornei *et al.* 2012). The slope of the correlation depends on the dominant physical outflow process. A linear correlation, $v_{\mathrm{out}} \propto \mathrm{SFR}$, is expected for radiation pressure dominant outflows (Sharma *et al.* 2011),

while shallower slopes are indicative of ram pressure dominant outflows (Heckman *et al.* 2000). Using the derived outflow velocities and stellar mass, we plan to constrain what is the dominant physical outflow process in LAEs. In this thesis, we have found that, at a given stellar mass, LAEs have higher outflow velocities compared to LBGs. This might be related to with their high radiation pressure caused by their high ionization state.

Concerning outflow properties, we also plan to constrain mass outflow/inflow rates which are one of the most important parameters in galaxy formation. We have derived outflow velocities and $N_{\rm HI}$ from the modeling. As discussed in Verhamme *et al.* (2008), assuming the size of outflow radius, we can derive neutral gas mass ejected by outflows, and mass outflow rates. These quantities, in conjunction with metallicity, we can in turn constrain the inflow rates and mass loading factors of LAEs (e.g., Yabe *et al.* 2015).

From April in 2015, I plan to stay at the Center for Research in Astrophysics in Lyon (CRAL) in France. The commissioning data taken by VLT/MUSE is available. MUSE is a massive IFU spectrograph currently operating at VLT, which can target Lyα lines at $2.8 < z < 6.7$ with extremely high sensitivity (e.g., Richard *et al.* 2015). With these data, we plan to examine Lyα profile properties down to very faint LAEs. From results of Hagen *et al.* (2014) and Kusakabe *et al.* (2014), it is possible that Lyα profile properties differ depending on their luminosities. Since MUSE can simultaneously detect Lyα and CIII] 1909 lines for $z \sim 2.8 - 3.8$ LAEs, we can both investigate the Lyα profile property evolution and its dependency on luminosities. In addition, with a comparison to the photoionization model, CIII] 1909 can be used to constrain the gas ionization state (e.g., Stark *et al.* 2014). We plan to examine correlation between $\Delta v_{{\rm Ly}\alpha,{\rm r}}$ and ionization parameter, thereby directly inspecting the relation between Lyα profiles and LyC leakers.

Acknowledgments

I would like to begin expressing my sincere gratitude to three advisors, Associate Prof. Kazuhiro Shimasaku, Associate Prof. Masami Ouchi, and Prof. Sadanori Okamura. I deeply appreciate Associate Prof. Kazuhiro Shimasaku for giving me many helpful advices during my PhD course. Through daily discussions, he taught me how to have effective presentations and scientific writings. I also learned from him how to interpret scientific results. I am grateful to Associate Prof. Masami Ouchi, for giving me an interesting topic of near-infrared spectroscopy for LAEs. He also kindly gave me opportunities to go several observations and international conferences, thorough which I leaned how to survive in competitive societies. My gratitude goes to Prof. Sadanori Okamura for giving me helpful comments on my presentation, especially the first two years of my PhD course.

Associate Prof. Kentaro Motohara, Prof. Ryohei Kawabe, Prof. Kohtaro Kohno, Prof. Toru Yamada, and Associate Prof. Nobunari Kashikawa are my defense referees. I really appreciate them to have read and judged my thesis.

I would like to thank Dr. Kimihiko Nakajima, Dr. Yoshiaki Ono, and Dr. Takatoshi Shibuya, for their helping me completing this work as the thesis. Dr. Kimihiko Nakajima has successfully confirmed nebular emission lines with his PI observations of Keck/NIRSPEC and Subaru/FMOS, kindly providing me with reduced data. He also took me to the FMOS observation, through which I could understand FMOS data reduction. Dr. Yoshiaki Ono has offered me the result of stellar populations of the $z \sim 2.2$ LAE samples. Dr. Takatoshi Shibuya has successfully detected Lyα and LIS absorption lines from LRIS spectra, kindly providing me with reduced data. He also provided me with morphological properties such as the presence of merger and the ellipticity for the sample.

I appreciate Dr. Michael Rauch for taking me to an observation with Magellan/MagE, and teaching me how to reduce MagE data. I also enjoyed discussions with him.

I sincerely thank Dr. Anne Verhamme and Prof. Daniel Schaerer for inviting me to

the Observatory of Geneva, teaching me how to use their code, and daily discussions. I am grateful to Dr. Anne Verhamme for inviting me to her family in France and taking me to skiing in Alps. I really enjoyed French wine and cheese. My gratitude goes to people in the Observatory, Dr. Antonio Cava, Dr. Miroslava Dessauges-Zavadsky, Dr. Zamojski Michel, Dr. Hakim Atek, Dr. Ivana Orlitova, and Mr. Panos Sklias, for their hospitality. I really enjoyed jazz concert, watching six nations rugby games in a bar, and tasty foie gras with sweet white wine. During the stay, Dr. Anne Verhamme also took me to Le Centre de Recherche Astrophysique de Lyon (CRAL) in France, where I experienced the commissioning ceremony for the new IFU instrument, MUSE, installed on VLT. I thank Jeremy Blaizot, Joakim Rosdahl, and Bruno Guiderdoni, who allowed me to have a presentation there the next day.

I thank Dr. Yujin Yang for providing data of two LABs, Dr. Steven Finkelstein for providing the revised results of his work, Dr. Daniel Stark, Dr. Ann Zabludoff, Prof. Masayuki Umemura, Mr. Hannes Jensen, and Mr. Matthew Schenker for giving us various useful comments for the paper Hashimoto *et al.* (2013).

I also thank Dr. Thibault Garel and Dr. Claudia Lagos for their important comments on the results of Lyα profiles comparison.

I would like to thank my laboratory members, Dr. Yusei Koyama, Dr. Yoshiaki Ono, Dr. Kimihiko Nakajima, Mr. Shingo Shinogi, Mr. Ryosuke Goto, Mr. Ryota Kawamata, Ms. Haruka Kusakabe, with whom I shared many scientific ideas. I really enjoyed free discussions with them. I also thank the members of the observational cosmology group in the Institute for Cosmic Ray Research, Dr. Tomoki Saito, Dr. Rieko Momose, Dr. Suraphong Yuma, Mr. Akira Konno, Mr. Yoshiaki Naito, Mr. Masafumi Ishigaki, Ms. Hiroko Tamazawa, Mr. Seiji Fujimoto, and Mr. Yuichi Harikane, for useful comments in meetings and daily lives.

I feel thankful to Prof. Goran Ostlin, Dr. Lucia Guaita, Dr. Matthew Hayes, Mr. Andreas Sandberg, and Mr. Thoger Rivera Thorsen, for kindly giving me an opportunity to have a presentation in an international conference focused on the Ly line held in Stockholm. My gratitude goes to Prof. Len Cowie, Prof. Ester Hu, Prof. James Rhoads, Associate Prof. Mark Dijkstra, Dr. Sebastiano Cantalupo, Dr. Peter Laursen, Dr. Moire Prescott, Dr. Claudia Scarlata, Dr. Dawn Erb, Mr. Ryan Trainor, Mr. Alex Hagen, Mr. Fluorent Duval, Mr. Christoph Behrens, for their helpful discussions and comments.

I express my sincere gratitude to my parents, Hiroyuki Hashimoto and Takako Hashimoto, and my sister, Urara Hashimoto, for their support and understanding

through my life. I also deeply thank my grandmothers, Sumi Hashimoto and Michiko Watanabe, for their support. I would like to appreciate my girl friend, Nobuko Gan, for her support and understanding.

Bibliography

Abraham, R. G., van den Bergh, S., Glazebrook, K., Ellis, R. S., Santiago, B. X., Surma, P. & Griffiths, R. E. (1996). *The Morphologies of Distant Galaxies. II. Classifications from the Hubble Space Telescope Medium Deep Survey.* The Astrophysical Journal, Supplement, **107**, 1.

Atek, H., Kunth, D., Schaerer, D., Mas-Hesse, J. M., Hayes, M., Östlin, G. & Kneib, J.-P. (2014). *Influence of physical galaxy properties on Lyα escape in star-forming galaxies.* Astronomy & Astrophysics, **561**, A89.

Baldwin, J. A., Phillips, M. M. & Terlevich, R. (1981). *Classification parameters for the emission-line spectra of extragalactic objects.* **93**, 5–19.

Barnes, L. A. & Haehnelt, M. G. (2009). *A joint model for the emission and absorption properties of damped Lyα absorption systems.* Monthly Notices of the Royal Astronomical Society, **397**, 511–519.

Barnes, L. A., Haehnelt, M. G., Tescari, E. & Viel, M. (2011). *Galactic winds and extended Lyα emission from the host galaxies of high column density quasi-stellar object absorption systems.* Monthly Notices of the Royal Astronomical Society, **416**, 1723–1738.

Becker, G. D., Rauch, M. & Sargent, W. L. W. (2007). *The Evolution of Optical Depth in the Lyα Forest: Evidence Against Reionization at z˜6.* The Astrophysical Journal, **662**, 72–93.

Behrens, C., Dijkstra, M. & Niemeyer, J. C. (2014). *Beamed Lyα emission through outflow-driven cavities.* Astronomy & Astrophysics, **563**, A77.

Bond, N. A., Feldmeier, J. J., Matković, A., Gronwall, C., Ciardullo, R. & Gawiser, E. (2010). *Evidence for Spatially Compact Lyα Emission in z = 3.1 Lyα-emitting Galaxies.* The Astrophysical Journal, Letters, **716**, L200–L204.

Bond, N. A., Gawiser, E., Gronwall, C., Ciardullo, R., Altmann, M. & Schawinski, K. (2009). *Sizes of LYα-emitting Galaxies and Their Rest-frame Ultraviolet Components at z = 3.1.* The Astrophysical Journal, **705**, 639–649.

Bruzual, G. & Charlot, S. (2003). *Stellar population synthesis at the resolution of 2003.* Monthly Notices of the Royal Astronomical Society, **344**, 1000–1028.

Calzetti, D., Armus, L., Bohlin, R. C., Kinney, A. L., Koornneef, J. & Storchi-Bergmann, T. (2000). *The Dust Content and Opacity of Actively Star-forming Galaxies.* The Astrophysical Journal, **533**, 682–695.

Cantalupo, S., Arrigoni-Battaia, F., Prochaska, J. X., Hennawi, J. F. & Madau, P. (2014). *A cosmic web filament revealed in Lyman-α emission around a luminous high-redshift quasar.* Nature, **506**, 63–66.

Cantalupo, S., Lilly, S. J. & Haehnelt, M. G. (2012). *Detection of dark galaxies and circum-galactic filaments fluorescently illuminated by a quasar at z = 2.4.* Monthly Notices of the Royal Astronomical Society, **425**, 1992–2014.

Cantalupo, S., Porciani, C., Lilly, S. J. & Miniati, F. (2005). *Fluorescent Lyα Emission from the High-Redshift Intergalactic Medium.* The Astrophysical Journal, **628**, 61–75.

Cardamone, C. N., van Dokkum, P. G., Urry, C. M., Taniguchi, Y., Gawiser, E., Brammer, G., Taylor, E., Damen, M., Treister, E., Cobb, B. E., Bond, N., Schawinski, K., Lira, P., Murayama, T., Saito, T. & Sumikawa, K. (2010). *The Multiwavelength Survey by Yale-Chile (MUSYC): Deep Medium-band Optical Imaging and High-quality 32-band Photometric Redshifts in the ECDF-S.* The Astrophysical Journal, Supplement, **189**, 270–285.

Choi, J.-H. & Nagamine, K. (2011). *Multicomponent and variable velocity galactic outflow in cosmological hydrodynamic simulations.* Monthly Notices of the Royal Astronomical Society, **410**, 2579–2592.

Chonis, T. S., Blanc, G. A., Hill, G. J., Adams, J. J., Finkelstein, S. L., Gebhardt, K., Kollmeier, J. A., Ciardullo, R., Drory, N., Gronwall, C., Hagen, A., Overzier, R. A., Song, M. & Zeimann, G. R. (2013). *The Spectrally Resolved Lyα Emission of Three Lyα-selected Field Galaxies at z ˜ 2.4 from the HETDEX Pilot Survey.* The Astrophysical Journal, **775**, 99.

Conselice, C. J., Bershady, M. A. & Jangren, A. (2000). *The Asymmetry of Galaxies: Physical Morphology for Nearby and High-Redshift Galaxies.* The Astrophysical Journal, **529**, 886–910.

Cooke, J., Berrier, J. C., Barton, E. J., Bullock, J. S. & Wolfe, A. M. (2010). *Lyman break galaxy close and interacting pairs at z ˜ 3.* Monthly Notices of the Royal Astronomical Society, **403**, 1020–1035.

Cowie, L. L., Barger, A. J. & Hu, E. M. (2011). *Lyα Emitting Galaxies as Early Stages in Galaxy Formation.* The Astrophysical Journal, **738**, 136.

Daddi, E., Dickinson, M., Morrison, G., Chary, R., Cimatti, A., Elbaz, D., Frayer, D., Renzini, A., Pope, A., Alexander, D. M., Bauer, F. E., Giavalisco, M., Huynh, M., Kurk, J. & Mignoli, M. (2007). *Multiwavelength Study of Massive Galaxies at z˜2. I. Star Formation and Galaxy Growth.* The Astrophysical Journal, **670**, 156–172.

Deharveng, J.-M., Small, T., Barlow, T. A., Péroux, C., Milliard, B., Friedman, P. G., Martin, D. C., Morrissey, P., Schiminovich, D., Forster, K., Seibert, M., Wyder, T. K., Bianchi, L., Donas, J., Heckman, T. M., Lee, Y.-W., Madore, B. F., Neff, S. G., Rich, R. M., Szalay, A. S., Welsh, B. Y. & Yi, S. K. (2008). *Lyα-Emitting Galaxies at 0.2z0.35 from GALEX Spectroscopy.* The Astrophysical Journal, **680**, 1072–1082.

Dekel, A., Birnboim, Y., Engel, G., Freundlich, J., Goerdt, T., Mumcuoglu, M., Neistein, E., Pichon, C., Teyssier, R. & Zinger, E. (2009). *Cold streams in early massive hot haloes as the main mode of galaxy formation.* Nature, **457**, 451–454.

Dessauges-Zavadsky, M., D'Odorico, S., Schaerer, D., Modigliani, A., Tapken, C. & Vernet, J. (2010). *Rest-frame ultraviolet spectrum of the gravitationally lensed galaxy "the 8 o'clock arc": stellar and interstellar medium properties.* Astronomy & Astrophysics, **510**, A26.

Dijkstra, M. (2014). *Lyman Alpha Emitting Galaxies as a Probe of Reionization.* ArXiv e-prints .

Dijkstra, M., Haiman, Z. & Spaans, M. (2006). *Lyα Radiation from Collapsing Protogalaxies. I. Characteristics of the Emergent Spectrum.* The Astrophysical Journal, **649**, 14–36.

Dijkstra, M. & Loeb, A. (2009). *Acceleration of galactic supershells by Lyα radiation.* Monthly Notices of the Royal Astronomical Society, **396**, 377–384.

Dunkley, J., Komatsu, E., Nolta, M. R., Spergel, D. N., Larson, D., Hinshaw, G., Page, L., Bennett, C. L., Gold, B., Jarosik, N., Weiland, J. L., Halpern, M., Hill, R. S., Kogut, A., Limon, M., Meyer, S. S., Tucker, G. S., Wollack, E. & Wright, E. L. (2009). *Five-Year Wilkinson Microwave Anisotropy Probe Observations: Likelihoods and Parameters from the WMAP Data.* The Astrophysical Journal, Supplement, **180**, 306–329.

Duval, F., Schaerer, D., Östlin, G. & Laursen, P. (2014). *Lyman α line and*

continuum radiative transfer in a clumpy interstellar medium. Astronomy & Astrophysics, **562**, A52.

Ellis, R. S., McLure, R. J., Dunlop, J. S., Robertson, B. E., Ono, Y., Schenker, M. A., Koekemoer, A., Bowler, R. A. A., Ouchi, M., Rogers, A. B., Curtis-Lake, E., Schneider, E., Charlot, S., Stark, D. P., Furlanetto, S. R. & Cirasuolo, M. (2013). *The Abundance of Star-forming Galaxies in the Redshift Range 8.5-12: New Results from the 2012 Hubble Ultra Deep Field Campaign.* The Astrophysical Journal, Letters, **763**, L7.

Erb, D. K., Pettini, M., Shapley, A. E., Steidel, C. C., Law, D. R. & Reddy, N. A. (2010). *Physical Conditions in a Young, Unreddened, Low-metallicity Galaxy at High Redshift.* The Astrophysical Journal, **719**, 1168–1190.

Erb, D. K., Shapley, A. E., Pettini, M., Steidel, C. C., Reddy, N. A. & Adelberger, K. L. (2006a). *The Mass-Metallicity Relation at z˜2.* The Astrophysical Journal, **644**, 813–828.

Erb, D. K., Steidel, C. C., Shapley, A. E., Pettini, M., Reddy, N. A. & Adelberger, K. L. (2006b). *The Stellar, Gas, and Dynamical Masses of Star-forming Galaxies at z ˜ 2.* The Astrophysical Journal, **646**, 107–132.

Erb, D. K., Steidel, C. C., Trainor, R. F., Bogosavljevic, M., Shapley, A. E., Nestor, D. B., Kulas, K. R., Law, D. R., Strom, A. L., Rudie, G. C., Reddy, N. A., Pettini, M., Konidaris, N. P., Mace, G., Matthews, K. & McLean, I. S. (2014). *The Ly-alpha Profiles of Faint Galaxies at z˜2-3 with Systemic Redshifts from Keck-MOSFIRE.* ArXiv e-prints .

Fan, X., Strauss, M. A., Becker, R. H., White, R. L., Gunn, J. E., Knapp, G. R., Richards, G. T., Schneider, D. P., Brinkmann, J. & Fukugita, M. (2006). *Constraining the Evolution of the Ionizing Background and the Epoch of Reionization with z˜6 Quasars. II. A Sample of 19 Quasars.* The Astronomical Journal, **132**, 117–136.

Faucher-Giguère, C.-A., Kereš, D., Dijkstra, M., Hernquist, L. & Zaldarriaga, M. (2010). *Lyα Cooling Emission from Galaxy Formation.* The Astrophysical Journal, **725**, 633–657.

Finkelstein, S. L., Hill, G. J., Gebhardt, K., Adams, J., Blanc, G. A., Papovich, C., Ciardullo, R., Drory, N., Gawiser, E., Gronwall, C., Schneider, D. P. & Tran, K.-V. (2011). *The HETDEX Pilot Survey. III. The Low Metallicities of High-redshift Lyα Galaxies.* The Astrophysical Journal, **729**, 140.

Gawiser, E., Francke, H., Lai, K., Schawinski, K., Gronwall, C., Ciardullo, R., Quadri, R., Orsi, A., Barrientos, L. F., Blanc, G. A., Fazio, G., Feldmeier, J. J., Huang, J.-s., Infante, L., Lira, P., Padilla, N., Taylor, E. N., Treister, E., Urry, C. M., van Dokkum, P. G. & Virani, S. N. (2007). *Lyα-Emitting Galaxies at z = 3.1: L* Progenitors Experiencing Rapid Star Formation.* The Astrophysical Journal, **671**, 278–284.

Genzel, R., Newman, S., Jones, T., Förster Schreiber, N. M., Shapiro, K., Genel, S., Lilly, S. J., Renzini, A., Tacconi, L. J., Bouché, N., Burkert, A., Cresci, G., Buschkamp, P., Carollo, C. M., Ceverino, D., Davies, R., Dekel, A., Eisenhauer, F., Hicks, E., Kurk, J., Lutz, D., Mancini, C., Naab, T., Peng, Y., Sternberg, A., Vergani, D. & Zamorani, G. (2011). *The Sins Survey of z ˜ 2 Galaxy Kinematics: Properties of the Giant Star-forming Clumps.* The Astrophysical Journal, **733**, 101.

Guaita, L., Acquaviva, V., Padilla, N., Gawiser, E., Bond, N. A., Ciardullo, R., Treister, E., Kurczynski, P., Gronwall, C., Lira, P. & Schawinski, K. (2011). *Lyα-emitting Galaxies at z = 2.1: Stellar Masses, Dust, and Star Formation Histories from Spectral Energy Distribution Fitting.* The Astrophysical Journal, **733**, 114.

Guaita, L., Francke, H., Gawiser, E., Bauer, F. E., Hayes, M., Östlin, G. & Padilla, N. (2013). *Magellan/MMIRS near-infrared multi-object spectroscopy of nebular emission from star-forming galaxies at 2 z 3.* Astronomy & Astrophysics, **551**, A93.

Guaita, L., Gawiser, E., Padilla, N., Francke, H., Bond, N. A., Gronwall, C., Ciardullo, R., Feldmeier, J. J., Sinawa, S., Blanc, G. A. & Virani, S. (2010). *Lyα-emitting Galaxies at z = 2.1 in ECDF-S: Building Blocks of Typical Present-day Galaxies?* The Astrophysical Journal, **714**, 255–269.

Hagen, A., Ciardullo, R., Gronwall, C., Acquaviva, V., Bridge, J., Zeimann, G. R., Blanc, G. A., Bond, N. A., Finkelstein, S. L., Song, M., Gawiser, E., Fox, D. B., Gebhardt, H., Malz, A. I., Schneider, D. P., Drory, N., Gebhardt, K. & Hill, G. J. (2014). *Spectral Energy Distribution Fitting of HETDEX Pilot Survey Lyα Emitters in COSMOS and GOODS-N.* The Astrophysical Journal, **786**, 59.

Hansen, M. & Oh, S. P. (2006). *Lyman α radiative transfer in a multiphase medium.* Monthly Notices of the Royal Astronomical Society, **367**, 979–1002.

Harikane, Y., Ouchi, M., Yuma, S., Rauch, M., Nakajima, K. & Ono, Y. (2014). *MOSFIRE and LDSS3 Spectroscopy for an [OII] Blob at z=1.18: Gas Outflow and Energy Source*. ArXiv e-prints .

Harrington, J. P. (1973). *The scattering of resonance-line radiation in the limit of large optical depth*. Monthly Notices of the Royal Astronomical Society, **162**, 43.

Hashimoto, T., Ouchi, M., Shimasaku, K., Ono, Y., Nakajima, K., Rauch, M., Lee, J. & Okamura, S. (2013). *Gas Motion Study of Lyα Emitters at z ˜ 2 Using FUV and Optical Spectral Lines*. The Astrophysical Journal, **765**, 70.

Heckman, T. M., Armus, L. & Miley, G. K. (1990). *On the nature and implications of starburst-driven galactic superwinds*. The Astrophysical Journal, Supplement, **74**, 833–868.

Heckman, T. M., Borthakur, S., Overzier, R., Kauffmann, G., Basu-Zych, A., Leitherer, C., Sembach, K., Martin, D. C., Rich, R. M., Schiminovich, D. & Seibert, M. (2011). *Extreme Feedback and the Epoch of Reionization: Clues in the Local Universe*. The Astrophysical Journal, **730**, 5.

Heckman, T. M., Lehnert, M. D., Strickland, D. K. & Armus, L. (2000). *Absorption-Line Probes of Gas and Dust in Galactic Superwinds*. The Astrophysical Journal, Supplement, **129**, 493–516.

Hu, E. M. & McMahon, R. G. (1996). *Detection of Lyman-α-emitting galaxies at redshift 4.55*. Nature, **382**, 231–233.

Iwata, I., Inoue, A. K., Matsuda, Y., Furusawa, H., Hayashino, T., Kousai, K., Akiyama, M., Yamada, T., Burgarella, D. & Deharveng, J.-M. (2009). *Detections of Lyman Continuum from Star-Forming Galaxies at z ˜ 3 through Subaru/Suprime-Cam Narrow-Band Imaging*. The Astrophysical Journal, **692**, 1287–1293.

Jensen, H., Laursen, P., Mellema, G., Iliev, I. T., Sommer-Larsen, J. & Shapiro, P. R. (2013). *On the use of Lyα emitters as probes of reionization*. Monthly Notices of the Royal Astronomical Society, **428**, 1366–1381.

Jiang, L., Egami, E., Fan, X., Windhorst, R. A., Cohen, S. H., Davé, R., Finlator, K., Kashikawa, N., Mechtley, M., Ouchi, M. & Shimasaku, K. (2013). *Physical Properties of Spectroscopically Confirmed Galaxies at z = 6. II. Morphology of the Rest-frame UV Continuum and Lyα Emission*. The Astrophysical Journal, **773**, 153.

Jones, T. A., Ellis, R. S., Schenker, M. A. & Stark, D. P. (2013). *Keck Spec-*

troscopy of Gravitationally Lensed z ˜= 4 Galaxies: Improved Constraints on the Escape Fraction of Ionizing Photons. The Astrophysical Journal, **779**, 52.

Kashikawa, N., Shimasaku, K., Malkan, M. A., Doi, M., Matsuda, Y., Ouchi, M., Taniguchi, Y., Ly, C., Nagao, T., Iye, M., Motohara, K., Murayama, T., Murozono, K., Nariai, K., Ohta, K., Okamura, S., Sasaki, T., Shioya, Y. & Umemura, M. (2006). *The End of the Reionization Epoch Probed by Lyα Emitters at z = 6.5 in the Subaru Deep Field.* The Astrophysical Journal, **648**, 7–22.

Kashikawa, N., Shimasaku, K., Matsuda, Y., Egami, E., Jiang, L., Nagao, T., Ouchi, M., Malkan, M. A., Hattori, T., Ota, K., Taniguchi, Y., Okamura, S., Ly, C., Iye, M., Furusawa, H., Shioya, Y., Shibuya, T., Ishizaki, Y. & Toshikawa, J. (2011). *Completing the Census of Lyα Emitters at the Reionization Epoch.* The Astrophysical Journal, **734**, 119.

Kashino, D., Silverman, J. D., Rodighiero, G., Renzini, A., Arimoto, N., Daddi, E., Lilly, S. J., Sanders, D. B., Kartaltepe, J., Zahid, H. J., Nagao, T., Sugiyama, N., Capak, P., Carollo, C. M., Chu, J., Hasinger, G., Ilbert, O., Kajisawa, M., Kewley, L. J., Koekemoer, A. M., Kovač, K., Le Fèvre, O., Masters, D., McCracken, H. J., Onodera, M., Scoville, N., Strazzullo, V., Symeonidis, M. & Taniguchi, Y. (2013). *The FMOS-COSMOS Survey of Star-forming Galaxies at z ˜ 1.6. I. Hα-based Star Formation Rates and Dust Extinction.* The Astrophysical Journal, Letters, **777**, L8.

Kelson, D. D. (2003). *Optimal Techniques in Two-dimensional Spectroscopy: Background Subtraction for the 21st Century.* **115**, 688–699.

Kewley, L. J. & Dopita, M. A. (2002). *Using Strong Lines to Estimate Abundances in Extragalactic H II Regions and Starburst Galaxies.* The Astrophysical Journal, Supplement, **142**, 35–52.

Kollmeier, J. A., Zheng, Z., Davé, R., Gould, A., Katz, N., Miralda-Escudé, J. & Weinberg, D. H. (2010). *Lyα Emission from Cosmic Structure. I. Fluorescence.* The Astrophysical Journal, **708**, 1048–1075.

Komatsu, E., Smith, K. M., Dunkley, J., Bennett, C. L., Gold, B., Hinshaw, G., Jarosik, N., Larson, D., Nolta, M. R., Page, L., Spergel, D. N., Halpern, M., Hill, R. S., Kogut, A., Limon, M., Meyer, S. S., Odegard, N., Tucker, G. S., Weiland, J. L., Wollack, E. & Wright, E. L. (2011). *Seven-year Wilkinson Microwave Anisotropy Probe (WMAP) Observations: Cosmological Interpretation.* The Astrophysical Journal, Supplement, **192**, 18.

Kornei, K. A., Shapley, A. E., Erb, D. K., Steidel, C. C., Reddy, N. A., Pettini, M. & Bogosavljević, M. (2010). *The Relationship between Stellar Populations and Lyα Emission in Lyman Break Galaxies.* The Astrophysical Journal, **711**, 693–710.

Kornei, K. A., Shapley, A. E., Martin, C. L., Coil, A. L., Lotz, J. M., Schiminovich, D., Bundy, K. & Noeske, K. G. (2012). *The Properties and Prevalence of Galactic Outflows at z = 1 in the Extended Groth Strip.* ArXiv e-prints .

Kulas, K. R., Shapley, A. E., Kollmeier, J. A., Zheng, Z., Steidel, C. C. & Hainline, K. N. (2012). *The Kinematics of Multiple-peaked Lyα Emission in Star-forming Galaxies at z ˜ 2-3.* The Astrophysical Journal, **745**, 33.

Kunth, D., Mas-Hesse, J. M., Terlevich, E., Terlevich, R., Lequeux, J. & Fall, S. M. (1998). *HST study of Lyman-alpha emission in star-forming galaxies: the effect of neutral gas flows.* Astronomy & Astrophysics, **334**, 11–20.

Kusakabe, H., Shimasaku, K., Nakajima, K. & Ouchi, M. (2014). *First direct implications for the dust extinction and star formation of typical Ly{\alpha} emitters from their faint infrared luminosities.* ArXiv e-prints .

Larson, R. B. (1974). *Effects of supernovae on the early evolution of galaxies.* Monthly Notices of the Royal Astronomical Society, **169**, 229–246.

Laursen, P., Duval, F. & Östlin, G. (2013). *On the (Non-)Enhancement of the Lyα Equivalent Width by a Multiphase Interstellar Medium.* The Astrophysical Journal, **766**, 124.

Law, D. R., Steidel, C. C., Shapley, A. E., Nagy, S. R., Reddy, N. A. & Erb, D. K. (2012). *An HST/WFC3-IR Morphological Survey of Galaxies at z = 1.5-3.6. I. Survey Description and Morphological Properties of Star-forming Galaxies.* The Astrophysical Journal, **745**, 85.

Le Fèvre, O., Abraham, R., Lilly, S. J., Ellis, R. S., Brinchmann, J., Schade, D., Tresse, L., Colless, M., Crampton, D., Glazebrook, K., Hammer, F. & Broadhurst, T. (2000). *Hubble Space Telescope imaging of the CFRS and LDSS redshift surveys - IV. Influence of mergers in the evolution of faint field galaxies from z˜1.* Monthly Notices of the Royal Astronomical Society, **311**, 565–575.

Lidman, C., Hayes, M., Jones, D. H., Schaerer, D., Westra, E., Tapken, C., Meisenheimer, K. & Verhamme, A. (2012). *The properties of the brightest Lyα emitters at z=5.7.* Monthly Notices of the Royal Astronomical Society, **420**, 1946–1958.

Madau, P. (1995). *Radiative transfer in a clumpy universe: The colors of high-redshift*

galaxies. The Astrophysical Journal, **441**, 18–27.

Malhotra, S., Rhoads, J. E., Finkelstein, S. L., Hathi, N., Nilsson, K., McLinden, E. & Pirzkal, N. (2012). *Sizing up Lyα and Lyman Break Galaxies*. The Astrophysical Journal, Letters, **750**, L36.

Martin, C. L. (2005). *Mapping Large-Scale Gaseous Outflows in Ultraluminous Galaxies with Keck II ESI Spectra: Variations in Outflow Velocity with Galactic Mass*. The Astrophysical Journal, **621**, 227–245.

McCracken, H. J., Capak, P., Salvato, M., Aussel, H., Thompson, D., Daddi, E., Sanders, D. B., Kneib, J.-P., Willott, C. J., Mancini, C., Renzini, A., Cook, R., Le Fèvre, O., Ilbert, O., Kartaltepe, J., Koekemoer, A. M., Mellier, Y., Murayama, T., Scoville, N. Z., Shioya, Y. & Tanaguchi, Y. (2010). *The COSMOS-WIRCam Near-Infrared Imaging Survey. I. BzK-Selected Passive and Star-Forming Galaxy Candidates at z gsim 1.4*. The Astrophysical Journal, **708**, 202–217.

McLinden, E. M., Finkelstein, S. L., Rhoads, J. E., Malhotra, S., Hibon, P., Richardson, M. L. A., Cresci, G., Quirrenbach, A., Pasquali, A., Bian, F., Fan, X. & Woodward, C. E. (2011). *First Spectroscopic Measurements of [O III] Emission from Lyα Selected Field Galaxies at z ˜ 3.1*. The Astrophysical Journal, **730**, 136.

Mosleh, M., Williams, R. J., Franx, M., Gonzalez, V., Bouwens, R. J., Oesch, P., Labbe, I., Illingworth, G. D. & Trenti, M. (2012). *The Evolution of Mass-Size Relation for Lyman Break Galaxies from z = 1 to z = 7*. The Astrophysical Journal, Letters, **756**, L12.

Murray, N., Quataert, E. & Thompson, T. A. (2005). *On the Maximum Luminosity of Galaxies and Their Central Black Holes: Feedback from Momentum-driven Winds*. The Astrophysical Journal, **618**, 569–585.

Nakajima, K. & Ouchi, M. (2014). *Ionization state of inter-stellar medium in galaxies: evolution, SFR-M_*-Z dependence, and ionizing photon escape*. Monthly Notices of the Royal Astronomical Society, **442**, 900–916.

Nakajima, K., Ouchi, M., Shimasaku, K., Hashimoto, T., Ono, Y. & Lee, J. C. (2013). *First Spectroscopic Evidence for High Ionization State and Low Oxygen Abundance in Lya Emitters*. ArXiv e-prints .

Nakajima, K., Ouchi, M., Shimasaku, K., Ono, Y., Lee, J. C., Foucaud, S., Ly, C., Dale, D. A., Salim, S., Finn, R., Almaini, O. & Okamura, S. (2012). *Average*

Metallicity and Star Formation Rate of Lyα Emitters Probed by a Triple Narrowband Survey. The Astrophysical Journal, **745**, 12.

Nestor, D. B., Shapley, A. E., Kornei, K. A., Steidel, C. C. & Siana, B. (2013). *A Refined Estimate of the Ionizing Emissivity from Galaxies at z ˜= 3: Spectroscopic Follow-up in the SSA22a Field.* The Astrophysical Journal, **765**, 47.

Neufeld, D. A. (1990). *The transfer of resonance-line radiation in static astrophysical media.* The Astrophysical Journal, **350**, 216–241.

Neufeld, D. A. (1991). *The escape of Lyman-alpha radiation from a multiphase interstellar medium.* The Astrophysical Journal, Letters, **370**, L85–L88.

Newman, S. F., Genzel, R., Förster-Schreiber, N. M., Shapiro Griffin, K., Mancini, C., Lilly, S. J., Renzini, A., Bouché, N., Burkert, A., Buschkamp, P., Carollo, C. M., Cresci, G., Davies, R., Eisenhauer, F., Genel, S., Hicks, E. K. S., Kurk, J., Lutz, D., Naab, T., Peng, Y., Sternberg, A., Tacconi, L. J., Vergani, D., Wuyts, S. & Zamorani, G. (2012). *The SINS/zC-SINF Survey of z ˜ 2 Galaxy Kinematics: Outflow Properties.* The Astrophysical Journal, **761**, 43.

Nilsson, K. K., Møller, P., Möller, O., Fynbo, J. P. U., Michałowski, M. J., Watson, D., Ledoux, C., Rosati, P., Pedersen, K. & Grove, L. F. (2007). *A multi-wavelength study of z = 3.15 Lyman-α emitters in the GOODS South Field.* Astronomy & Astrophysics, **471**, 71–82.

Oke, J. B. & Gunn, J. E. (1983). *Secondary standard stars for absolute spectrophotometry.* The Astrophysical Journal, **266**, 713–717.

Ono, Y., Ouchi, M., Curtis-Lake, E., Schenker, M. A., Ellis, R. S., McLure, R. J., Dunlop, J. S., Robertson, B. E., Koekemoer, A. M., Bowler, R. A. A., Rogers, A. B., Schneider, E., Charlot, S., Stark, D. P., Shimasaku, K., Furlanetto, S. R. & Cirasuolo, M. (2013). *Evolution of the Sizes of Galaxies over 7 z 12 Revealed by the 2012 Hubble Ultra Deep Field Campaign.* The Astrophysical Journal, **777**, 155.

Ono, Y., Ouchi, M., Mobasher, B., Dickinson, M., Penner, K., Shimasaku, K., Weiner, B. J., Kartaltepe, J. S., Nakajima, K., Nayyeri, H., Stern, D., Kashikawa, N. & Spinrad, H. (2012). *Spectroscopic Confirmation of Three z-dropout Galaxies at z = 6.844-7.213: Demographics of Lyα Emission in z ˜ 7 Galaxies.* The Astrophysical Journal, **744**, 83.

Ono, Y., Ouchi, M., Shimasaku, K., Akiyama, M., Dunlop, J., Farrah, D., Lee, J. C., McLure, R., Okamura, S. & Yoshida, M. (2010a). *Stellar populations of*

Lyα emitters at z = 3-4 based on deep large area surveys in the Subaru-SXDS/UKIDSS-UDS Field. Monthly Notices of the Royal Astronomical Society, **402**, 1580–1598.

Ono, Y., Ouchi, M., Shimasaku, K., Dunlop, J., Farrah, D., McLure, R. & Okamura, S. (2010b). *Stellar Populations of Lyα Emitters at z ˜ 6-7: Constraints on the Escape Fraction of Ionizing Photons from Galaxy Building Blocks.* The Astrophysical Journal, **724**, 1524–1535.

Osterbrock, D. E. & Ferland, G. J. (2006). *Astrophysics of gaseous nebulae and active galactic nuclei.*

Östlin, G., Hayes, M., Duval, F., Sandberg, A., Rivera-Thorsen, T., Marquart, T., Orlitová, I., Adamo, A., Melinder, J., Guaita, L., Atek, H., Cannon, J. M., Gruyters, P., Herenz, E. C., Kunth, D., Laursen, P., Mas-Hesse, J. M., Micheva, G., Otí-Floranes, H., Pardy, S. A., Roth, M. M., Schaerer, D. & Verhamme, A. (2014). *The Lyα Reference Sample. I. Survey Outline and First Results for Markarian259.* The Astrophysical Journal, **797**, 11.

Ota, K., Iye, M., Kashikawa, N., Shimasaku, K., Kobayashi, M., Totani, T., Nagashima, M., Morokuma, T., Furusawa, H., Hattori, T., Matsuda, Y., Hashimoto, T. & Ouchi, M. (2008). *Reionization and Galaxy Evolution Probed by z = 7 Lyα Emitters.* The Astrophysical Journal, **677**, 12–26.

Ouchi, M., Shimasaku, K., Akiyama, M., Simpson, C., Saito, T., Ueda, Y., Furusawa, H., Sekiguchi, K., Yamada, T., Kodama, T., Kashikawa, N., Okamura, S., Iye, M., Takata, T., Yoshida, M. & Yoshida, M. (2008). *The Subaru/XMM-Newton Deep Survey (SXDS). IV. Evolution of Lyα Emitters from z=3.1 to 5.7 in the 1 deg^2 Field: Luminosity Functions and AGN.* The Astrophysical Journal, Supplement, **176**, 301–330.

Ouchi, M., Shimasaku, K., Furusawa, H., Saito, T., Yoshida, M., Akiyama, M., Ono, Y., Yamada, T., Ota, K., Kashikawa, N., Iye, M., Kodama, T., Okamura, S., Simpson, C. & Yoshida, M. (2010). *Statistics of 207 Lyα Emitters at a Redshift Near 7: Constraints on Reionization and Galaxy Formation Models.* The Astrophysical Journal, **723**, 869–894.

Pagel, B. E. J., Edmunds, M. G., Blackwell, D. E., Chun, M. S. & Smith, G. (1979). *On the composition of H II regions in southern galaxies. I - NGC 300 and 1365.* Monthly Notices of the Royal Astronomical Society, **189**, 95–113.

Pardy, S. A., Cannon, J. M., Östlin, G., Hayes, M., Rivera-Thorsen, T., Sandberg, A., Adamo, A., Freeland, E., Herenz, E. C., Guaita, L., Kunth,

D., Laursen, P., Mas-Hesse, J. M., Melinder, J., Orlitová, I., Otí-Floranes, H., Puschnig, J., Schaerer, D. & Verhamme, A. (2014). *The Lyman Alpha Reference Sample: III. Properties of the Neutral ISM from GBT and VLA Observations.* ArXiv e-prints .

Partridge, R. B. & Peebles, P. J. E. (1967). *Are Young Galaxies Visible?* The Astrophysical Journal, **147**, 868.

Peng, C. Y., Ho, L. C., Impey, C. D. & Rix, H.-W. (2002). *Detailed Structural Decomposition of Galaxy Images.* The Astronomical Journal, **124**, 266–293.

Pentericci, L., Fontana, A., Vanzella, E., Castellano, M., Grazian, A., Dijkstra, M., Boutsia, K., Cristiani, S., Dickinson, M., Giallongo, E., Giavalisco, M., Maiolino, R., Moorwood, A., Paris, D. & Santini, P. (2011). *Spectroscopic Confirmation of z ˜ 7 Lyman Break Galaxies: Probing the Earliest Galaxies and the Epoch of Reionization.* The Astrophysical Journal, **743**, 132.

Pettini, M., Kellogg, M., Steidel, C. C., Dickinson, M., Adelberger, K. L. & Giavalisco, M. (1998). *Infrared Observations of Nebular Emission Lines from Galaxies at Z ˜= 3.* The Astrophysical Journal, **508**, 539–550.

Pettini, M. & Pagel, B. E. J. (2004). *[OIII]/[NII] as an abundance indicator at high redshift.* Monthly Notices of the Royal Astronomical Society, **348**, L59–L63.

Pettini, M., Rix, S. A., Steidel, C. C., Adelberger, K. L., Hunt, M. P. & Shapley, A. E. (2002). *New Observations of the Interstellar Medium in the Lyman Break Galaxy MS 1512-cB58.* The Astrophysical Journal, **569**, 742–757.

Pettini, M., Shapley, A. E., Steidel, C. C., Cuby, J.-G., Dickinson, M., Moorwood, A. F. M., Adelberger, K. L. & Giavalisco, M. (2001). *The Rest-Frame Optical Spectra of Lyman Break Galaxies: Star Formation, Extinction, Abundances, and Kinematics.* The Astrophysical Journal, **554**, 981–1000.

Pirzkal, N., Malhotra, S., Rhoads, J. E. & Xu, C. (2007). *Optical-to-Mid-Infrared Observations of Lyα Galaxies at z˜5 in the Hubble Ultra Deep Field: A Young and Low-Mass Population.* The Astrophysical Journal, **667**, 49–59.

Press, W. H., Teukolsky, S. A., Vetterling, W. T. & Flannery, B. P. (1992). *Numerical recipes in C. The art of scientific computing.*

Prochaska, J. X. (2006). *On the Perils of Curve-of-Growth Analysis: Systematic Abundance Underestimates for the Gas in Gamma-Ray Burst Host Galaxies.* The Astrophysical Journal, **650**, 272–280.

Rakic, O., Schaye, J., Steidel, C. C. & Rudie, G. C. (2011). *Calibrating galaxy*

redshifts using absorption by the surrounding intergalactic medium. Monthly Notices of the Royal Astronomical Society, **414**, 3265–3271.

Rauch, M., Becker, G. D., Haehnelt, M. G., Gauthier, J.-R., Ravindranath, S. & Sargent, W. L. W. (2011). *Filamentary infall of cold gas and escape of Lyα and hydrogen ionizing radiation from an interacting high-redshift galaxy.* Monthly Notices of the Royal Astronomical Society, **418**, 1115–1126.

Rauch, M., Haehnelt, M., Bunker, A., Becker, G., Marleau, F., Graham, J., Cristiani, S., Jarvis, M., Lacey, C., Morris, S., Peroux, C., Röttgering, H. & Theuns, T. (2008). *A Population of Faint Extended Line Emitters and the Host Galaxies of Optically Thick QSO Absorption Systems.* The Astrophysical Journal, **681**, 856–880.

Reddy, N. A., Steidel, C. C., Pettini, M., Adelberger, K. L., Shapley, A. E., Erb, D. K. & Dickinson, M. (2008). *Multiwavelength Constraints on the Cosmic Star Formation History from Spectroscopy: the Rest-Frame Ultraviolet, Hα, and Infrared Luminosity Functions at Redshifts 1.9 ˜ z ˜ 3.4.* The Astrophysical Journal, Supplement, **175**, 48–85.

Rhoads, J. E. & Malhotra, S. (2001). *Lyα Emitters at Redshift z = 5.7.* The Astrophysical Journal, Letters, **563**, L5–L9.

Rhoads, J. E., Malhotra, S., Richardson, M. L. A., Finkelstein, S. L., Fynbo, J. P. U., McLinden, E. M. & Tilvi, V. S. (2014). *The Dynamical Masses, Densities, and Star Formation Scaling Relations of Lyα Galaxies.* The Astrophysical Journal, **780**, 20.

Richard, J., Patricio, V., Martinez, J., Bacon, R., Clément, B., Weilbacher, P., Soto, K., Wisotzki, L., Vernet, J., Pello, R., Schaye, J., Turner, M. & Martinsson, T. (2015). *MUSE observations of the lensing cluster SMACSJ2031.8-4036: new constraints on the mass distribution in the cluster core.* Monthly Notices of the Royal Astronomical Society, **446**, L16–L20.

Rosdahl, J. & Blaizot, J. (2012). *Extended Lyα emission from cold accretion streams.* Monthly Notices of the Royal Astronomical Society, **423**, 344–366.

Salpeter, E. E. (1955). *The Luminosity Function and Stellar Evolution.* The Astrophysical Journal, **121**, 161.

Santos, M. R. (2004). *Probing reionization with Lyman α emission lines.* Monthly Notices of the Royal Astronomical Society, **349**, 1137–1152.

Schaerer, D. & de Barros, S. (2009). *The impact of nebular emission on the ages of*

z 6 galaxies. Astronomy & Astrophysics, **502**, 423–426.

Schaerer, D., Hayes, M., Verhamme, A. & Teyssier, R. (2011). *Grid of Lyα radiation transfer models for interpreting distant galaxies.* Astronomy & Astrophysics, **531**, A12.

Schaerer, D. & Verhamme, A. (2008). *3D Lyα radiation transfer. II. Fitting the Lyman break galaxy MS 1512-cB58 and implications for Lyα emission in high-z starbursts.* Astronomy & Astrophysics, **480**, 369–377.

Schenker, M. A., Ellis, R. S., Konidaris, N. P. & Stark, D. P. (2013). *Contamination of Broadband Photometry by Nebular Emission in High-redshift Galaxies: Investigations with Keck's MOSFIRE Near-infrared Spectrograph.* The Astrophysical Journal, **777**, 67.

Schenker, M. A., Ellis, R. S., Konidaris, N. P. & Stark, D. P. (2014). *Line-emitting Galaxies beyond a Redshift of 7: An Improved Method for Estimating the Evolving Neutrality of the Intergalactic Medium.* The Astrophysical Journal, **795**, 20.

Schenker, M. A., Stark, D. P., Ellis, R. S., Robertson, B. E., Dunlop, J. S., McLure, R. J., Kneib, J.-P. & Richard, J. (2012). *Keck Spectroscopy of Faint 3 z 8 Lyman Break Galaxies: Evidence for a Declining Fraction of Emission Line Sources in the Redshift Range 6 z 8.* The Astrophysical Journal, **744**, 179.

Seaton, M. J. (1979). *Interstellar extinction in the UV.* Monthly Notices of the Royal Astronomical Society, **187**, 73P–76P.

Shapiro, K. L., Genzel, R., Quataert, E., Förster Schreiber, N. M., Davies, R., Tacconi, L., Armus, L., Bouché, N., Buschkamp, P., Cimatti, A., Cresci, G., Daddi, E., Eisenhauer, F., Erb, D. K., Genel, S., Hicks, E. K. S., Lilly, S. J., Lutz, D., Renzini, A., Shapley, A., Steidel, C. C. & Sternberg, A. (2009). *The SINS Survey: Broad Emission Lines in High-Redshift Star-Forming Galaxies.* The Astrophysical Journal, **701**, 955–963.

Shapley, A. E., Erb, D. K., Pettini, M., Steidel, C. C. & Adelberger, K. L. (2004). *Evidence for Solar Metallicities in Massive Star-forming Galaxies at z ˜ 2.* The Astrophysical Journal, **612**, 108–121.

Shapley, A. E., Steidel, C. C., Pettini, M. & Adelberger, K. L. (2003). *Rest-Frame Ultraviolet Spectra of z˜3 Lyman Break Galaxies.* The Astrophysical Journal, **588**, 65–89.

Shapley, A. E., Steidel, C. C., Pettini, M., Adelberger, K. L. & Erb, D. K. (2006). *The Direct Detection of Lyman Continuum Emission from Star-forming Galax-*

ies at z˜3. The Astrophysical Journal, **651**, 688–703.

Sharma, M., Nath, B. B. & Shchekinov, Y. (2011). *Dust-driven Wind from Disk Galaxies.* The Astrophysical Journal, Letters, **736**, L27.

Shibuya, T., Ouchi, M., Nakajima, K., Hashimoto, T., Ono, Y., Rauch, M., Gauthier, J.-R., Shimasaku, K., Goto, R., Mori, M. & Umemura., M. (2014a). *What is the Physical Origin of Strong Lyα Emission? II. Gas Kinematics and Distribution of Lyα Emitters.* The Astrophysical Journal, **788**, 74.

Shibuya, T., Ouchi, M., Nakajima, K., Yuma, S., Hashimoto, T., Shimasaku, K., Mori, M. & Umemura, M. (2014b). *What is the Physical Origin of Strong Lyα Emission? I. Demographics of Lyα Emitter Structures.* The Astrophysical Journal, **785**, 64.

Song, M., Finkelstein, S. L., Gebhardt, K., Hill, G. J., Drory, N., Ashby, M. L. N., Blanc, G. A., Bridge, J., Chonis, T., Ciardullo, R., Fabricius, M., Fazio, G. G., Gawiser, E., Gronwall, C., Hagen, A., Huang, J.-S., Jogee, S., Livermore, R., Salmon, B., Schneider, D. P., Willner, S. P. & Zeimann, G. R. (2014). *The HETDEX Pilot Survey. V. The Physical Origin of Lyα Emitters Probed by Near-infrared Spectroscopy.* The Astrophysical Journal, **791**, 3.

Soto, K. T., Martin, C. L., Prescott, M. K. M. & Armus, L. (2012). *The Emission-line Spectra of Major Mergers: Evidence for Shocked Outflows.* The Astrophysical Journal, **757**, 86.

Stark, D. P., Ellis, R. S., Chiu, K., Ouchi, M. & Bunker, A. (2010). *Keck spectroscopy of faint 3 z 7 Lyman break galaxies - I. New constraints on cosmic reionization from the luminosity and redshift-dependent fraction of Lyman α emission.* Monthly Notices of the Royal Astronomical Society, **408**, 1628–1648.

Stark, D. P., Ellis, R. S. & Ouchi, M. (2011). *Keck Spectroscopy of Faint 3z7 Lyman Break Galaxies: A High Fraction of Line Emitters at Redshift Six.* The Astrophysical Journal, Letters, **728**, L2.

Stark, D. P., Richard, J., Siana, B., Charlot, S., Freeman, W. R., Gutkin, J., Wofford, A., Robertson, B., Amanullah, R., Watson, D. & Milvang-Jensen, B. (2014). *Ultraviolet emission lines in young low-mass galaxies at z 2: physical properties and implications for studies at z 7.* Monthly Notices of the Royal Astronomical Society, **445**, 3200–3220.

Steidel, C. C., Erb, D. K., Shapley, A. E., Pettini, M., Reddy, N., Bogosavljević, M., Rudie, G. C. & Rakic, O. (2010). *The Structure and Kinematics of*

the Circumgalactic Medium from Far-ultraviolet Spectra of z ˜= 2-3 Galaxies. The Astrophysical Journal, **717**, 289–322.

Tremonti, C. A., Heckman, T. M., Kauffmann, G., Brinchmann, J., Charlot, S., White, S. D. M., Seibert, M., Peng, E. W., Schlegel, D. J., Uomoto, A., Fukugita, M. & Brinkmann, J. (2004). *The Origin of the Mass-Metallicity Relation: Insights from 53,000 Star-forming Galaxies in the Sloan Digital Sky Survey.* The Astrophysical Journal, **613**, 898–913.

Vanzella, E., Grazian, A., Hayes, M., Pentericci, L., Schaerer, D., Dickinson, M., Cristiani, S., Giavalisco, M., Verhamme, A., Nonino, M. & Rosati, P. (2010). *The unusual N IV] -emitter galaxy GDS J033218.92-275302.7: star formation or AGN-driven winds from a massive galaxy at z = 5.56.* Astronomy & Astrophysics, **513**, A20.

Vargas, C. J., Bish, H., Acquaviva, V., Gawiser, E., Finkelstein, S. L., Ciardullo, R., Ashby, M. L. N., Feldmeier, J., Ferguson, H., Gronwall, C., Guaita, L., Hagen, A., Koekemoer, A., Kurczynski, P., Newman, J. A. & Padilla, N. (2014). *To Stack or Not to Stack: Spectral Energy Distribution Properties of Lyα-emitting Galaxies at z = 2.1.* The Astrophysical Journal, **783**, 26.

Verhamme, A., Dubois, Y., Blaizot, J., Garel, T., Bacon, R., Devriendt, J., Guiderdoni, B. & Slyz, A. (2012). *Lyman-α emission properties of simulated galaxies: interstellar medium structure and inclination effects.* Astronomy & Astrophysics, **546**, A111.

Verhamme, A., Orlitova, I., Schaerer, D. & Hayes, M. (2014). *On the use of Lyman-alpha to detect Lyman continuum leaking galaxies.* ArXiv e-prints .

Verhamme, A., Schaerer, D., Atek, H. & Tapken, C. (2008). *3D Lyα radiation transfer. III. Constraints on gas and stellar properties of z ˜ 3 Lyman break galaxies (LBG) and implications for high-z LBGs and Lyα emitters.* Astronomy & Astrophysics, **491**, 89–111.

Verhamme, A., Schaerer, D. & Maselli, A. (2006). *3D Lyα radiation transfer. I. Understanding Lyα line profile morphologies.* Astronomy & Astrophysics, **460**, 397–413.

Yabe, K., Ohta, K., Akiyama, M., Iwamuro, F., Tamura, N., Yuma, S., Dalton, G. & Lewis, I. (2015). *The Gas Inflow and Outflow Rate in Star-forming Galaxies at z ˜ 1.4.* The Astrophysical Journal, **798**, 45.

Yajima, H., Li, Y., Zhu, Q., Abel, T., Gronwall, C. & Ciardullo, R. (2012). *Were Progenitors of Local L* Galaxies Lyα Emitters at High Redshift?* The Astro-

physical Journal, **754**, 118.

Yamada, T., Matsuda, Y., Kousai, K., Hayashino, T., Morimoto, N. & Umemura, M. (2012). *Profiles of Lyα Emission Lines of the Emitters at z = 3.1.* The Astrophysical Journal, **751**, 29.

Yang, Y., Zabludoff, A., Jahnke, K. & Davé, R. (2014). *The Properties of Lyman Alpha Nebulae: Gas Kinematics from Non-resonant Lines.* ArXiv e-prints .

Yang, Y., Zabludoff, A., Jahnke, K., Eisenstein, D., Davé, R., Shectman, S. A. & Kelson, D. D. (2011). *Gas Kinematics in Lyα Nebulae.* The Astrophysical Journal, **735**, 87.

Zheng, Z. & Miralda-Escudé, J. (2002). *Monte Carlo Simulation of Lyα Scattering and Application to Damped Lyα Systems.* The Astrophysical Journal, **578**, 33–42.

Zheng, Z. & Wallace, J. (2014). *Anisotropic Lyman-alpha Emission.* The Astrophysical Journal, **794**, 116.